

CONSTRAINTS ON THE DEFORMATIONAL HISTORY OF
THE TIJERAS CAÑONCITO FAULT SYSTEM,
NORTH-CENTRAL NEW MEXICO

John Charles Abbott

**Geotechnical
Information Center**

**N.M. BUREAU OF MINES
AND MINERAL RESOURCES
SOCORRO, N.M. 87801**

Department of Earth and Environmental Science
New Mexico Tech
Socorro, New Mexico

Submitted in partial fulfillment of the requirements for the degree of
Master of Science in Geology

May 1995

ABSTRACT

The regionally extensive, northeast-striking Tijeras-Cañoncito fault system includes a number of sub-vertical faults. Most major faults within the fault system strike northeast, although the strikes of some major and most minor faults are oblique to the system. The fault system has a complex history of recurrent movement. Slip was partitioned among major and minor faults. Slickenside striae record strike-slip, dip-slip, and oblique-slip movements, though strike-slip movement was dominant. The width of the fault zone, the intensity of deformation, and tectonic mixing within the fault zone together suggest significant displacement on the fault system.

The oldest documented activity occurred during the Laramide orogeny (80-40 Ma). Right-lateral strike-slip motion is recorded by minor faults and slickenside striae. Analysis of paleocurrent indicators and paleogeography indicates synchronous extensional subsidence of the Paleogene Galisteo basin. Taken together, these data suggest that the Tijeras-Cañoncito fault system accommodated right-lateral, transtensional motion during the Laramide orogeny. This movement sense is consistent with regional deformation patterns.

Apatite fission-track ages of 21.4 ± 3.3 to 25.9 ± 2.6 Ma on both sides of the fault preclude major vertical displacement on the Tijeras fault (a major fault within the Tijeras-Cañoncito fault system) in the late Oligocene to early Miocene. Neogene deformation is indicated by extreme brecciation of an Oligocene porphyritic intrusive rock that is overlain by Quaternary(?) surficial deposits. Slickenside striae and orientations of minor faults that suggest left-lateral transtensional motion locally cut the intrusive rock and are interpreted to be related to extension associated with the formation of the Rio Grande rift. Regional extension directions indicate that northeast-striking faults could be expected to accommodate rift-related deformation by left-lateral transtensional motion. Quaternary surficial deposits are known to be offset in two locations, indicating Quaternary activity.

ACKNOWLEDGMENTS

I would like to thank Laurel Goodwin, Paul Bauer, Steve Cather, and Dave Johnson for serving on my thesis committee. I found a mentor and friend in each of them. Laurel, my primary advisor, deserves special thanks. She was the reason I chose to attend this school, and has never given me reason to second-guess my decision. I will miss her professionalism, enthusiasm, and friendship. I sincerely thank Shari Kelley, who took me under her wing and introduced me to fission-track dating. I also thank the many colleagues and friends who shared their knowledge of New Mexico geology or aided with data collection: Orin Anderson, Chris Beck, Chuck Chapin, Bob Colpitts, John Farren, Charlie Ferranti, Bill Haneberg, Bruce Harrison, John Hawley, Karl Karlstrom, Keith Kelson, Eric Kirby, Dave Love, Spencer Lucas, Joe Marcoline, Steve Maynard, Peter Mozley, Terry Pollock, Steve Ralser, Bob Redden, Allan Sanford, John Sigda, Dave Sivils, and Tom Sheppler. I benefitted much from discussions with each of them.

I appreciate generous financial support from the New Mexico Bureau of Mines and Mineral Resources, the New Mexico Geological Society, the Roswell Geological Society, the Matuszeski Fund of the Graduate Association and the Alumni and Development Office, Anita and Anton Budding, and the New Mexico Tech Graduate Student Research Fund. I commend them for their support of students.

A final note of thanks to those special people without whom this thesis would not have been completed. Aaron Cross put it all in perspective, and was kind enough to wash me out of Socorro with a hose. Meltem Zorlu was an enthusiastic field companion and provided ample inspiration for me to swiftly finish the thesis. *Seni cok seviyorum, canim benim.* Lastly, I graciously thank my parents for their unending support throughout my entire academic career, and I dedicate this thesis to them.

TABLE OF CONTENTS

Abstract	i
Acknowledgements	ii
Table of Contents	iii
List of Figures	v
List of Tables	viii
List of Appendices	ix
List of Plates	x
Introduction	1
Part I: PALEOGENE SYNOROGENIC SEDIMENTATION IN THE GALISTEO BASIN RELATED TO THE TIJERAS-CAÑONCITO FAULT SYSTEM	3
Abstract	4
Introduction	5
Geological Setting	5
The Tijeras-Cañoncito fault system	5
Stratigraphy of the Galisteo basin	7
Stratigraphic Thickness	10
Spatial Variation in Lithology	10
Paleocurrents	12
Treatment of data	12
Lower unit	13
Upper unit	19
Discussion and Conclusions	25
Part II: A SPECTACULAR EXPOSURE OF THE TIJERAS FAULT, WITH EVIDENCE FOR QUATERNARY MOTION	
Abstract	29
Introduction	30
The Tijeras-Cañoncito fault system	30
Regional geology	33
Terminology of fault rocks and minor faults	34
The Streamcut Exposure of the Tijeras Fault near Golden	35
Bedrock geology	35

Surficial deposits	42
Fault slickenside data	46
Discussion	50
Conclusion	55
Part III: EVIDENCE FOR REACTIVATION OF THE TIJERAS-CAÑONCITO FAULT SYSTEM FROM THE LARAMIDE TO THE QUATERNARY	
Introduction	57
The Tijeras-Cañoncito fault system	59
Previous Studies	63
Precambrian	63
Paleozoic	64
Mesozoic - early Cenozoic	65
Middle - late Cenozoic	65
Evidence for the Timing and Character of Motion on the Tijeras- Cañoncito Fault System	67
Field observations	67
Precambrian	67
Late Paleozoic	68
Fission-Track Analysis	69
Faults and Fault Slickensides	81
East-northeast-striking faults	90
Northwest-striking faults	96
North- and north-northeast-striking faults	96
Northeast-striking faults	97
Summary of slickenside data and interpretations	98
Conclusions	101
REFERENCES	104-112
APPENDICES	113-161
PLATES	back pocket

LIST OF FIGURES

Part I: PALEOGENE SYNOROGENIC SEDIMENTATION IN THE GALISTEO BASIN RELATED TO THE TIJERAS-CAÑONCITO FAULT SYSTEM

Figure 1-1.	Location map of the Tijeras-Cañoncito fault system and known exposures of strata of the Galisteo basin	6
Figure 1-2.	Basal conglomerate of the upper unit of the Galisteo basin	9
Figure 1-3.	Thicknesses of strata of the Galisteo basin	11
Figure 1-4.	Paleocurrent rose diagrams of the lower unit in the Cerrillos-Lamy area	14-15
Figure 1-5.	Resultant vector means of paleocurrents in the lower unit in the Cerrillos-Lamy area	16-17
Figure 1-6.	Synthesis of all paleocurrent data in the lower unit of the Galisteo basin	18
Figure 1-7.	Paleocurrent rose diagrams of the upper unit in the Cerrillos-Lamy area	20-21
Figure 1-8.	Resultant vector means of paleocurrents in the upper unit in the Cerrillos-Lamy area	22-23
Figure 1-9.	Synthesis of all paleocurrent data in the upper unit of the Galisteo basin	24

Part II: A SPECTACULAR EXPOSURE OF THE TIJERAS FAULT, WITH EVIDENCE FOR QUATERNARY MOTION

Figure 2-1.	Location of the streamcut exposure	32
Figure 2-2.	Illustrations of selected parts of the streamcut exposure	36-37

Figure 2-3.	Oligocene(?) porphyry overlain by Holocene(?) imbricated gravel surficial deposit	38
Figure 2-4.	Tectonic mixing	39
Figure 2-5.	Brecciated Proterozoic Cibola gneiss	41
Figure 2-6.	Quaternary(?) fault	43
Figure 2-7.	Apparent Holocene(?) faults	45
Figure 2-8.	Equal area, lower hemisphere projection of poles to 62 minor faults	47
Figure 2-9.	Equal area, lower hemisphere projection of poles to 20 fault slickensides	48
Figure 2-10.	Pitches of 20 fault striae from slickenside surfaces near the margin of the fault zone	49
Figure 2-11.	Anticipated Riedel shear geometries	52
Figure 2-12.	Schematic diagram of Neogene rifting	53

Part III: EVIDENCE FOR REACTIVATION OF THE TIJERAS-CAÑONCITO FAULT SYSTEM FROM THE LARAMIDE TO THE QUATERNARY

Figure 3-1.	Location map and major structural elements of the Tijeras-Cañoncito fault system	60
Figure 3-2.	Major structural elements of the Tijeras-Cañoncito fault system near Tijeras graben and Monte Largo horst	62
Figure 3-3.	Sample localities for fission-track analysis	71
Figure 3-4.	Comparison of fission-track dates in and adjacent to the Tijeras fault zone	72

Figure 3-5.	Schematic illustration of the effect of the timing of uplift of the Monte Largo horst on fission-track dates	75-76
Figure 3-6.	Histograms of confined fission-track lengths in apatite	79
Figure 3-7.	Time-temperature inversion model for sample ML02	80
Figure 3-8.	Schematic diagram of Neogene rifting	82
Figure 3-9.	Fault and slickenline data from the Proterozoic Tijeras greenstone	83-84
Figure 3-10.	Fault and slickenline data from the Proterozoic Cibola gneiss	85
Figure 3-11.	Fault and slickenline data from the Permian Abo Formation.....	86
Figure 3-12.	Fault and slickenline data from the Jurassic Morrison Formation	87
Figure 3-13.	Fault and slickenline data from the Cretaceous Dakota Formation	88
Figure 3-14.	Fault and slickenline data from the rocks in the streamcut exposure near Golden	89
Figure 3-15.	Polished fault surface in the Tijeras greenstone with well developed horizontal slickenside striae indicating strike-slip motion	91
Figure 3-16.	Anticipated Riedel shear geometries	92
Figure 3-17.	Simplified geologic map of the northeastern part of the Tijeras 7.5" quadrangle	93-94
Figure 3-18.	Two fault surfaces in the Abo Formation of similar orientation that record different kinematic histories	100

LIST OF TABLES

Table 3-1. Fission-track sample descriptions and etching procedures 70

LIST OF APPENDICES

APPENDIX A: Sedimentological data from the Galisteo basin in the Cerrillos-
Lamy area 113-126

APPENDIX B: Detailed log of the streamcut exposure near Golden 127-132

APPENDIX C: Minor fault and fault slickenside data for rocks in the streamcut
exposure near Golden 133-135

APPENDIX D: Fission-track age data 136-143

APPENDIX E: Graphical representation of fission-track age data 144-152

APPENDIX F: Apatite confined fission-track lengths 153

APPENDIX G: Minor fault and fault slickenside data 154-161

LIST OF PLATES

PLATE 1: Measurement sites in the Galisteo basin in the Cerrillos-Lamy area. Site numbers are keyed to Appendix A back pocket

(a) sites 1-158 and 288-304.

Map is from the Madrid and Cerrillos 7.5" U.S.G.S. topographic quadrangles.

(b) sites 159-246 and 251-287 and 329-340.

Map is from the Picture Rock and Captain Davis Mountain 7.5" U.S.G.S. topographic quadrangles.

(c) sites 247-250.

Map is from the Captain Davis Mountain 7.5" U.S.G.S. topographic quadrangle.

(d) sites 305-328.

Map is from the Galisteo 7.5" U.S.G.S. topographic quadrangle.

(e) sites 341-363.

Map is from the Galisteo 7.5" U.S.G.S. topographic quadrangle.

INTRODUCTION

The Tijeras-Cañoncito fault system is arguably one of the most commonly mentioned fault systems in New Mexico. The fault system is mentioned regularly in discussions that range in scope from the Proterozoic crustal evolution of New Mexico to seismic hazard assessment of Albuquerque and Santa Fe. Unfortunately, many of these discussions have been misdirected by a poor understanding of the deformational history of the fault system. Though the fault system has been of interest for decades, previous workers generally considered the Tijeras-Cañoncito fault system as a peripheral topic in their studies. This thesis is notable because it is the first major study that focuses solely on the deformational history of the fault system.

Current interest in the Tijeras-Cañoncito fault system prompted me to present the results of my research in a readily accessible form. My thesis comprises a trio of manuscripts intended for publication in widely distributed professional journals. Each manuscript was written to stand alone as a separate journal article. The text in the published manuscripts is very similar to the thesis version, though the thesis version contains a few additional photographs and all of the raw data in appendices.

Part I focuses on the Paleogene deformational history of the fault system. I test a hypothesis proposed by Steve Cather that the fault system acted as a releasing bend in the right-lateral system of the Southern Rocky Mountains during the Laramide orogeny. I entertain the possibility that the fault system controlled extensional subsidence of the Paleogene Galisteo basin to the northwest. I test the model by examining the sedimentology and stratigraphic thickness variations of Paleogene strata adjacent to the fault system.

Part II is a detailed description of a single, recently discovered, 160-m-wide exposure of the Tijeras fault. The exposure is a remarkable window into the internal structure of the fault zone. It reveals a spectacular example of tectonic mixing and illustrates key relationships of reactivation of the fault system in the Neogene and Quaternary.

Part III summarizes the current understanding of the Tijeras-Cañoncito fault system. I integrate new fission-track and slickenside data with regional deformation patterns. Several previously published observations are re-interpreted in terms of the new understanding of the fault system. This is the most comprehensive summary to date of the deformational history of the Tijeras-Cañoncito fault system. The conclusion section of this manuscript serves as a summary for the entire thesis.

I do not consider this thesis as the definitive work on the Tijeras-Cañoncito fault system, rather as a foundation and springboard for further study. Several questions remain, which I present in hopes of piquing some curiosities: (1) Does the Tijeras-Cañoncito fault system connect with other fault systems? A possible relationship with the Tijeras accommodation zone is of particular interest as it may yield insight into the mechanics and evolution of accommodation zones in continental rifts. (2) Is the fault system older than Laramide in age? Detailed stratigraphic analysis of Upper Paleozoic strata across the Tijeras and Guitierrez faults may provide insight into possible Ancestral Rocky Mountain deformation accommodated by the Tijeras-Cañoncito fault system. (3) How active was the Tijeras-Cañoncito fault system during the Quaternary? Of the two known exposures of the Tijeras-Cañoncito fault system, both reveal unequivocal evidence of faulted surficial deposits, but with opposite apparent displacement directions. The nature and timing of Quaternary movement is poorly constrained. (4) What is the slip vector for each deformational event? Structural relationships suggest substantial right- and left-lateral strike-slip motion in the Tertiary, though no piercing points have yet been identified to establish the magnitude of slip. (5) What effect does the fault system have on groundwater flow patterns? The Tijeras fault is a breccia zone locally over 160 m wide, and likely has a strong influence on the subsurface hydrology.

Part I

PALEOGENE SYNOROGENIC SEDIMENTATION IN THE GALISTEO BASIN
RELATED TO THE TIJERAS-CAÑONCITO FAULT SYSTEM

John C. Abbott
Steven M. Cather*
and
Laurel B. Goodwin

Department of Earth and Environmental Science
New Mexico Tech
Socorro, New Mexico

*New Mexico Bureau of Mines and Mineral Resources
Socorro, New Mexico

in press

1995 New Mexico Geological Society Guidebook 46

ABSTRACT

The strata between the Cretaceous Mesaverde Group and the Oligocene Espinazo Formation were deposited in a synorogenic, continental basin (the Galisteo basin) during the Laramide orogeny. Three lines of evidence suggest that the Tijeras-Cañoncito fault system controlled extensional subsidence of the Galisteo basin. First, stratigraphic thickening and highly variable paleocurrent directions adjacent to the fault system in both the Hagan and Cerrillos-Lamy areas indicate that the axis of the basin was parallel to the fault system. Second, there were large components of fault-parallel paleoflow in the lower unit of the basin adjacent to the fault system near Galisteo Creek. Paleoflow was both to the northeast and to the southwest, recording fault control on sediment dispersal. Third, the Tijeras-Cañoncito fault system is the only major fault system identified in the area, and is the most plausible structural control on Paleogene extensional subsidence. Although the fault system appears to have controlled a large part of the extensional subsidence of the basin, the fault system was not the southeastern boundary of the basin. The presence of Paleogene strata on the southeast fault block, the lack of scarp-derived deposits, and the scarcity of northwesterly paleoflow adjacent to the fault system preclude major uplift and denudation of the southeast fault block during the Laramide, and suggest the fault system was located within the basin. Because the southeast block was not emergent, the maximum displacement magnitude of the Paleogene dip-slip component on the Tijeras-Cañoncito fault system is constrained to approximately the thickness of the strata of the Galisteo basin (about 1300 m, northwest-side-down).

INTRODUCTION

It has long been recognized that the strata of the Galisteo basin thicken substantially to the southeast, and this observation has been used repeatedly to suggest that the sediments were deposited in an actively subsiding basin during the Laramide orogeny (Stearns, 1943; 1953; Gorham, 1979; Gorham and Ingersoll, 1979; Ingersoll et al., 1990; Cather, 1992). Ingersoll et al. (1990) used the thickening to the southeast as evidence to suggest there was important structural control on subsidence, and they were the first to speculate that the Tijeras-Cañoncito fault system was the southeastern boundary of the Galisteo basin. Cather (1992) developed this hypothesis in a regional tectonic model wherein the Tijeras-Cañoncito fault system acted as a releasing bend in the right-lateral strike-slip system of the southern Rocky Mountains, and controlled extensional subsidence in a half-graben to the northwest of the fault system in the Paleogene. In this paper, we test this hypothesis by examining the sedimentology and paleocurrents of the strata of the Galisteo basin adjacent to the Tijeras-Cañoncito fault system.

GEOLOGICAL SETTING

The Tijeras-Cañoncito fault system

The Tijeras-Cañoncito fault system comprises a number of northeast-striking, sub-vertical faults, including the Tijeras, Guitierrez, San Lazarus, Los Angeles, and Lamy faults (Fig. 1-1). The fault system is regionally extensive; it has been mapped for more than 80 km from Kirtland Air Force Base on the southwest (about 16 km east of Albuquerque), to the Cañoncito area on the northeast (about 20 km south of Santa Fe). Following Lisenbee et al. (1979), Woodward (1984), and Maynard et al. (1990), we prefer the name "Tijeras-Cañoncito fault system" over "Tijeras fault zone" when referring to the entire structure. Both names are entrenched in the literature and are often used synonymously. We prefer "Tijeras-Cañoncito

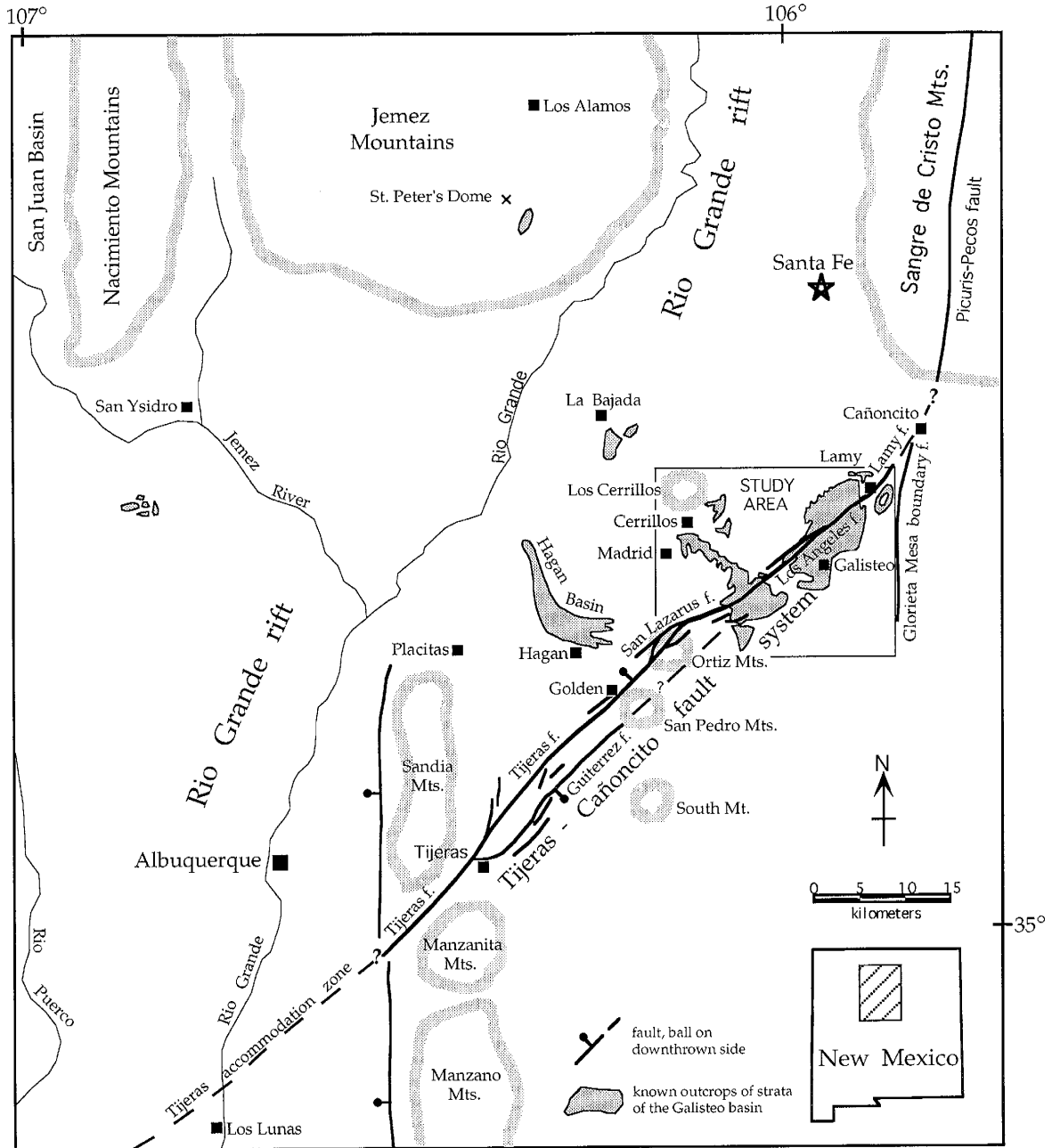


Figure 1-1. Location map of the Tijeras-Cañoncito fault system and known exposures of strata of the Galisteo basin.

fault system" because it approximately locates the structure, and also distinguishes it from the Tijeras fault, which is only part of the system.

The Tijeras-Cañoncito fault system has a history of recurrent movement. Slickenlines on minor fault surfaces record strike-slip, dip-slip, and oblique-slip motion (Abbott et al., Part III). Lisenbee et al. (1979) suggested that the fault system was active in the Proterozoic and in the Pennsylvanian, but unequivocal evidence of such activity is lacking (Abbott et al., Part III). The oldest documented activity is Laramide (80-40 Ma) in age. Laramide activity is supported by the results of this as well as other studies. En echelon folds (Chapin and Cather, 1981, p. 48) and fault slickenlines (Abbott and Goodwin, 1995; Abbott et al., Part III) in Mesozoic and Paleozoic rocks record right-lateral strike-slip motion. The Laramide orogeny is the only post-Mesozoic deformational event that is consistent with right-lateral motion on the Tijeras-Cañoncito fault system. Neogene activity is supported by strongly brecciated Oligocene rocks within the fault system in the Ortiz and San Pedro Mountains (Fig. 1-1; Maynard et al., 1990; Abbott and Goodwin, 1995), as well as slickenlines that record left-lateral motion on the fault system. Faulted surficial deposits provide clear evidence for reactivation of the Tijeras fault in the Quaternary (Lisenbee et al., 1979; Abbott and Goodwin, 1995).

Stratigraphy of the Galisteo basin

Strata between the Upper Cretaceous Mesaverde Group (Holmes, 1877) and the Oligocene Espinazo Formation (Stearns, 1953) have traditionally been assigned to the Galisteo Formation (Hayden, 1869). These strata consist of fluvial mudstone, sandstone, and conglomerate up to 1295 m thick (Gorham, 1979). Excellent lithologic descriptions of these strata have been made in the Hagan Basin (Stearns, 1943; Harrison, 1949; Gorham, 1979), in the Cerrillos-Lamy area (Stearns, 1943; Lucas, 1982), and in the vicinity of St. Peter's Dome about 10 km south of Los Alamos (Cather, 1992). Measured sections are provided by Harrison (1949), Gorham (1979), and Lucas (1982). In a forthcoming paper (Lucas et al., in prep), it will be

proposed that these strata should be subdivided into two formations. In light of imminent revision to the stratigraphic nomenclature, the term "Galisteo Formation" is abandoned in this paper. Herein we recognize two informal lithostratigraphic units. Based on close similarities in age, distribution, and sedimentology, we consider both units to have been deposited in the Galisteo basin, and we refer to them collectively as the strata of the Galisteo basin. The lower unit unconformably overlies the Mesaverde Group. In the Cerrillos-Lamy area, the unconformity has been mapped by Stearns (1953), Disbrow and Stoll (1957), Bachman (1975), and Johnson (1975). It consists of about 121 m of yellowish-brown and gray sandstone, mudstone, pebbly sandstone, and minor conglomerate. In the Cerrillos-Lamy area, the lower unit is equivalent to units 10-21 of Lucas' (1982) measured section; in the Hagan Basin, the lower unit is the strata below the Lw-css member of Gorham (1979). The upper lithostratigraphic unit unconformably overlies the lower unit. The contact is marked by a basal conglomerate that is ubiquitous in the Cerrillos-Lamy area (Fig. 1-2). The basal conglomerate is 1-3 m of clast-supported pebble conglomerate. Clasts have a high degree of sphericity, and are composed of quartzite, gray limestone, chert, and sandstone. Good exposures of the basal conglomerate are present in four localities: ne1/4, sec. 19, T14N, R8E; se1/4, se1/4, sec. 36, T15N, R9E; w1/2, se1/4, sec. 16, T14N, R8E; and nw1/4, sw1/4, sec. 6, T13N, R9E (Plate 1). The upper unit is a red-bed sequence about 974 m thick of red mudstone, light gray sandstone, and conglomerate. In the Cerrillos-Lamy area, the upper unit is equivalent to units 22-82 of Lucas' (1982) measured section; in the Hagan Basin, the upper unit is the strata above the Lb-ss, mdst member of Gorham (1979). Late Wasatchian through Duchesnean vertebrate fossils from this interval suggest that deposition of the upper unit spanned the entire Eocene (Lucas, 1982). The upper contact of the upper unit has been chosen in slightly different stratigraphic positions by different workers. Lucas (1982) provides a strong argument for locating it at the base of the lowermost major debris flow deposit or tuff of the overlying thick volcanic strata. This practice is accepted here.



Figure 1-2. Basal conglomerate of the upper unit of the Galisteo basin. Yellow pebbly sands of the lower unit (foreground) are unconformably overlain by a basal pebble conglomerate (lower to middle part of photo) of the upper unit. Brown cannonball concretion (~30 cm in diameter) at lower right lies slightly below the contact. Concretions such as this one are common in the lower unit, but rare or absent in the upper unit. Red beds of the upper unit crop out on the upper part of the slope. View to south; photo taken in se1/4, se1/4, sec. 36, T15N, R9E.

STRATIGRAPHIC THICKNESS

Strata of the Galisteo basin thicken substantially to the southeast (Fig. 1-3). Stearns (1943) depicted an increase in stratigraphic thickness from about 350 m near La Bajada to about 1300 m near Lamy and Hagan. Gorham (1979) demonstrated that strata of the Galisteo basin thicken to the southeast in the Hagan Basin from 261 m to 1295 m. Both units contribute to the southeast thickening in the Hagan Basin; the lower unit thickens from 0 to 450 m, and the upper unit thickens from 261 to 850 m. This variation in thickness is not the result of post-Galisteo erosion, because deposition of the Espinazo Formation followed without interruption (Stearns, 1943). The variation in thickness is also not the result of onlap onto irregular topography. Though basal scours are present in both units, the local relief is small and limited to channels less than a few meters deep. There is no evidence for much local irregularity on either surface. One exception to the trend of southeastward thickening is the exposure near St. Peters Dome. At this locality, Cather (1992) noted that the strata of the Galisteo basin are over 630 m thick.

SPATIAL VARIATION IN LITHOLOGY

In the Cerrillos-Lamy area, there is no systematic relationship in either unit between lithology and geographic location. The exposures immediately adjacent to the Tijeras-Cañoncito fault system, for instance, are similar in grain size and facies to exposures elsewhere in the Cerrillos-Lamy area. Though an outcrop in either unit generally consists of beds ranging in coarseness from conglomerate to mudstone, the relative abundances of conglomerate, sandstone, and mudstone (Appendix A) in an outcrop are similar throughout the Cerrillos-Lamy area (about 2/73/25 in the lower unit, and 5/40/55 in the upper unit). It is therefore not possible to delineate and contour areas in either unit within the Cerrillos-Lamy area based on overall coarseness. Similarly, it is not possible to contour the Cerrillos-Lamy area based on maximum clast sizes. Stearns (1943) noted that the maximum-size clasts in the strata of the Galisteo

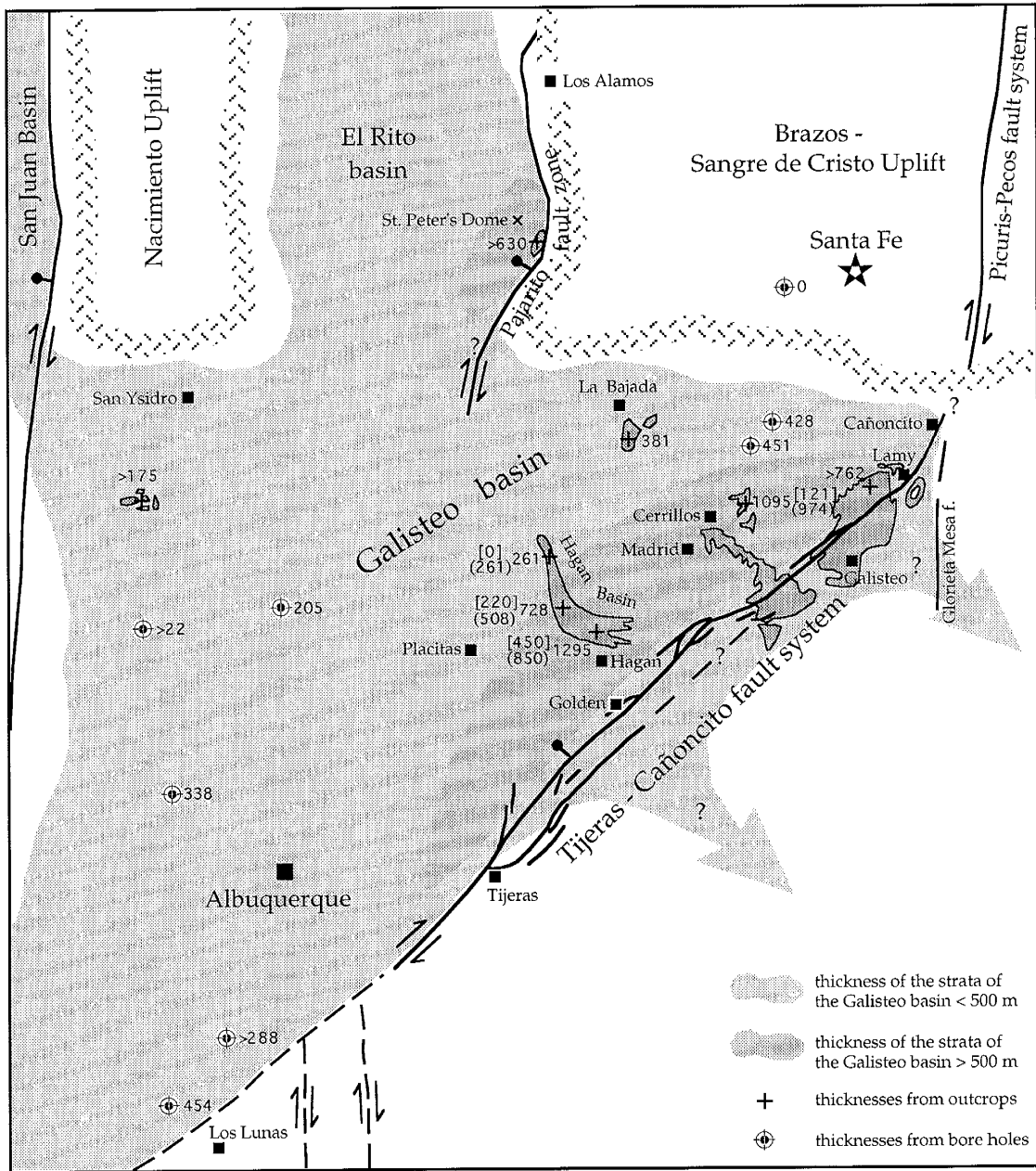


Figure 1-3. Thicknesses (in meters) of strata of the Galisteo basin. In addition to total thickness of undifferentiated strata of the Galisteo basin, local thickness of the lower unit [brackets] and upper unit (parentheses) are indicated. Bore hole data are compiled from Lozinsky (1988; 1994). Outcrop thicknesses are from Stearns (1943), Gorham (1979), and Cather (1992).

basin in the Cerrillos-Lamy area are generally similar in size and composition to those in the Hagan Basin. The exposures near St. Peter's Dome are considerably coarser than in the Hagan Basin and the Cerrillos-Lamy area, and are more proximal piedmont deposits (Cather, 1992).

PALEOCURRENTS

Treatment of data

Bedding in the Cerrillos-Lamy area has been tilted up to 120° by subsequent deformation, so paleocurrent indicators must be restored to their original orientations. It is assumed that bedding was rotated about a single horizontal axis to its present orientation. The effect of tilting on the paleocurrent direction is removed, therefore, by restoring bedding to horizontal with one rotation about the line of strike.

Most paleocurrent measurements in the lower unit in the Cerrillos-Lamy area are of planar cross-stratification, although trough cross-stratification was also noted (Appendix A). The most abundant paleocurrent indicator in the upper unit is planar cross-stratification, though pebble imbrication, trough cross-stratification, and ripple cross-laminations are also locally present (Appendix A). Rose diagrams include all paleocurrent indicators in an area of exposure. Resultant vector means in each unit were calculated for high-order paleocurrent indicators (pebble imbrication and trough cross-stratification), for low-order paleocurrent indicators (planar cross-stratification and ripple cross-laminations), and for all paleocurrent indicators.

Several potential sources of paleocurrent variance are identified. There is a natural variation inherent in the formation of paleocurrent indicators (Allen, 1967; Smith, 1972). Some paleocurrent variance arises from the procedure of rotating the paleocurrent indicator to its original depositional orientation. The assumption that bedding was rotated about a single horizontal axis is certainly not infallible, and the possibility of rotations about other axes has

the potential to radically alter the restored paleocurrent direction. Finally, variance in paleocurrent rose diagrams may arise by grouping paleocurrents by geographic location, not stratigraphic position. Each paleocurrent rose diagram potentially reflects paleoflow of interfingering axial deposits with deposits that prograded transverse to the basin axis.

Lower unit

Paleocurrent directions in the lower unit are highly variable (Figs. 1-4 and 1-5). Most of these paleocurrent indicators are planar cross-beds, though three measurements from exposures about 3 km east of Cerrillos are of trough cross-stratification that record paleoflow toward 308°, 330°, and 341°. The mean vector of three measurements of trough cross-stratification (326°) is considerably different than the mean vector of 5 measurements of planar cross-stratification (133°). Paleocurrents are most variable adjacent to the Tijeras-Cañoncito fault system. Rose diagrams of paleocurrents from these areas are polymodal, recording significant paleoflow in all directions. The strongest components of paleoflow were to the northeast and southwest, sub-parallel to the fault system. The same trends are evident at a larger scale (Fig. 1-6). In the Cerrillos-Lamy area, paleocurrent rose diagrams in the lower unit are polymodal, with large components of paleoflow sub-parallel to the fault system. In the Hagan Basin, paleoflow in the lower unit was dominantly to the south-southeast (Gorham, 1979).

Figure 1-4. Paleocurrent rose diagrams of the lower unit in the Cerrillos-Lamy area. Rose diagrams are roughly scaled to represent the number of measurements. Black part of rose diagrams represents measurements where exposure afforded good three-dimensional control on the orientation of the paleocurrent indicator. Gray part of rose diagrams represents measurements from poorer exposure, where each measurement records only a component of the paleocurrent direction.

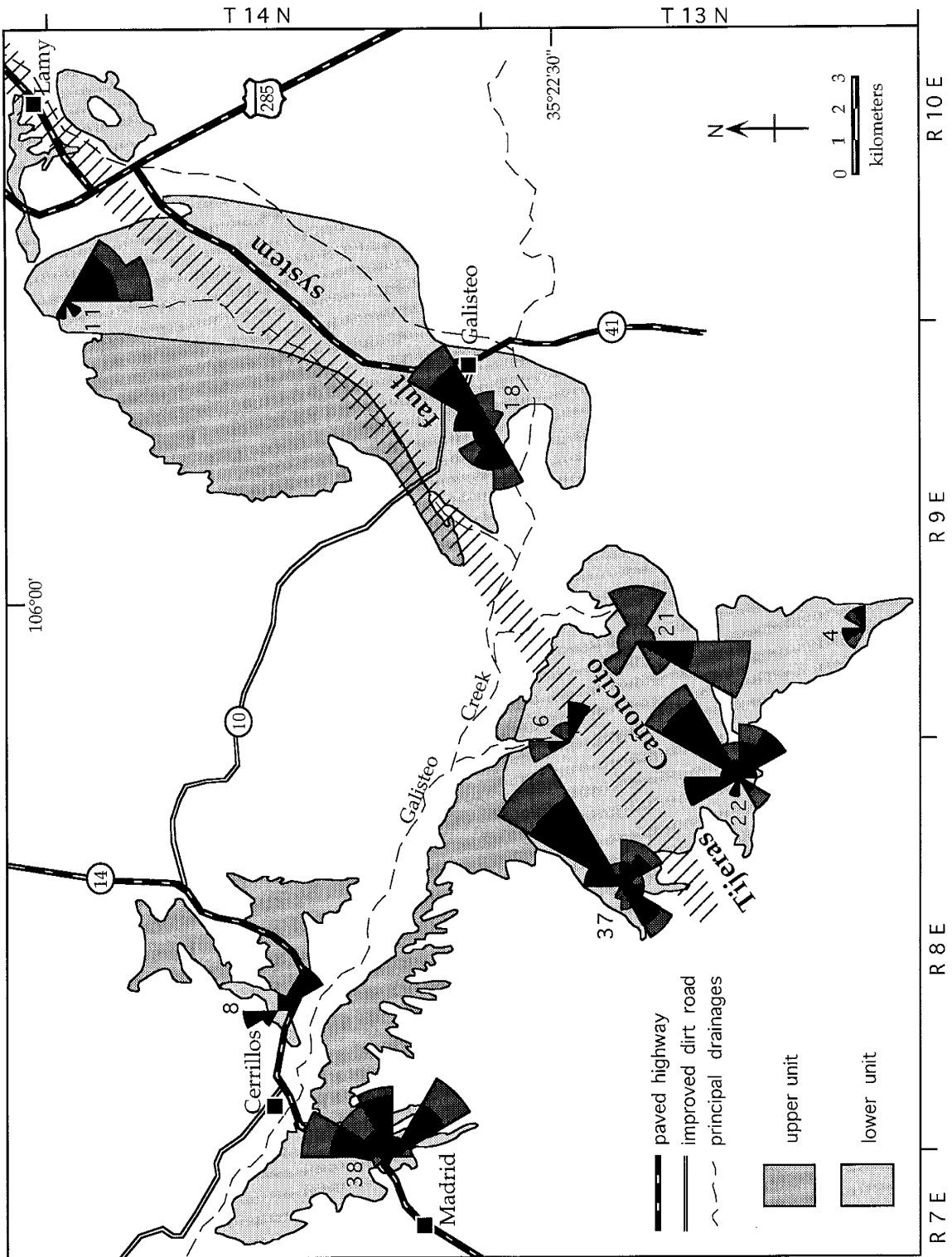
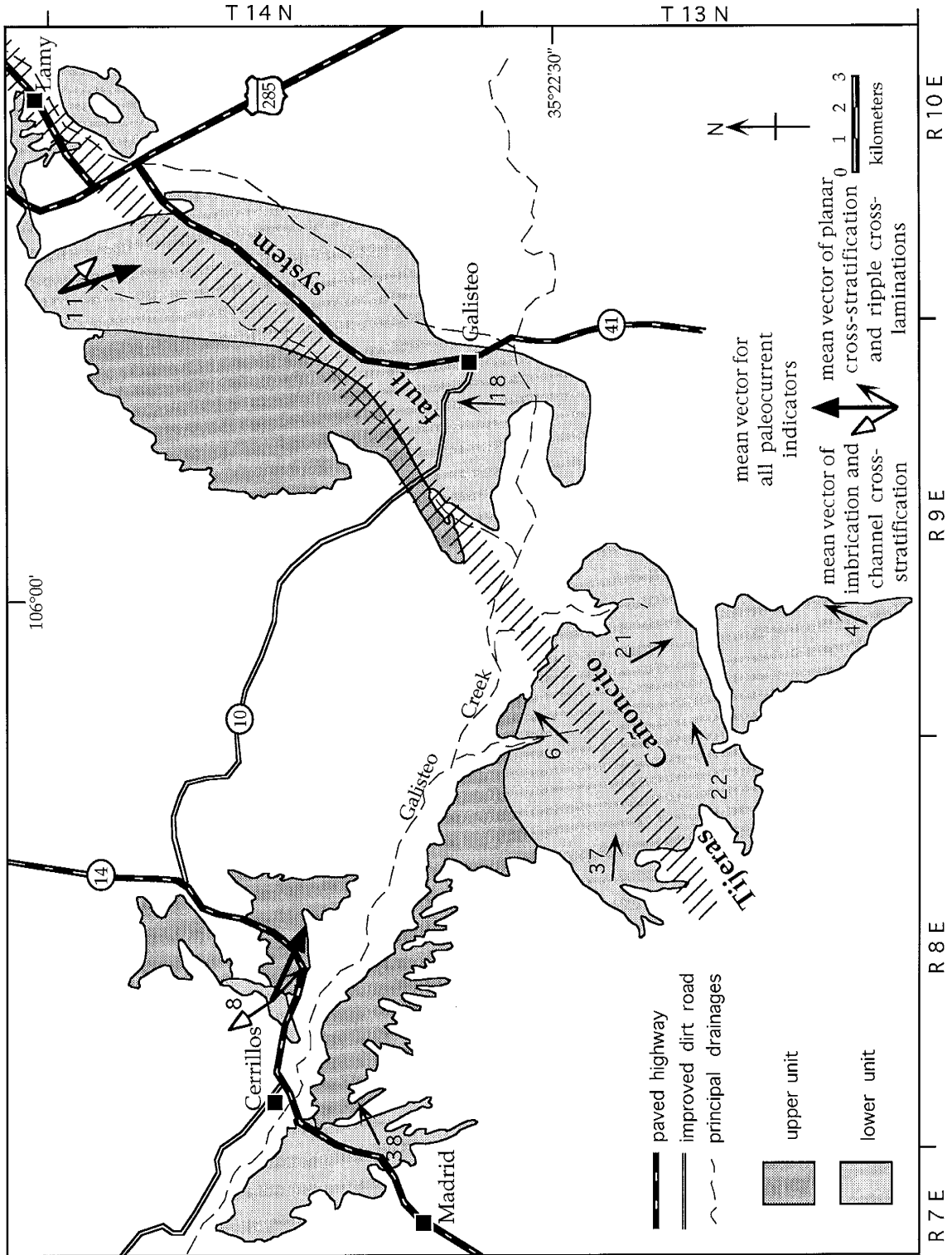


Figure 1-5. Resultant vector means of paleocurrents in the lower unit in the Cerrillos-Lamy area.



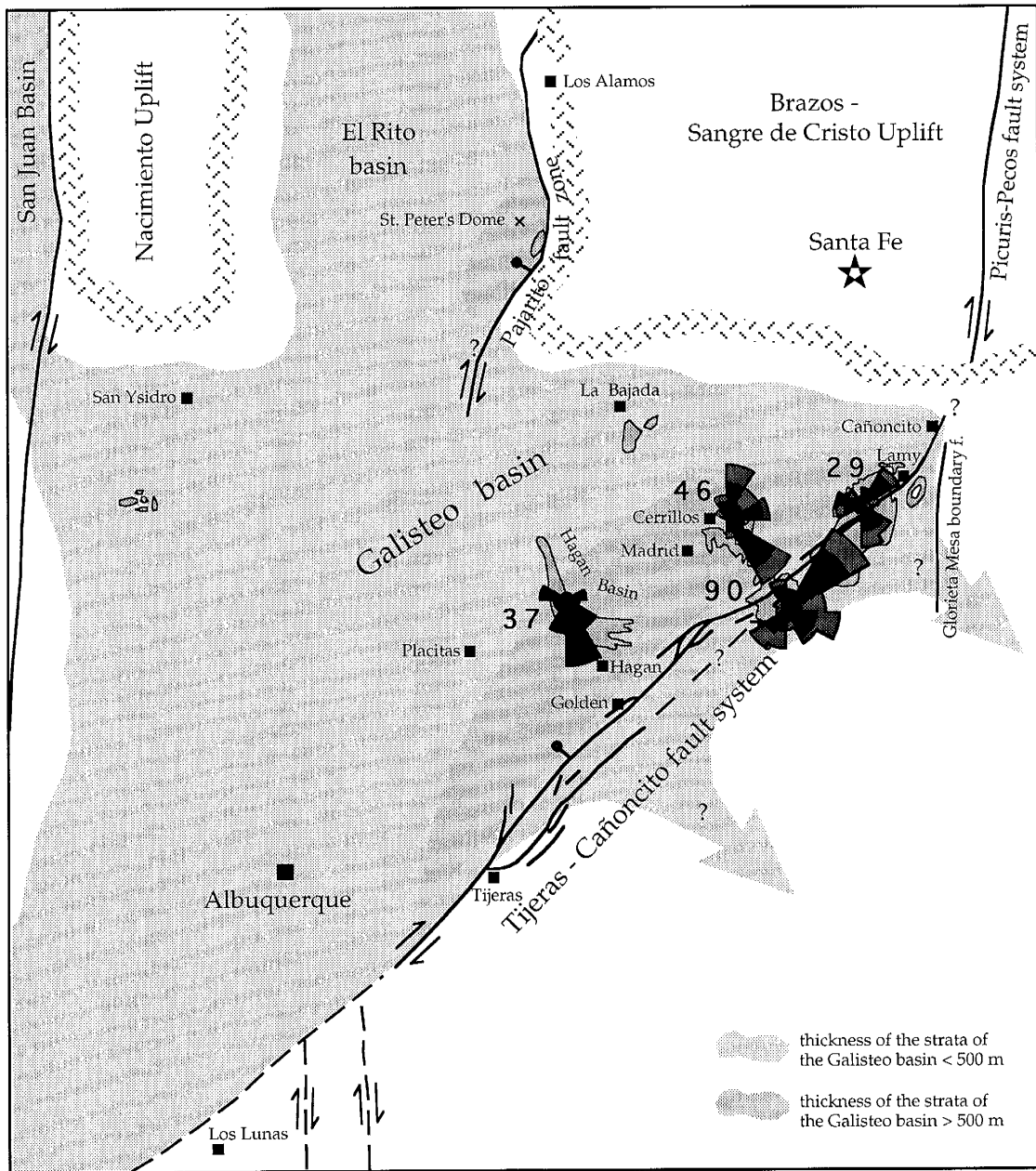


Figure 1-6. Synthesis of all paleocurrent data in the lower unit of the Galisteo basin. Data in the Hagan Basin are from Gorham (1979).

Upper unit

Paleocurrent directions in the upper unit are also highly variable (Fig. 1-7). Paleocurrent indicators record considerable paleoflow in almost all directions. Despite high variability in individual paleocurrent directions, computed vector resultants are quite similar, with net paleoflow generally to the east and east-northeast (Fig. 1-8). A significant deviation from this trend is in exposures about 4 km west of the village of Galisteo, where paleocurrent indicators record westward paleoflow. Acknowledging the paucity of high-order paleocurrent indicators, there is general similarity between the mean vector resultants of high-order and low-order paleocurrent indicators. At a larger scale, paleocurrent directions in the Cerrillos-Madrid area are highly variable, but record a general eastward paleoflow (Fig. 1-9). Immediately adjacent to the Tijeras-Cañoncito fault system, paleoflow was more to the southeast. In the Hagan Basin, paleoflow was predominantly to the southeast and south (Gorham, 1979). A rose diagram of paleocurrents from the exposure near St. Peter's Dome is bimodal, with paleoflow to the south-southeast and northwest (Cather, 1992).

Figure 1-7. Paleocurrent rose diagrams of the upper unit in the Cerrillos-Lamy area. Rose diagrams are roughly scaled to represent the number of measurements. Black part of rose diagrams represents measurements where exposure afforded good three-dimensional control on the orientation of the paleocurrent indicator. Gray part of rose diagrams represents measurements from poorer exposure, where each measurement records only a component of the paleocurrent direction.

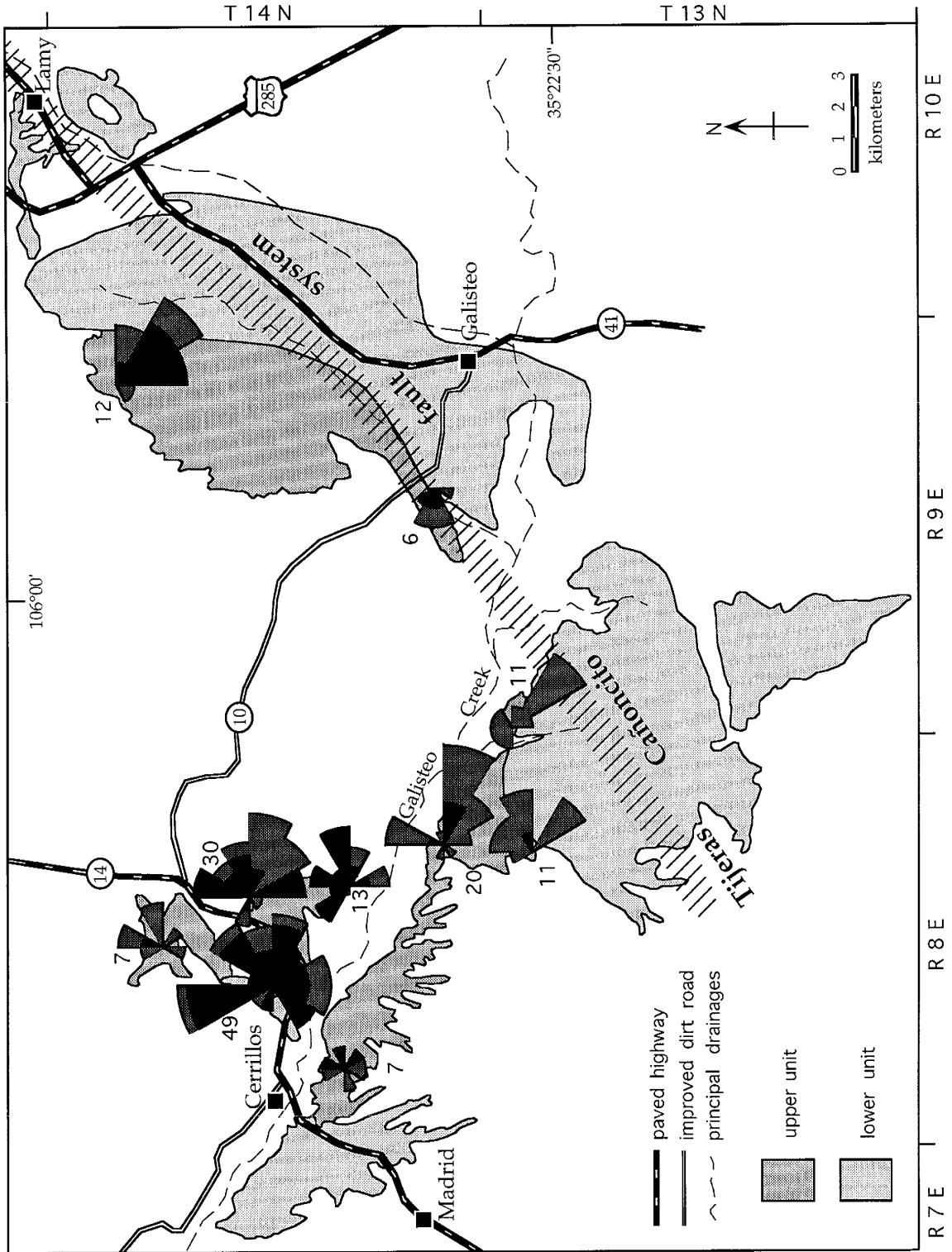
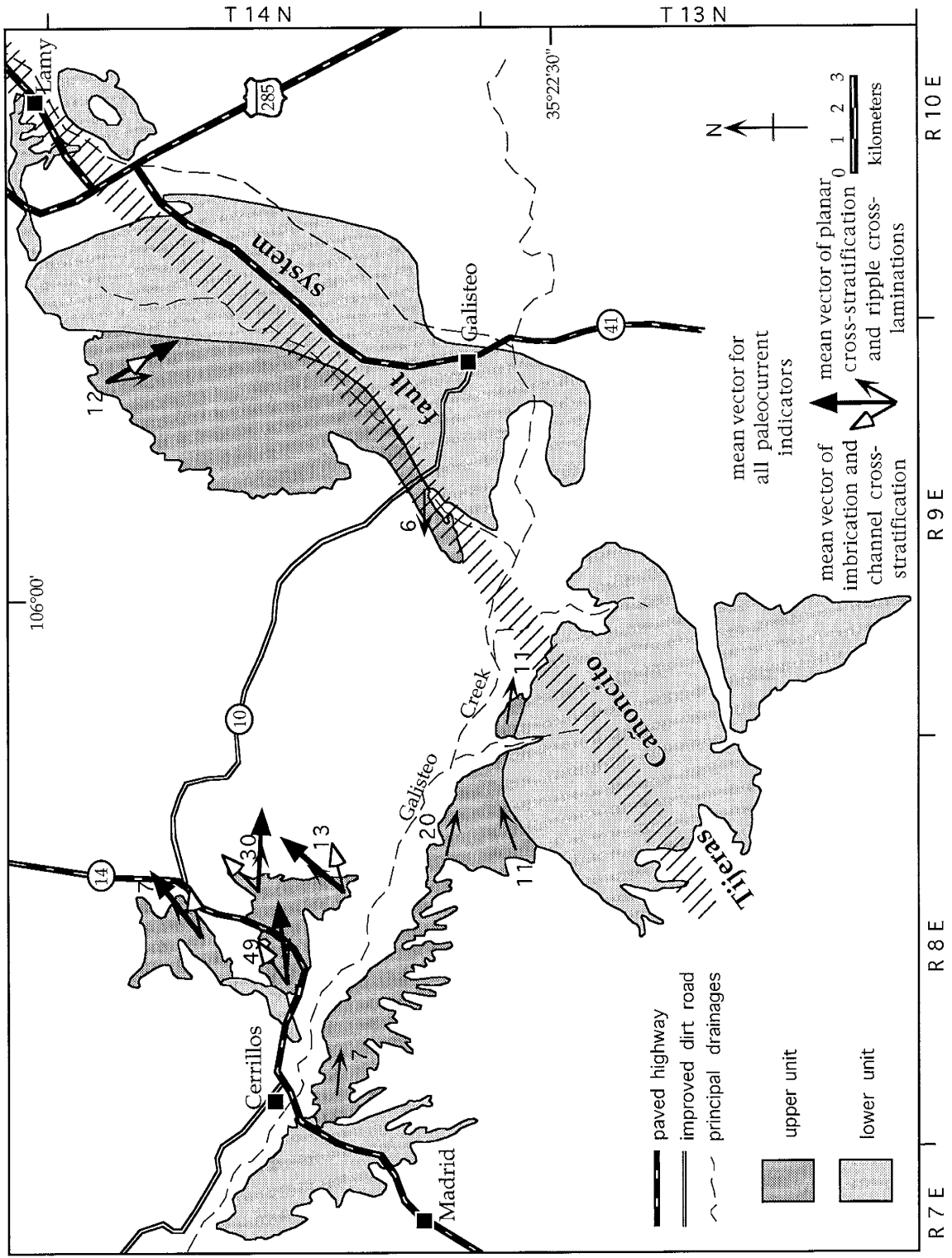


Figure 1-8. Resultant vector means of paleocurrents in the upper unit in the Cerrillos-Lamy area.

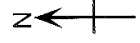


T 14 N
T 13 N
R 10 E
R 9 E
R 8 E
R 7 E

— paved highway
— improved dirt road
- - - principal drainages

■ upper unit
■ lower unit

mean vector for all paleocurrent indicators
mean vector of imbrication and channel cross-stratification
mean vector of planar cross-stratification and ripple laminations



0 1 2 3
kilometers

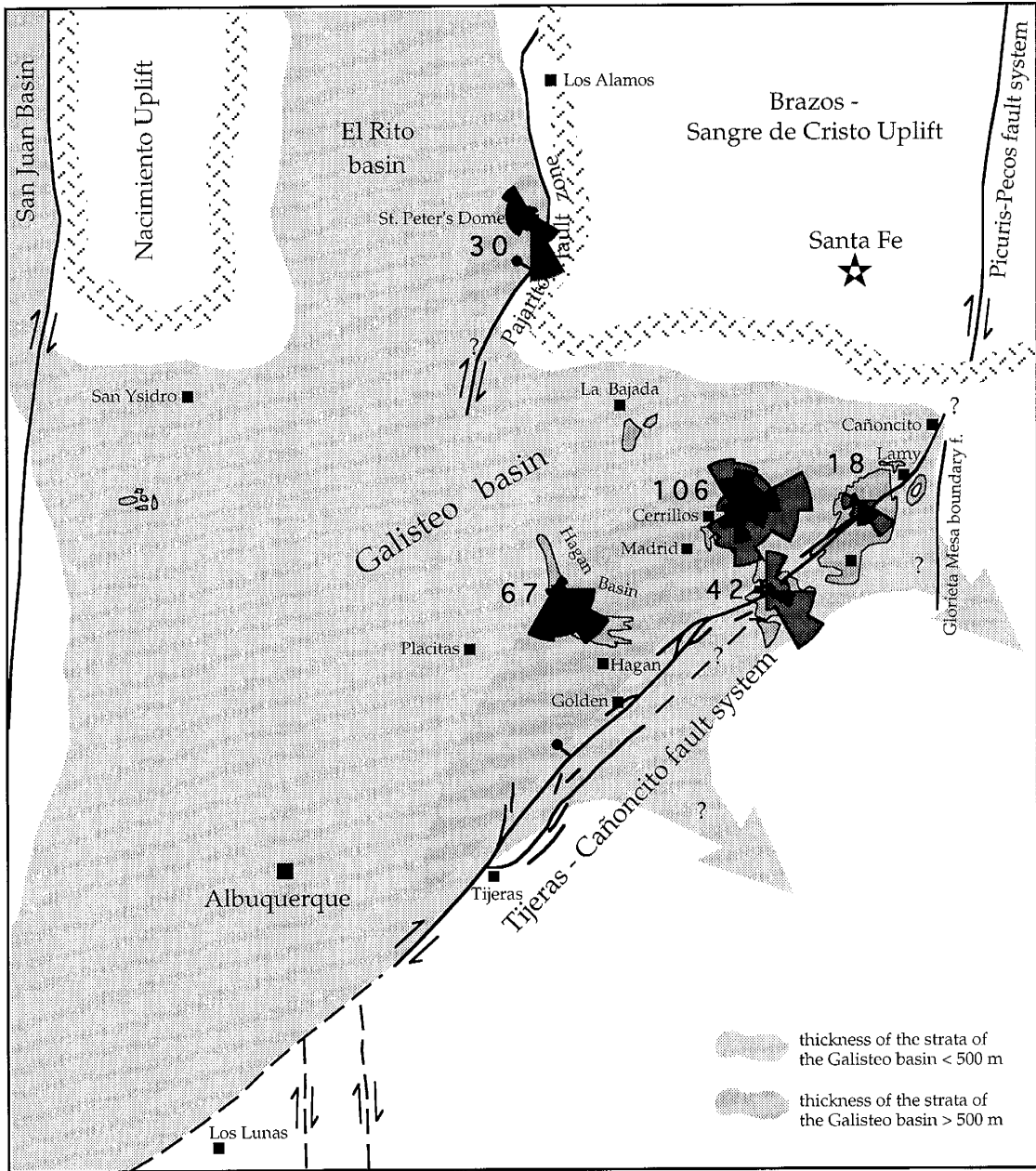


Figure 1-9. Synthesis of all paleocurrent data in the upper unit of the Galisteo basin. Data in the Hagan Basin are from Gorham (1979); data from exposures near St. Peter's Dome are from Cather (1992).

DISCUSSION AND CONCLUSIONS

Although there is clearly a progressive thickening of the strata of the Galisteo basin towards the Tijeras-Cañoncito fault system, thickness data alone do not preclude continuation of the basin southeast of the structure. The southeast side of the Tijeras-Cañoncito fault system is currently a structural high, so the thickness of strata removed by uplift and erosion subsequent to the Eocene is unknown.

The paleocurrents and sedimentology of the strata of the Galisteo basin provide additional insight into the development of the basin. Paleocurrent directions in both units are highly variable in the Cerrillos-Lamy area. Paleocurrent indicators from exposures of the upper unit on the southeast margin of the fault zone record paleotransport to the west, and paleocurrent indicators in the lower unit adjacent to the fault system record large components of paleotransport parallel to the fault system, both to the northeast and to the southwest. About 3 km east of Cerrillos, the computed vector resultants of high-order paleocurrents are roughly opposite that of low order paleocurrents. These observations are consistent with a basin axis in the Cerrillos-Lamy area. Bimodal and polymodal paleocurrent rose diagrams probably reflect paleoflow of interfingering axial deposits and deposits that prograded transverse to the basin axis. Geographic and stratigraphic variations in paleocurrents in the Hagan Basin suggest that the Hagan area was also near or within the basin axis (Gorham and Ingersoll, 1979). Thus, it appears that the basin axis paralleled the Tijeras-Cañoncito fault system.

Three lines of evidence suggest that the fault system was a control on subsidence and sediment dispersal. First, the axis of the basin was sub-parallel to the fault system. This is indicated by stratigraphic thickening adjacent to the fault system, and by highly variable paleocurrent directions adjacent to the fault system in both the Hagan and Cerrillos-Lamy areas. Second, there are large components of fault-parallel paleoflow in the lower unit in exposures adjacent to the fault system near Galisteo Creek. Paleoflow was both to the northeast and to the southwest, recording fault control on sediment dispersal. Third, the

Tijeras-Cañoncito fault system is the only major fault system identified in the area, and is the most plausible structural control on Paleogene extensional subsidence.

The southeast block of the Tijeras-Cañoncito fault system in the Laramide was not a major topographic high and significant source of sediment during deposition of the strata of the Galisteo basin. The lithologies in both units are similar throughout the Cerrillos-Lamy area. This demonstrates that coarse, proximal piedmont deposits did not prograde northwestward from the southeast fault block. Strata of the lower unit and Cretaceous strata currently exposed on the southeast fault block preclude major uplift and denudation of the southeast fault block during the Laramide orogeny. Although the fault system appears to have controlled a large part of the extensional subsidence of the basin, the fault system was not the southeastern boundary of the basin. The presence of Paleogene strata on the southeast fault block, the lack of scarp-derived deposits, and the scarcity of northwesterly paleoflow adjacent to the fault system suggest the fault system was within the basin.

Because the southeast block was not emergent, the maximum displacement magnitude of the Paleogene dip-slip component on the Tijeras-Cañoncito fault system is constrained to approximately the stratigraphic thickness of the strata of the Galisteo basin (~1300 m, northwest-side-down). This is a maximum estimate because the thickness of the strata of the Galisteo basin deposited on the southeast fault block is unknown. Though sedimentological study of strata of the Galisteo basin offers no constraints on the magnitude of horizontal displacement, the strike-slip component may have been substantial, as indicated by Laramide-age slickenside striations from other parts of the fault system that record a dominant component of strike-slip motion (Abbott and Goodwin, 1995; Abbott et al., Part III). Structures indicative of right-lateral motion within the fault system and extensional subsidence of the Galisteo basin to the northwest support Cather's (1992) hypothesis that the Tijeras-Cañoncito fault system accommodated right-lateral transtensional motion in the Paleogene.

In summary, stratigraphic thickening and highly variable paleocurrent directions in the strata of the Galisteo basin adjacent to the Tijeras-Cañoncito fault system suggest the fault

system was a significant control on basin subsidence and sedimentation. The presence of Paleogene strata on the southeast fault block, the scarcity of northwest paleoflow, and the lack of scarp-derived deposits indicate that the Tijeras-Cañoncito fault system was not the southeastern boundary of the Galisteo basin. The fault system appears to have operated within the basin. Because the southeast block was not emergent, the maximum displacement magnitude of the Paleogene dip-slip component on the Tijeras-Cañoncito fault system is constrained to approximately the stratigraphic thickness of the strata of the Galisteo basin (~1300 m, northwest-side-down).

Part II

A SPECTACULAR EXPOSURE OF THE TIJERAS FAULT,
WITH EVIDENCE FOR QUATERNARY MOTION

John C. Abbott
and
Laurel B. Goodwin

Department of Earth and Environmental Science
New Mexico Tech

in press

1995 New Mexico Geological Society Guidebook 46

ABSTRACT

The regionally extensive Tijeras-Cañoncito fault system comprises a number of northeast-striking, sub-vertical faults, including the Tijeras fault. Slickenlines on minor fault surfaces within the fault zone exhibit a wide range in orientation and record a complex history of strike-slip, oblique-slip, and dip-slip motion on the fault system. The oldest documented movement is Laramide (Late Cretaceous - early Tertiary) in age. A recently discovered streamcut provides the best known exposure of the Tijeras fault. It reveals a strongly but heterogeneously deformed zone more than 160 meters wide, within which Proterozoic, Pennsylvanian, Permian, and Oligocene(?) age rocks are faulted. Quaternary(?) surficial deposits are locally faulted. The streamcut includes a population of minor faults that are interpreted as right-lateral synthetic Riedel shears, which is consistent with Laramide-age deformation. Neogene deformation is indicated by extreme brecciation of an Oligocene(?) porphyritic intrusive rock and by slickenlines that suggest left-lateral strike-slip motion. Left-lateral strike-slip motion is consistent with the development of the Rio Grande rift in the Neogene. Quaternary(?) activity is recorded in the streamcut by a fault that juxtaposes Quaternary(?) surficial deposits against an Oligocene(?) porphyritic intrusive rock; this fault does not offset an overlying Holocene(?) imbricated gravel deposit. The length of the Tijeras-Cañoncito fault system, the width of the fault zone, and the intense deformation within the Tijeras fault zone, all suggest substantial post-Pennsylvanian displacement on the fault system. Slickenside striae indicate that movement within the fault system was dominantly strike-slip.

INTRODUCTION

The Tijeras-Cañoncito fault system

The Tijeras-Cañoncito fault system comprises a number of northeast-striking, sub-vertical faults, including the Tijeras, Guitierrez, San Lazarus, Los Angeles, and Lamy faults. The system is regionally extensive; it has been mapped for more than 80 km from Kirtland Air Force Base on the southwest (about 16 km southeast of Albuquerque) to the Cañoncito area on the northeast (about 20 km south of Santa Fe). The fault system may continue southwestward into the Rio Grande rift as the Tijeras accommodation zone, one of several places in the rift where the sense of asymmetry of half grabens reverses (Russell and Snelson, 1990; 1994; May and Russell, 1994), or it may link with the north-striking faults that bound the Rio Grande rift on the east. Following Lisenbee et al. (1979), Woodward (1984), and Maynard et al. (1990), we prefer the name "Tijeras-Cañoncito fault system" over "Tijeras fault zone" when referring to the entire group of faults. Both names are entrenched in the literature and are used synonymously. We prefer "Tijeras-Cañoncito fault system" because it approximately locates the structure and distinguishes it from the Tijeras fault, which is only part of the system.

The Tijeras-Cañoncito fault system has a history of recurrent motion. Slickenlines on minor fault surfaces record strike-slip, oblique-slip, and dip-slip motion (Abbott et al., Part III). Lisenbee et al. (1979) suggested the fault system was active in the Proterozoic and in the Pennsylvanian, but unequivocal evidence of such activity is lacking. The oldest documented movement on the fault system is Laramide (late Cretaceous - early Tertiary) in age (Abbott et al., 1995). Lisenbee et al. (1979) also documented offset of colluvium of probable Quaternary age, indicating reactivation of the fault system in the Quaternary. All deformation along the Tijeras-Cañoncito fault system has been brittle; there is no evidence of ductile shearing at any time in its history (Abbott et al., Part III).

The Tijeras-Cañoncito fault system is poorly exposed along much of its length. There are, however, two locations that offer excellent exposure where the internal character of the zone can be directly observed and offset of surficial deposits is apparent. The first locality is a roadcut on westbound I-40 in Tijeras Canyon. It is here that Lisenbee et al. (1979) documented movement of probable Quaternary age: brecciated Proterozoic Tijeras greenstone (Kelley and Northrop, 1975) is in fault contact with unconsolidated colluvium. Though no paleontologic or radiometric dates have been obtained, the colluvium is probably Pleistocene in age (B. Harrison and D. Love, personal commun., 1994), and thus records Pleistocene and/or Holocene activity. The apparent displacement is northwest-side-down, although there are no constraints on either the magnitude of slip or the true slip direction. The rest of the exposed fault zone in Tijeras Canyon is composed of intensely brecciated Proterozoic greenstone and gneiss (Kelley and Northrop, 1975).

The second locality is a recently discovered streamcut, which is the focus of this paper. The exposure lies roughly midway along the Tijeras-Cañoncito fault system near the village of Golden. The arroyo containing the streamcut intersects state route NM-14 about 6.5 km south of Golden in T12N, R6E (Fig. 2-1). The exposure is located only tens of meters downstream of the roadside. The stream has incised a channel generally 1-3 m deep, exposing a fault zone more than 160 m wide in a cross-section transverse to the strike of the Tijeras fault. When discovered in late summer 1994, the exposure appeared very fresh, and it seems likely that the exposure was created or enlarged during that summer. On subsequent visits to the site in the months that followed, it was evident that modern stream deposits were steadily aggrading and the exposure was beginning to be covered. The streamcut provides the most spectacular and informative known exposure of the Tijeras fault.

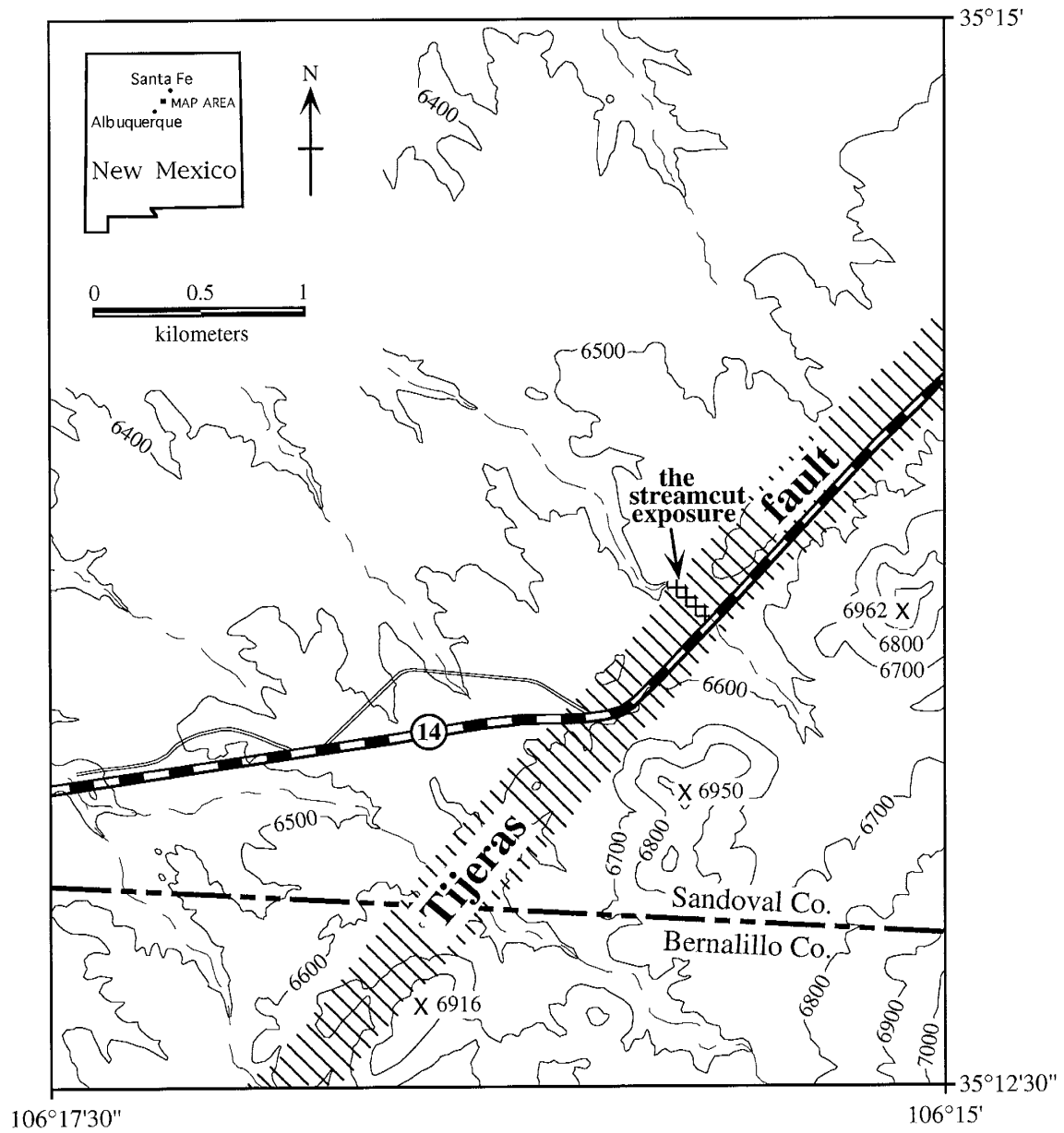


Figure 2-1. Location of the streamcut exposure. The area shown is in T12N, R6E on the Sandia Park U.S.G.S. 7.5' topographic quadrangle.

Regional geology

Proterozoic basement rocks exposed in the vicinity of the Tijeras-Cañoncito fault system are coarse crystalline plutonic rocks and greenschist- to amphibolite-grade metamorphic rocks (Lambert 1961; Huzarski, 1971; Kelley and Northrop, 1975; Connolly, 1982; Vernon, 1986). The basement rocks are overlain by up to several thousand meters of Upper Paleozoic and Mesozoic sedimentary strata (Kelley and Northrop, 1975). These beds record a Late Pennsylvanian - Early Permian orogenic event associated with formation of the Ancestral Rocky Mountains (Baars, 1982; Beck and Chapin, 1991), followed by multiple Mesozoic transgressions and regressions (Molenaar, 1977; 1983). Renewed tectonic activity during the Late Cretaceous - early Tertiary Laramide orogeny resulted in high-angle faulting, and the formation of basement-cored uplifts and associated intermontane basins in north-central New Mexico (Chapin and Cather, 1981; Chapin and Nelson, 1986; Martinez, 1989; Cabezas, 1991; Cather, 1992). A significant component of right-lateral strike-slip movement occurred on north-striking faults during the Laramide orogeny (Chapin and Cather, 1981; Hamilton, 1981; Cather, 1992; Karlstrom and Daniel, 1993). A period of relative tectonic quiescence marked by widespread volcanic and igneous activity followed Laramide deformation (Stearns, 1953; Cather, 1989). A shallow intrusive center, the San Pedro - Ortiz porphyry belt, was emplaced in and around the Tijeras-Cañoncito fault system in the Oligocene (Bachman and Mehnert, 1978; Woodward, 1984; Maynard et al., 1991). From the Miocene through the Holocene, the region accommodated significant east-west extension with formation of the north-trending Rio Grande rift (Keller and Cather, 1994). The rift appears to have developed with a small component of left-lateral motion (Kelley, 1982; Chapin and Cather, 1994; Lewis and Baldrige, 1994; Salyards et al., 1994).

Terminology of fault rocks and minor faults

The Tijeras fault, as exposed by the streamcut, is a zone more than 160 m wide of brittlely deformed bedrock. We follow Sibson (1977) in subdividing incohesive cataclastic rocks into fault breccia and fault gouge. In fault breccia, visible fragments of the parent rock comprise at least 30% of the rock mass, whereas fault gouge contains less than 30% visible fragments. Both breccia and gouge locally exhibit a strong fabric. In keeping with Chester et al. (1985), we refer to this fabric as a cataclastic foliation.

Minor faults referred to herein are mesoscopic surfaces marked by a discernible clay fault gouge, fault slickenside surface, and/or lithologic discontinuity. Fault gouge is abundant in the most intensely deformed part of the fault zone (units 1-19 of Appendix B). The gouge typically is considerably lighter in color than the wall rocks from which it presumably was derived. It generally occurs in planar to curvilinear zones less than a few centimeters wide. In the strongly deformed units, gouge zones anastomose around lens-shaped pods of somewhat less deformed material. Fault slickensides are only present in less deformed bedrock near the margin of the fault zone. We follow Fleuty (1975) in defining a fault slickenside as a polished and commonly, though not invariably, striated brittle shear surface. Slickenside striae are linear structures on a slickenside that form by friction parallel to the direction of movement. In a few instances, the sense of movement can be deduced from structures developed on the fault slickenside. The criteria we used to determine the sense of shear on a fault slickenside are described by Petit (1987).

THE STREAMCUT EXPOSURE OF THE TIJERAS FAULT NEAR GOLDEN

Bedrock geology

The geology of the streamcut is described in a detailed log measured from southeast to northwest (Appendix B). Thicknesses given in the log reflect the true thicknesses of each unit measured transverse to the strike of the Tijeras fault (taken to be 045°, Emerick, 1950), not the apparent thickness in the streamcut. The exposure can be subdivided into three parts based on the intensity of deformation.

The first 92.9 m of the log (the upstream, southeastern end) covers the most extensively deformed section (units 1-19), wherein rocks of many different ages and lithologies have been juxtaposed and locally mixed (Fig. 2-2). Lithologies in this section include: Proterozoic Cibola gneiss, interbedded shale and thin limestone beds interpreted to be late Paleozoic in age, limestone of the Pennsylvanian Madera Group, carbonate-rich sandstone interpreted to be the San Ysidro Member of the Permian Yeso Formation, and an Oligocene(?) porphyritic intrusive rock (Fig. 2-3). By association with other porphyritic intrusive rocks in the nearby San Pedro - Ortiz porphyry belt (Bachman and Mehnert, 1978; Maynard et al., 1990), the porphyritic intrusive rock in the fault zone is probably Oligocene in age. The rocks in this section are so intensely brecciated that field identification of the parent material is locally impossible (e.g., units 4, 10, and 17, Appendix B). Unidentifiable units may be zones in which different rocks have been tectonically mixed. Mixing is clearly evident in unit 8 (Figs. 2-2a and 2-4) where a block of limestone of the Madera Group is set in a matrix of strongly brecciated Cibola gneiss. Also in unit 8, faulting mixed Pennsylvanian(?) black shales with Cibola gneiss. The strongly brecciated units in the first section of the fault zone typically exhibit a foliation defined by innumerable slip surfaces and anastomosing zones of fault gouge. The foliation is sub-vertical and strikes northeast, sub-parallel to the trend of the Tijeras-Cañoncito fault system. Sedimentary bedding and relict gneissic foliations are generally not discernible in the first

Figure 2-2. Illustrations of selected parts of the streamcut exposure. Views are to the northeast. Detailed descriptions of each unit are provided in Appendix 1. (a) Southeast end of the streamcut exposure. Note Quaternary(?) fault between units 1 and 3 which places Quaternary sandy gravel and carbonate-rich mottled clay against Oligocene(?) porphyry (see Fig. 2-6). This view shows apparent dip; the true dip of the faults and cataclastic foliation is sub-vertical. Note the Holocene(?) imbricated gravel overlies the faults and foliated domains, and is not itself deformed. (b) Zone of tectonic mixing. Unit 8 is a dramatic example of tectonic mixing, wherein a limestone knocker of the Pennsylvanian Madera Group is set in a matrix of strongly brecciated Proterozoic Cibola gneiss. Black shales are locally mixed with Cibola gneiss.

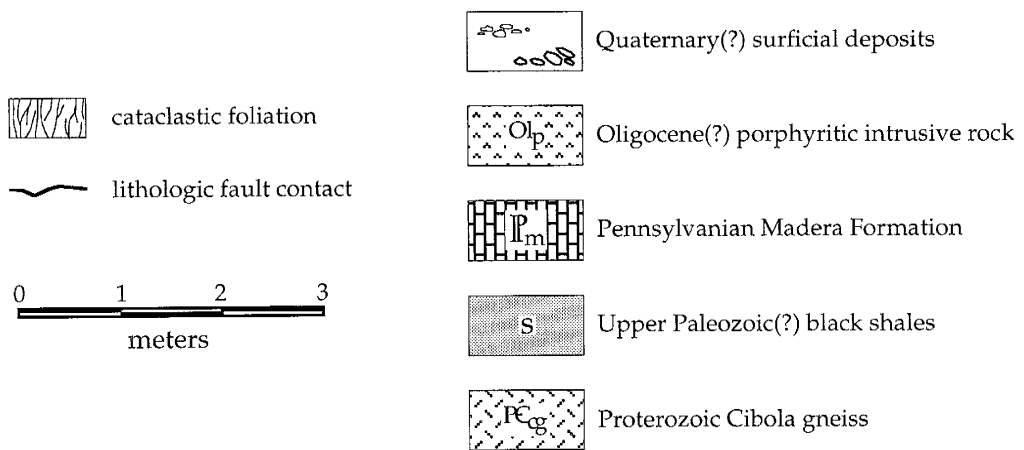
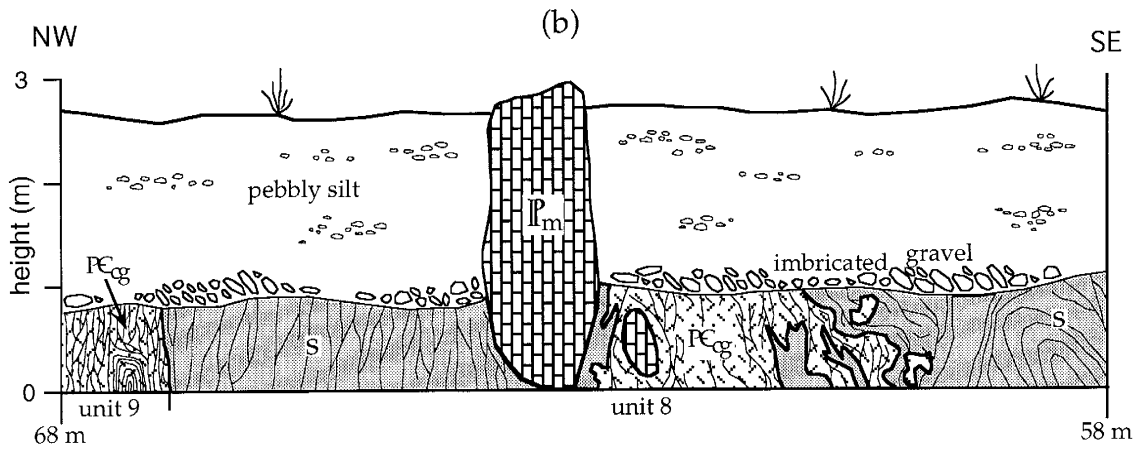
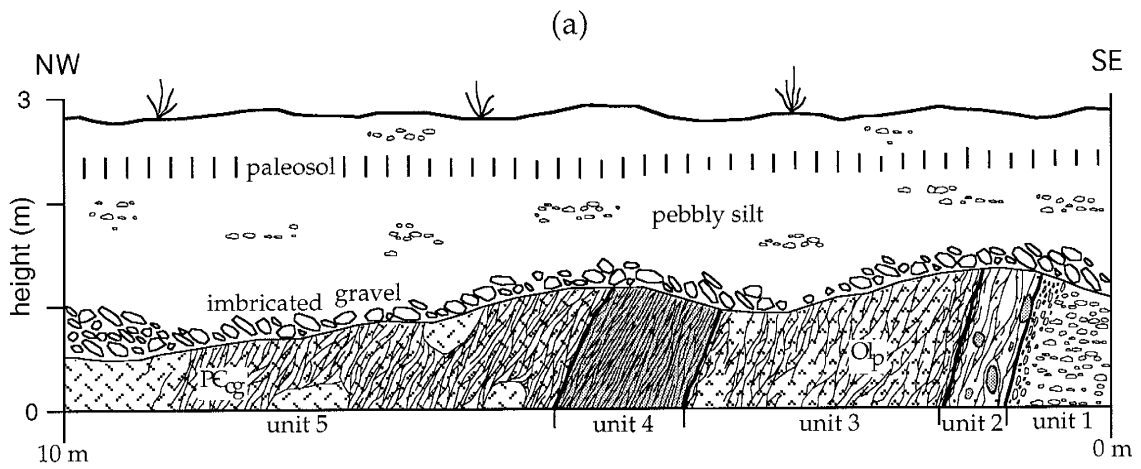




Figure 2-3. Oligocene(?) porphyry of unit 16 overlain by Holocene(?) imbricated gravel surficial deposit. The porphyry is strongly brecciated, recording Oligocene(?) and/or Neogene faulting. Somewhat more intact porphyry is evident at right.



Figure 2-4. Tectonic mixing is illustrated in unit 8. A knocker of limestone from the Pennsylvanian Madera Group (m) is set in a matrix of brecciated Proterozoic Cibola gneiss (cg). Upper Paleozoic(?) black shales (s) are mixed with Cibola gneiss at far left. All bedrock units are unconformably overlain by a Holocene(?) pebbly silt (ps) surficial deposit. View is to the southwest.

section, except in places where the breccia contains relatively intact blocks on the order of a meter or more in diameter (Fig. 2-5). These blocks are fractured, and shatter easily under the blow of a hammer. No slickensides have been identified in this section of the fault zone.

The next 46.1 m (units 20-26) are characterized by moderate to locally strong deformation of Upper Paleozoic sedimentary rocks. Exposed bedrock units include limestone of the Pennsylvanian Madera Group and sandstone and mudstone of the Permian Abo Formation. Rocks in two small exposures (units 20 and 24) are not readily identifiable, but probably are late Paleozoic in age. Bedding in mudstones and siltstones is completely overprinted by a cataclastic foliation, but bedding is locally preserved in sandstones and invariably preserved in limestones. Unit 25 is a good example of this, and provides clear evidence that deformation is localized in finer-grained rocks. Two exposures of the Madera Group (units 21 and 23), separated by only 14 m, have considerably different bedding orientations, which likely is a consequence of differential rotation of blocks within the fault zone. Although gouge-filled fault zones are numerous in the sandstones, slickensides are uncommon.

The last 23.0 m of the streamcut (units 27-29) is characterized by significantly less deformation than in the previous two sections. The Abo Formation is the only bedrock unit exposed. Bedding is evident in all sandstones and in some mudstones. Bedding orientations are fairly consistent in this section, and are considerably less steep than those upstream. In unit 27, conjugate sets of north-striking, high-angle faults show apparent normal separations, resulting in a series of horsts and grabens. Several gouge zones are present, though the gouge is more silty and less clayey than upstream. The sandstone beds preserve abundant fault slickensides. Major slip surfaces are less abundant downstream. This style of deformation continues downstream for at least another 100 m, but is not included in the descriptive log.

In summary, the bedrock is heterogeneously deformed in a zone more than 160 m wide. Rocks of various ages and lithologies have been juxtaposed, including Cibola gneiss, Upper Paleozoic(?) black shales, limestone of the Madera Group, Abo and Yeso(?) Formations, and an Oligocene(?) porphyritic intrusive rock. Cibola gneiss, Upper Paleozoic(?) black shales, and



Figure 2-5. Brecciated Proterozoic Cibola gneiss of unit 7. Two blocks of relatively more intact gneiss, each about 1 m across, are set in a matrix of strongly brecciated gneiss (under hammer). Gneiss is overlain by unfaulted Quaternary(?) surficial deposits.

limestone of the Madera Group have locally been mixed by faulting. Brittle faulting has locally destroyed sedimentary bedding and original gneissic foliations. Where preserved, bedding is generally steep and sub-parallel to the Tijeras fault, but dips shallowly at the margin and outside of the fault zone. A cataclastic foliation is developed in much of the zone, and its orientation is consistently sub-parallel to the Tijeras fault. Fault slickensides are abundant near the margin of the fault zone.

Surficial deposits

Quaternary(?) surficial deposits overlie the bedrock and are locally disrupted by the Tijeras fault. The surficial deposits are described in some detail as they record Quaternary(?) faulting. Determining the relative ages of all of the surficial units was ambiguous in the main streamcut because faulting has disrupted the section. However, relative ages were confirmed by correlation with undisturbed exposures on the southeast side of the highway.

The oldest surficial deposit is a carbonate-rich mottled clay (unit 2, Appendix B). It is clearly faulted and has been dragged along the fault (Figs. 2-2a and 2-6). It is 0.5 m wide, and contains a strong, northeast-striking, sub-vertical foliation defined by anastomosing white gouge zones and elongate cobbles oriented parallel to the foliation. The unit is mostly clay and silt, and was probably derived largely from a carbonate paleosol horizon exposed on the southeast side of the highway. It also contains several outsized clasts up to 30 cm in maximum diameter, which may have been incorporated from another surficial deposit. The deposit is probably not older than Quaternary in age (B. Harrison and D. Love, personal commun., 1994). A 5-10 cm wide zone of white gouge and strongly brecciated porphyritic intrusive rock separates the carbonate-rich mottled clay unit from adjacent bedrock. The apparent displacement along this fault is southeast-side-down, which is opposite that of the previously documented Quaternary(?) fault in Tijeras Canyon (Lisenbee et al, 1979). No attempt has been made to determine the relative timing of Quaternary(?) faulting in the streamcut area with that in



Figure 2-6. Quaternary(?) fault. The Quaternary(?) sandy gravel (sg, unit 1, Appendix B) is in fault contact with the Quaternary(?) carbonate-rich mottled clay (crmc, unit 2). Unit 2 is in fault contact with a brecciated Oligocene(?) porphyry (Ol_p, unit 3). All are overlain by Holocene(?) imbricated gravel (ig) and pebbly silt (ps) deposits.



Figure 2-7. Apparent Holocene(?) faults. The Holocene(?) imbricated gravel (ig) surficial deposit appears to be offset in two places. At lower right, a large, elongate cobble of the imbricated gravel surficial deposit lies in the plane of a fault in the Proterozoic Cibola gneiss (cg). This cobble may have rotated by faulting. At lower left, about 1.5 m downstream, a fault appears to juxtapose Cibola gneiss (cg) against the imbricated gravel surficial deposit, but excavation showed the gravel was deposited in a channel that truncated the fault. The overlying pebbly silt (ps) and paleosol (A) do not appear to be offset.

Fault slickenside data

The orientations of 62 minor faults from bedrock exposures throughout the streamcut are shown in Figure 2-8 and Appendix C. The orientations of these faults vary widely, but the vast majority are steeply dipping ($>60^\circ$). Three populations of minor faults are identified, none of which are parallel to the orientation of the Tijeras fault ($045^\circ, 90^\circ$). The most pronounced population is sub-vertical, strikes about 060° , and is present throughout the fault zone. Kinematic data from this population along other segments of the Tijeras-Cañoncito fault system indicate right-lateral strike-slip motion (Abbott et al., Part III). Five minor faults in the Oligocene(?) porphyritic intrusive rock contribute to this population. A second population of faults is sub-vertical and strikes north-northeast. Three minor faults in the Oligocene(?) porphyritic intrusive rock contribute to this population. A third population is composed of sub-vertical, northwest-striking faults oriented roughly perpendicular to the general trend of the fault zone. These faults account for about one-fifth of the entire sample of faults. Shear fractures (R criteria of Petit, 1987) on two slickensides that contribute to this population of faults record a dominant component of right-lateral strike-slip motion on the slickenside surface. Twenty of the 62 minor faults contain fault slickensides with well developed slickenside striae (Fig. 2-9). Eighteen of these are from unit 28, near the margin of the fault zone. The pitch (rake) of striae is generally small ($<45^\circ$). The striae record a large component of strike-slip ($\text{pitch} \leq 30^\circ$) and oblique-slip ($30^\circ < \text{pitch} < 60^\circ$) motion, with a subordinate amount of dip-slip ($\text{pitch} \geq 60^\circ$) motion (Fig. 2-10).

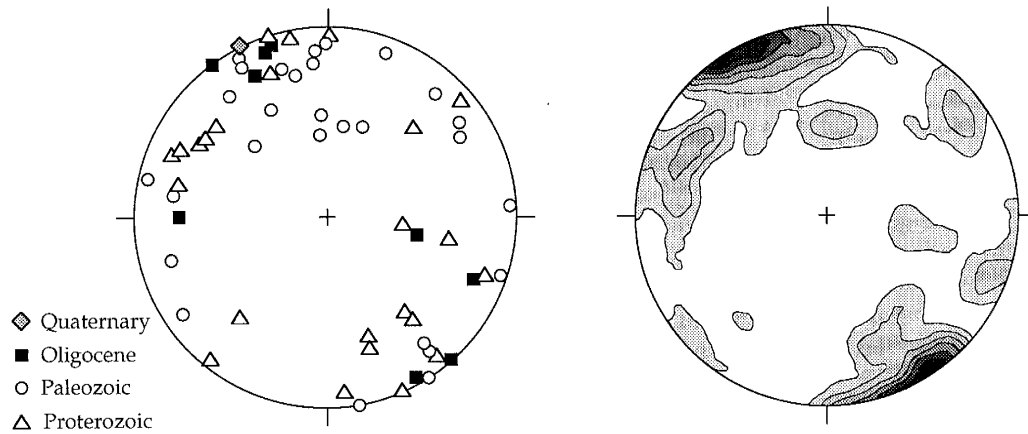


Figure 2-8. Equal area, lower hemisphere projection of poles to 62 minor faults. Most faults dip steeply. Three populations of faults are identified: ENE-striking, NNE-striking, and NW-striking. Open triangles represent faults that cut Proterozoic rocks, open circles represent faults that cut Upper Paleozoic rocks, closed squares represent faults that cut the Oligocene(?) porphyry, and the shaded diamond represents the Quaternary(?) fault in unit 2. Contoured in multiples of random distribution (mrd). White is less than 1 mrd, each subsequent contour represents an increase in one mrd. The data are plotted and contoured using the program and method of Starkey (1977).

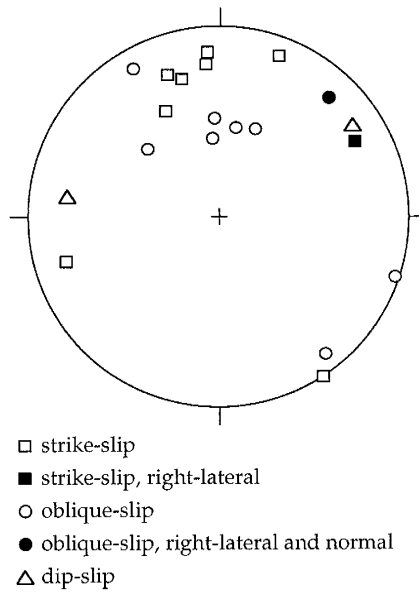


FIGURE 2-9. Equal area, lower hemisphere projection of poles to 20 fault slickensides. Open squares represent strike-slip faults (pitch of striation $\leq 30^\circ$); open circles represent oblique-slip faults ($30^\circ < \text{pitch} < 60^\circ$); open triangles represent dip-slip faults (pitch $\geq 60^\circ$); closed symbols represent faults with a component of right-lateral slip.

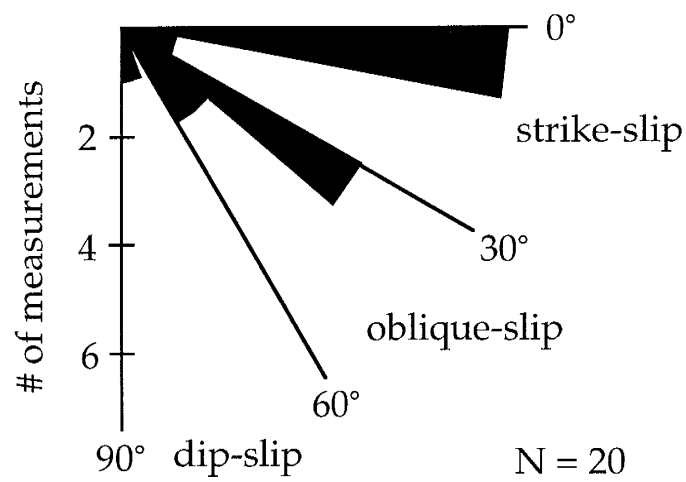


Figure 2-10. Pitches of 20 fault striae from slickenside surfaces near the margin of the fault zone. Each petal is 10°. Most faults record strike-slip ($\text{pitch} \leq 30^\circ$) or oblique-slip ($30^\circ < \text{pitch} < 60^\circ$) motion. Only two slickenside surfaces record dip-slip ($\text{pitch} \geq 60^\circ$) motion.

DISCUSSION

The magnitude of the net displacement accommodated by the Tijeras-Cañoncito fault system has not been determined because no piercing points have been identified. Vertical separations of Upper Paleozoic and Mesozoic strata are generally less than a few hundred meters. Several lines of evidence, however, suggest that there has been significant post-Pennsylvanian displacement along the fault system. First, the fault system is regionally extensive. It has been mapped for about 80 km through Upper Paleozoic and Mesozoic rocks. Though not impossible, it is energetically unfavorable to create such a long structure without accommodating a substantial amount of slip. Second, the fault zone is very wide, which also suggests the possibility of substantial displacement. The Tijeras fault alone is a zone more than 160 m wide of brecciated Proterozoic and Upper Paleozoic rocks. The Guiterrez fault, which parallels the Tijeras fault to the southeast, is also a major fault and may have accommodated as much or more slip than the Tijeras fault. Third, the intensity of deformation within the fault zone also suggests significant slip. Proterozoic, Pennsylvanian, and Oligocene(?) rocks are strongly brecciated within the fault zone. Locally, Proterozoic and Upper Paleozoic rocks are tectonically mixed (Figs. 2-2b and 2-4). These observations suggest substantial post-Pennsylvanian and/or post-Oligocene(?) displacement on the Tijeras-Cañoncito fault system.

The orientations of minor faults and slickenside striae help constrain the sense of motion and timing of deformation in the fault zone. Several populations of minor faults that are distinctly oblique to the trend of the Tijeras fault have been identified. We interpret these populations of minor faults in terms of Riedel shear geometries. The orientation of each population of minor faults suggests a certain sense of movement on the Tijeras-Cañoncito fault system. The timing of deformation is constrained by comparing the sense of movement recorded by rocks of different ages with our current understanding of the tectonic history of north-central New Mexico.

The most pronounced population of minor faults is sub-vertical and strikes about 060°. Slickenlines on these faults record mostly strike-slip and oblique-slip motion (Fig 2-9). This population of minor faults is properly oriented for slip as synthetic right-lateral Riedel shears during right-lateral motion on the Tijeras-Cañoncito fault system (Fig. 2-11a). Their orientations are inconsistent with Riedel shears developed during left-lateral motion. East-west to northeast-southwest shortening during the Laramide orogeny would have favored right-lateral transtensional motion on the Tijeras-Cañoncito fault system (Cather, 1992). These faults are therefore interpreted to be Laramide in age. One bit of evidence that seems to contradict this interpretation is the fact that this population of faults is also found in the Oligocene(?) porphyritic intrusive rock (Fig. 2-8). As the porphyritic intrusive rock is almost certainly post-Laramide in age, it might appear that this is evidence for post-Laramide right-lateral motion. This, however, is generally inconsistent with the Neogene tectonic history of north-central New Mexico. One possibility is that these faults are extensions of reactivated Laramide faults that propagated into the porphyritic intrusive rock during the Neogene and/or Quaternary. Alternatively, these faults may record Oligocene or early Miocene right-lateral motion on the Tijeras-Cañoncito fault system. This hypothesis is supported by the work by Best (1988), which suggests that a northerly least principle stress orientation persisted until the late Oligocene or early Miocene. A third possibility is that these faults accommodated right-lateral slip in a local transfer zone in an otherwise dominantly left-lateral regime in the Neogene.

A second population of minor faults is sub-vertical and strikes north-northeast. These faults are properly oriented for slip as synthetic left-lateral Riedel shears during left-lateral strike-slip motion on the Tijeras-Cañoncito fault system (Fig. 2-11b). Their orientation is inconsistent with Riedel shears formed in a right-lateral strike-slip regime. The Tijeras-Cañoncito fault system could have accommodated rifting through left-lateral transtension in the Neogene and Quaternary (Fig. 2-12). These north-northeast striking faults are therefore interpreted to be related to rifting in the Neogene and/or Quaternary. In an exposure of Abo

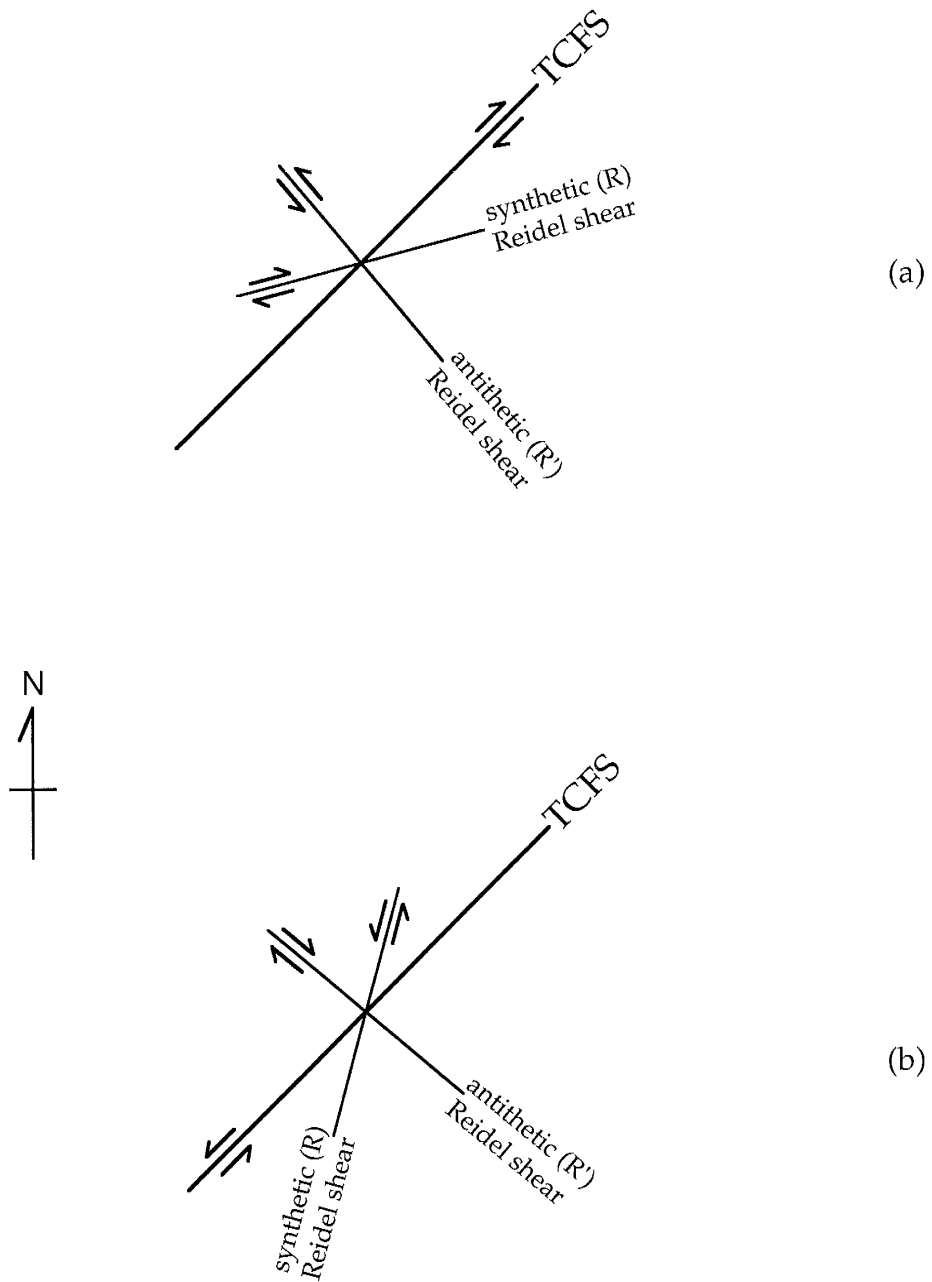


Figure 2-11. Anticipated Riedel shear geometries. (a) right-lateral motion on the Tijeras-Cañoncito fault system. (b) left-lateral motion on the Tijeras-Cañoncito fault system.

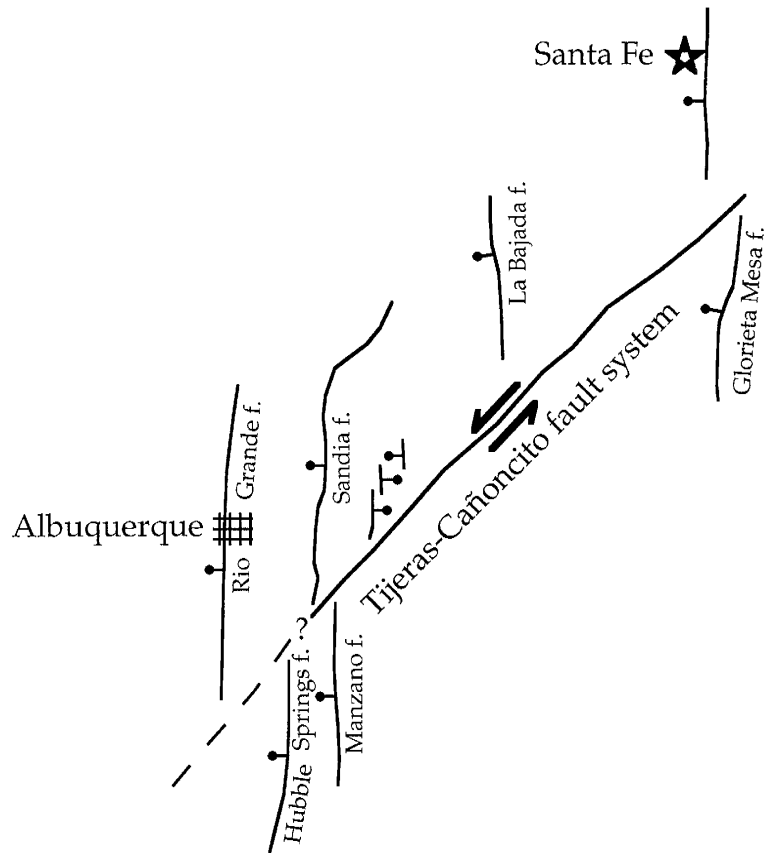


Figure 2-12. Schematic diagram of Neogene rifting. Left-lateral transtensional motion on the northeast-trending Tijeras-Cañoncito fault system, coupled with greater extension on the northwest side of the fault system, may have accommodated E-W extension during the Neogene and Quaternary.

Formation near the margin of the fault zone (unit 27), conjugate sets of north- to northeast-striking, high-angle minor faults have apparent normal separations which create a series of horsts and grabens. This geometry of faults is consistent with the development of the Rio Grande rift. There is firm evidence for mid- to late-Cenozoic deformation on the Tijeras fault in the intense deformation of the Oligocene(?) porphyritic intrusive rock and in offset of Quaternary(?) surficial deposits.

The third population is composed of sub-vertical, northwest-striking minor faults oriented roughly perpendicular to the Tijeras-Cañoncito fault system. They account for about one-fifth of all the minor faults. We interpret these to be antithetic Riedel shears, though their orientation does not suggest a particular sense of shear (see Fig. 2-11). However, two slickenside surfaces in this population exhibit synthetic and antithetic shears (R criteria of Petit, 1987) that record right-lateral motion. This is consistent with left-lateral motion on the Tijeras fault (Fig. 2-11b), and thus is probably related to the Tijeras fault accommodating the development of the Rio Grande rift in the Neogene.

CONCLUSION

A recently discovered streamcut across the Tijeras fault near Golden, New Mexico, is a spectacular window into the internal structure of the Tijeras-Cañoncito fault system. The fault zone is more than 160 m wide. Faulting locally mixed lithologies of diverse origins and geologic ages. Proterozoic, Pennsylvanian, Permian, and Oligocene(?) rocks in the fault zone are generally intensely brecciated, locally to the extent where field identification of the parent rock is impossible. In many areas of the fault zone, sedimentary bedding and gneissic foliations have been completely overprinted by a cataclastic foliation that is consistently sub-parallel to the Tijeras-Cañoncito fault system. Where preserved, bedding is sub-vertical within the fault zone, but is shallowly dipping at the margin and outside of the fault zone.

The streamcut exposure provides valuable insight into the deformational history of the Tijeras fault. Strongly deformed Proterozoic, Upper Paleozoic, and Oligocene(?) bedrock units are overlain by Quaternary(?) surficial deposits throughout most of the exposure. A population of minor faults that fits the orientation for right-lateral synthetic Riedel shears are interpreted to have formed by right-lateral motion on the Tijeras-Cañoncito fault system, consistent with deformation during the Laramide orogeny. In addition, three lines of evidence support Neogene activity. First, a porphyritic intrusive rock is intensely brecciated. By association with other porphyritic intrusive rocks in the nearby San Pedro - Ortiz porphyry belt, the brecciated porphyritic intrusive rock is probably Oligocene in age. The porphyritic intrusive rock is the only post-Laramide bedrock lithology present, and its intense deformation demonstrates that there has been significant post-Laramide movement on the Tijeras fault. The strongly deformed porphyritic intrusive rock is locally overlain by Quaternary(?) surficial deposits, suggesting that the post-Laramide deformation is bracketed in age between the Oligocene(?) and the Quaternary(?). Second, a population of minor faults fits the orientation for left-lateral synthetic Riedel shears in a left-lateral strike-slip regime. Given our understanding of the tectonics of the Rio Grande rift, it is expected that the Tijeras fault would

have accommodated left-lateral motion in the Neogene, and therefore this population of minor faults is interpreted to record Neogene activity. Third, two northwest-striking slickensides record right-lateral strike-slip motion. These are interpreted to be antithetic Riedel shears in a left-lateral strike-slip regime, which is consistent with the development of the Rio Grande rift in the Neogene.

Surficial deposits exposed by the streamcut provide clear evidence for Quaternary activity. Two Quaternary(?) surficial deposits were cut by and dragged along a fault, but are overlain by a Holocene(?) imbricated gravel. The apparent displacement on this fault is opposite that of the previously described Quaternary(?) fault in Tijeras Canyon (Lisenbee et al., 1979), but the relative timing of faulting in the streamcut and in Tijeras Canyon has not been determined.

The magnitude of displacement accommodated by the Tijeras-Cañoncito fault system has not been determined because no piercing points have been identified. The length of the fault system, the width of the fault zone, and the intense deformation within the fault zone, however, all suggest substantial displacement on the fault system.

Part III

EVIDENCE FOR REACTIVATION OF
THE TIJERAS-CAÑONCITO FAULT SYSTEM
FROM THE LARAMIDE TO THE QUATERNARY

John C. Abbott
Laurel B. Goodwin
and
Shari A. Kelley

Department of Earth and Environmental Science
New Mexico Tech

in preparation for publication

INTRODUCTION

North-central New Mexico contains the boundaries between several major geologic provinces: the Colorado Plateau, the Southern Rocky Mountains, the Basin and Range, and the Great Plains. The deformational history of the structures near the boundaries of these provinces is key to understanding the Phanerozoic tectonic history of New Mexico. The Tijeras-Cañoncito fault system is a regionally extensive structure in this area that is of particular interest because it strikes northeast, unlike most other major fault systems in New Mexico, which strike north. Determination of the timing and sense of movement on the Tijeras-Cañoncito fault system, and how it relates to regional faulting patterns, is important to understanding the tectonic development of New Mexico.

North-central New Mexico experienced major deformation during the Laramide orogeny (80-40 Ma) and during the development of the Rio Grande rift (24 Ma - present). During the Laramide orogeny, the Colorado Plateau behaved as a rigid block during east- to northeast-directed crustal shortening (Hamilton, 1981). Deformation to the east of the Colorado Plateau included high-angle faulting and the formation of basement-cored uplifts and associated intermontaine basins (Chapin and Cather, 1981; Chapin and Nelson, 1986; Martinez, 1989; Cabezas, 1991; Cather, 1992). It was formerly widely accepted that shortening was accommodated in large part by right-lateral transpressional motion on north-striking faults systems and left-lateral transpressional motion on the northeast-striking Tijeras-Cañoncito fault system (Slack and Campbell, 1976). More recently, however, it was proposed that the shortening was accommodated by right-lateral transpression on north-striking fault systems and right-lateral transtension on the Tijeras-Cañoncito fault system (Cather, 1992). Though the Tijeras-Cañoncito fault system has been a major element in most of the Laramide tectonic models proposed over the last several decades, until now there has been no investigation of kinematic data in the fault system.

Laramide-age shortening was succeeded by Basin and Range extension. From the Miocene through the Holocene, the region accommodated significant extension with the formation of the north-striking Rio Grande rift (Keller and Cather, 1994). The rift appears to have developed with a component of left-lateral motion (Kelley, 1982; Chapin and Cather, 1994; Salyards et al., 1994; Lewis and Baldrige, 1994). Laramide uplifts were locally inverted to Neogene basins. The deformational history of the Tijeras-Cañoncito fault system during rifting is of interest because little is known about the role of pre-existing oblique structures in the development of the Rio Grande rift. It has been suggested that such structures were reactivated as accommodation zones, which separate basins within the rift (Chapin et al., 1978; Chapin, 1988; Lozinsky, 1988; Chapin, 1989; Russell and Snelson, 1990, 1994; Chapin and Cather, 1994; Lewis and Baldrige, 1994; May and Russell, 1994).

The Tijeras-Cañoncito fault system was active in the Quaternary, and the possibility exists for reactivation in the future. The Quaternary history of the fault system is therefore of specific interest to assess the potential seismic hazard to Albuquerque, Santa Fe, and adjacent developing areas.

In this paper, we present new fault slickenside data, fission-track dates, and descriptions of structural and sedimentological relationships that are key to understanding the deformational history of the fault system. These data are integrated with previous observations to provide the most comprehensive summary to date of the deformational history of the fault system.

The Tijeras-Cañoncito fault system

The Tijeras-Cañoncito fault system comprises a number of northeast-striking, sub-vertical faults, including the Tijeras, Guiterrez, San Lazarus, Los Angeles, and Lamy faults (Fig. 3-1). The system is regionally extensive; it has been mapped for more than 80 km from Kirtland Air Force Base on the southwest (about 16 km southeast of Albuquerque) to the

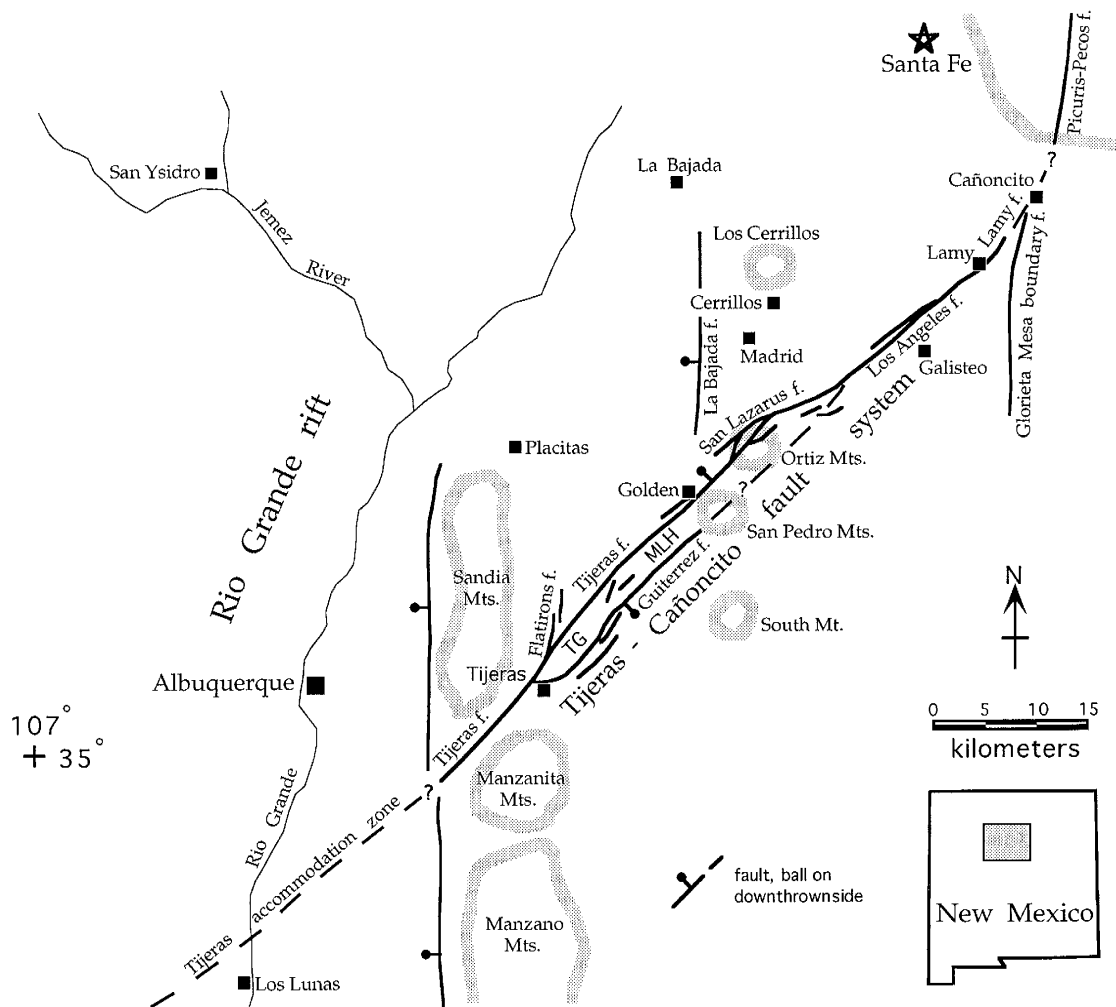


Figure 3-1. Location map and major structural elements of the Tijeras-Cañoncito fault system.

TG = Tijeras graben; MLH = Monte Largo horst.

Cañoncito area on the northeast (about 20 km southeast of Santa Fe). Following Lisenbee et al. (1979), Woodward (1984), and Maynard et al. (1990), we prefer the name "Tijeras-Cañoncito fault system" over "Tijeras fault zone" when referring to the entire group of faults. Both names are entrenched in the literature and are often used synonymously. We prefer "Tijeras-Cañoncito fault system" because it approximately locates the structure, and also distinguishes it from the Tijeras fault, which is only part of the system. The fault system may continue southwestward into the Rio Grande rift as the Tijeras accommodation zone, one of a number of places in the rift where the sense of asymmetry of half grabens reverses (Russell and Snelson, 1990; 1994; May and Russell, 1994), or it may link with the north-striking faults that bound the Rio Grande rift on the east. On the northeast end near Cañoncito, the fault system appears to link with the north-striking Picuris-Pecos fault system, though connectivity has not been demonstrated (Miller, et al., 1963; Booth, 1976).

Along much of its length, the Tijeras-Cañoncito fault system is characterized by parallel fault zones, between which horsts and grabens are present. The largest of these structures are the Monte Largo horst and the Tijeras graben, which are located between the Guitierrez and Tijeras faults (Fig. 3-2). These appear to be a single fault block, rotated about a horizontal axis perpendicular to the faults (Kelley and Northrop, 1975). Throw on the Guitierrez fault subsequent to deposition of the Upper Cretaceous Mesaverde Group is locally up to 1500 m (Kelley and Northrop, 1975). A key exposure of the Tijeras fault near the village of Golden reveals a strongly but heterogeneously deformed zone more than 160 m wide, wherein rocks of diverse lithologies and geologic ages are locally tectonically mixed (Abbott and Goodwin, 1995).

Despite decades of interest, our understanding of the Tijeras-Cañoncito fault system is surprisingly poor. The fault system clearly has a complex history of recurrent movement, but no piercing points have yet been identified to determine the magnitude of displacement for any episode of movement. Additionally, there was a considerable amount of Cenozoic movement, yet there are relatively few Cenozoic rocks exposed adjacent to the fault system to establish

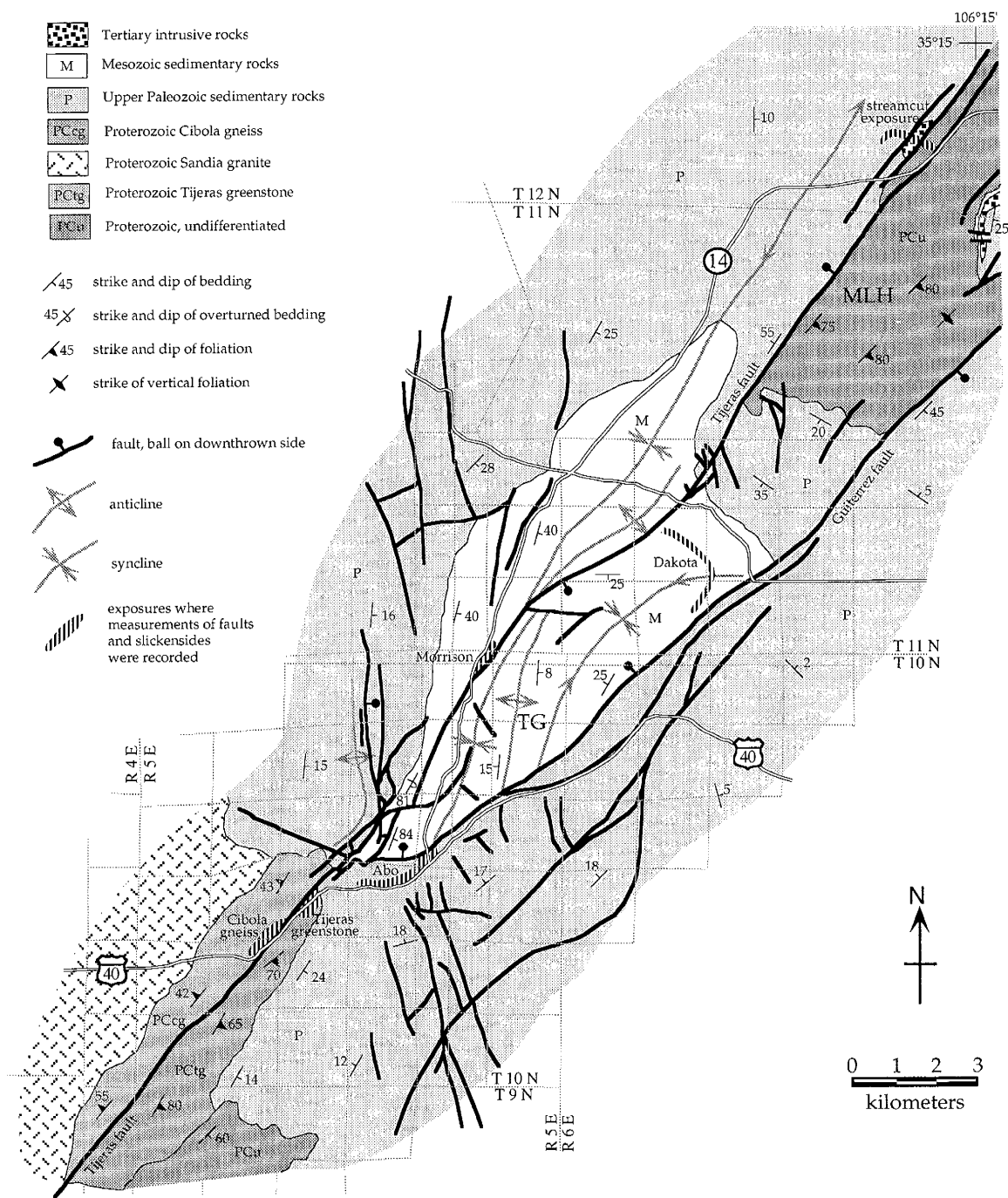


Figure 3-2. Major structural elements of the Tijeras-Cañoncito fault system near Tijeras graben (TG) and Monte Largo horst (MLH). Modified from Kelley and Northrop (1975).

the precise timing of this activity. Strain partitioning has also contributed to the structural complexity. The length of the fault system, the width of the Tijeras fault zone, and the intense deformation within the Tijeras fault zone, however, all suggest substantial displacement on the fault system.

PREVIOUS STUDIES

Many geologic maps are available for various sections of the Tijeras-Cañoncito fault system. There is considerable variability in the maps of any one area, which attests to the structural complexity of the fault system. Maps have been produced for the areas near Four Hills (unpubl. report for Sandia National Laboratories, 1993), Tijeras Canyon (Bruns, 1959; Myers and McKay, 1976; Connolly, 1981; Cavin, 1985; Gibbons, 1990; Karlstrom et al., 1994), Tijeras graben (Kelley and Northrop, 1975), Monte Largo Hills (Lambert, 1961; Huzarski, 1971), Golden (Emerick, 1950), San Pedro Mountains (Atkinson, 1961); Ortiz Mountains (Kay, 1986; Maynard et al., 1990; Maynard et al., 1991), Galisteo Creek (Stearns, 1953; Lisenbee, 1967; 1976; Bachman, 1975; Johnson, 1975), and Cañoncito (Goolsby, 1965; Booth, 1976). The geologic history of rocks adjacent to the Tijeras-Cañoncito fault system has been extensively studied, though the deformational history of the fault system has generally been only a peripheral topic.

Proterozoic

The oldest rocks in the vicinity of the Tijeras-Cañoncito fault system are exposed in Tijeras Canyon and in the Monte Largo horst (Fig. 3-2). In Tijeras Canyon, the Tijeras fault juxtaposes two different Proterozoic lithologies. On the southeast side of the fault is the Tijeras greenstone, a package of greenschist-grade metavolcanic and metasedimentary rocks (Bruns, 1959; Connolly, 1981). On the northwest side of the fault is the Cibola gneiss, an amphibolite-grade deformed granite that may be derived from the adjacent 1.42 Ga Sandia

granite (Kirby et al., 1995). Kirby et al. (1995) proposed that the Tijeras-Cañoncito fault system crosscuts a metamorphic aureole surrounding the Sandia granite. Based on quartz veins, simple pegmatite dikes, and minor aplite dikes in the Tijeras greenstone, which were interpreted to form an en echelon array, Lisenbee et al. (1979) and Connolly (1981) suggested that the initial movement on the Tijeras fault was coincident with intrusion of the Sandia granite. Connolly (1981) also concluded that intrusion of the nearby pluton caused amphibolite-facies metamorphism of the Cibola gneiss, based on the presence of sillimanite in the gneiss. Booth (1976) suggested that faults near Cañoncito accommodated deformation from the Proterozoic through the Neogene in the vicinity of the area where the Tijeras-Cañoncito fault may link with the Picuris-Pecos fault (Fig. 3-1). This area, and the proposed link between the fault systems, has not been explored in this study, and will not be addressed.

Paleozoic

Our understanding of the geologic history of north-central New Mexico between the Middle Proterozoic and the late Paleozoic is severely limited by the lack of rocks in this area from this interval. The next oldest rocks adjacent to the Tijeras-Cañoncito fault system are late Paleozoic in age. Lisenbee et al. (1979) noted that the Pennsylvanian Sandia Formation is generally thicker and coarser on the northwest side of the Tijeras fault, and attributed this sedimentation pattern to late Paleozoic motion on the fault system. They also noted small facies changes in Mississippian strata across small, high-angle, northwest-striking faults near the village of Tijeras. Similarly, they attributed the facies changes to Late Mississippian to Early Pennsylvanian faulting, which was not previously reported in the Sandia or Manzano Mountains. The relationship of these faults to the Tijeras-Cañoncito fault system, if any, is unknown.

Mesozoic - Early Cenozoic

Stearns (1953) described horizontal and vertical separations across the fault system in Cretaceous and Tertiary rocks near Galisteo Creek, and Emerick (1950) noted the complex structure of Paleozoic and Mesozoic strata in the fault system near the village of Golden. Several workers (Kelley and Northrop, 1975; Lisenbee et al., 1979; Chapin and Cather, 1981) interpreted folds oblique to the fault system to record right-lateral strike-slip motion in the Tertiary. Slack and Campbell (1976) interpreted the Tijeras-Cañoncito fault system as a left-lateral strike-slip fault to accommodate conjugate motion on the right-lateral Rio Puerco fault zone during the Laramide orogeny. Pronounced stratigraphic thickening and highly variable paleocurrents in the strata of the Paleogene Galisteo basin immediately adjacent to the Tijeras-Cañoncito fault system suggest the fault system was active in the Paleogene, and controlled extensional subsidence and sedimentation to the northwest (Cather, 1992; Abbott et al., 1995). Because the southeast block was not emergent, the maximum displacement magnitude of the Paleogene dip-slip component on the Tijeras-Cañoncito fault system is constrained to approximately the stratigraphic thickness of the strata of the Galisteo basin (about 1300 m, northwest-side-down; Abbott et al., 1995).

Middle - Late Cenozoic

A period of widespread volcanic and igneous activity followed Laramide deformation (Stearns, 1953; Cather, 1989). A shallow intrusive center, the San Pedro - Ortiz porphyry belt, was emplaced in and around the Tijeras-Cañoncito fault system in the Oligocene (Bachman and Mehnert, 1978; Woodward, 1984; Kay, 1986; Maynard et al., 1990; Maynard et al., 1991). Mineral deposits in the Ortiz Mountains are localized along the Tijeras-Cañoncito fault system, and there is clearly a genetic relationship between faulting and mineralization (Woodward, 1984; Kay, 1986; Maynard et al., 1990; Maynard et al., 1991). The relative timing of faulting,

intrusion, and mineralization is not well established. Maynard et al. (1990) maintain that intrusion and mineralization were contemporaneous with faulting, and that a K-Ar age based on hornblende from an igneous intrusive on the west side of the Ortiz Mountains constrains the timing of mid-Tertiary movement on the Tijeras-Cañoncito fault system to 30-34 Ma (early Oligocene). The possibility also exists that mineralization occurred on pre-existing fractures.

The Tijeras accommodation zone (Russell and Snelson, 1990; Lewis and Baldrige, 1994; May and Russell, 1994), which may be a southwestern continuation of the Tijeras-Cañoncito fault system, was clearly active in the Neogene. Seismic profiles (Russell and Snelson, 1994) and stratigraphic thicknesses of the basin sediments indicate that the northwest side of the Tijeras accommodation zone is downthrown as much as 3 km with respect to the southeast side (Lozinsky, 1988; 1994).

In Tijeras Canyon, the Tijeras fault clearly juxtaposed Proterozoic Tijeras greenstone against colluvium (Lisenbee et al., 1979) of probable Pleistocene age (B. Harrison and D. Love, personal commun., 1994). This activity must be Pleistocene(?) and/or younger in age. The apparent displacement direction of this fault is northwest-side-down. Near the village of Golden, Quaternary activity on the Tijeras fault is illustrated by relationships between faulting and sedimentation (Abbott and Goodwin, 1995). A streamcut exposes a fault strand of the Tijeras fault that incorporated a carbonate-rich mottled clay and pebbly gravel into the fault zone, but did not disrupt an overlying Holocene(?) imbricated gravel conglomerate. The carbonate-rich mottled clay and pebbly gravel are both older than the Holocene(?) imbricated gravel conglomerate, but are probably not older than Quaternary in age (B. Harrison and D. Love, personal commun., 1994). The apparent displacement direction of this fault (southeast-side-down) is opposite that of the previously described Quaternary(?) fault in Tijeras Canyon (Lisenbee et al., 1979); the relative timing of faulting in the two locations has not been determined.

Additional evidence for Quaternary activity on the Tijeras-Cañoncito fault system is found in the sediments of the Rio Grande rift. Gibbons (1990) suggested that the drainage

system from Tijeras Canyon was tectonically disrupted by Holocene interaction between the Tijeras and Hubble Springs faults, and Machette (1982) surveyed Holocene scarps that may be southwestern continuations of the Tijeras fault.

It is not known whether there has been any slip on the fault system in historical time, though several earthquakes have been recorded near or on the Tijeras fault in the past several decades (Sanford et al., 1991). The largest one (M.M. VI) occurred on November 6, 1947 near Tijeras and Cedar Crest (Kelley and Northrop, 1975).

EVIDENCE FOR TIMING AND CHARACTER OF MOTION ON THE TIJERAS-CAÑONCITO FAULT SYSTEM

Field Observations

Proterozoic

There is a marked discordance between the orientation of the Tijeras fault and the orientations of the main foliations developed on either side of it (Fig. 3-2). The foliation in the greenstone strikes sub-parallel to the strike of the Tijeras-Cañoncito fault system, but dips moderately to the southeast (Kelley and Northrop, 1975; Bruns, 1976; Connolly, 1981). The strike of the foliation in the gneiss is also sub-parallel to the strike of the fault system, but dips moderately to the northwest (Kelley and Northrop, 1975; Bruns, 1976; Connolly, 1981). There is no significant strain gradient in the Cibola gneiss and there is an absence of intensely sheared rocks in outcrop or as breccia clasts along the fault trace. Granitoid veins invariably lie within the plane of foliation, which locally strikes obliquely to the Tijeras fault.

We draw several conclusions from these observations. First, the Tijeras fault was not localized along a pre-existing Proterozoic ductile shear zone. This is indicated by the absence of foliations parallel to the fault and the absence of an increase in strain with proximity to the fault. In other words, the Tijeras fault was brittle from inception. Second, the pegmatite and

aplite dikes and veins appear to be an echelon only because they are intruded along the foliation in the Tijeras greenstone, which is itself locally oblique to the Tijeras fault. Therefore, there is no reason to conclude that faulting was coincident with intrusion of the Sandia granite, as suggested by Lisenbee et al. (1979) and Connolly (1981). Both of these conclusions are consistent with the observation that intrusion of the Sandia granite caused amphibolite facies metamorphism of the Cibola gneiss (Connolly, 1981). Ductile shearing, not brittle faulting, would be expected under amphibolite-facies conditions.

Late Paleozoic

On the southeast side of the Tijeras fault, the Sandia Formation is composed of roughly equal proportions of conglomerate, sandstone, and mudstone. The base of the formation is a matrix-supported sandy conglomerate about 1 m thick having rounded quartzite clasts up to 8 cm in diameter. On the northwest side of the fault, the basal conglomerate is 1 - 25 m thick, and the formation is dominated by sand and conglomerate, with lesser amounts of mudstone. Clasts in the conglomerate on the northwest fault block are generally similar in size to those on the southeast fault block, though locally there are boulders up to 1 m in diameter immediately adjacent to a ridge of Proterozoic quartzite that clearly was a topographic high in Pennsylvanian time. Lisenbee et al. (1979) believed the differences across the fault were due directly to syndepositional Pennsylvanian motion on the Tijeras fault, with the northwest side down. An alternative interpretation is that different facies were juxtaposed subsequent to deposition by strike-slip motion on the fault. Data supporting strike-slip movement is presented in the section on faults and slickensides. This interpretation is further supported by the fact that the Sandia Formation on the northwest fault block is highly variable in lithology and thickness, clearly demonstrating laterally abrupt facies changes within the formation.

FISSION-TRACK ANALYSIS

Apatite and zircon fission-track dates were determined for several rocks proximal to the Tijeras fault (Fig. 3-3; Table 3-1) in an attempt to constrain the timing of vertical displacement. Fission-track ages reveal the time that has elapsed since a rock cooled below the temperature at which fission tracks in a crystal lattice effectively accumulate; this temperature is known as the closure temperature. The closure temperature for apatite is about $100 \pm 25^\circ\text{C}$ over 1-10 m.y. (Harrison et al., 1979); the closure temperature for zircon is about $245 \pm 15^\circ\text{C}$ over 1 m.y. (Krishnaswami et al., 1974; Hurford, 1985). Fission-track dates on rocks from both sides of a fault zone can constrain the timing of relative uplift and cooling of the fault blocks, and therefore the timing of substantial vertical displacement on the fault zone. It does not constrain the timing or magnitude of strike-slip displacement because the two fault blocks do not undergo significantly different thermal effects as a result of horizontal movement. Based on stratigraphic relations, there is about 600-800 m of throw on the Tijeras fault in the area sampled.

Apatite and zircon were separated using standard heavy liquid and magnetic separation techniques (Naeser and Naeser, 1989). The external detector method of fission-track dating was used so that individual grain ages could be determined (Naeser, 1979). Samples were collected on a traverse across the Tijeras fault (Fig. 3-3). The units sampled include Proterozoic granite and granitic gneiss, Permian siltstone, porphyritic intrusive rock of suspected Oligocene age, and a Quaternary surficial deposit (Table 3-1).

The apatite fission-track ages of the bedrock units are similar (Table 3-1, Appendices D and E). The granite in the horst (ML01), the granitic gneiss near the southeast margin of the fault zone (ML02), the granitic gneiss in the fault zone (ML04), and the Abo siltstone on the northwest fault block (ML03), all have apatite fission-track ages between 21.4 ± 3.3 and 25.9 ± 2.6 Ma (Late Oligocene to Early Miocene; Fig. 3-4). These ages are similar to previously

Table 3-1. Fission-track sample descriptions and etching procedures. *Zircon etchant was a eutectic melt of 10g KOH and 7.2g NaOH @ 220°C.

sample name	lithology and geological setting	latitude, longitude	elevation (m)	fission-track dates (Ma) A = apatite Z = zircon	apatite etching procedure	zircon etching procedure*
ML01	Proterozoic granite from the Monte Largo horst near Indian Spring. The nearest known Tertiary intrusive is about 2.0 km away.	35°11.41", 106°25.51"	2134	A: 21.4 ± 3.3	22 secs in 5m HNO ₃ @ 25°C	2 hrs
ML02	brecciated Sandia granite from the southeastern margin of the fault zone. The nearest known Tertiary intrusive is about 1.0 km away.	35°13.21", 106°16.11"	2027	A: 24.9 ± 2.4	22 secs in 5m HNO ₃ @ 25°C	1 hr
ML03	Abo siltstone from the northwestern fault block. The nearest known Tertiary intrusive is about 100 m away.	35°13.69", 106°15.77"	1988	A: 25.1 ± 5.2 Z: 204.9 ± 15.0	22 secs in 5m HNO ₃ @ 25°C	6 hrs
porphyry	brecciated porphyritic intrusive rock within the fault zone (unit 16 of Abbott and Goodwin, in press)	35°13.66", 106°15.40"	1988	Z: 31.9 ± 2.0	22 secs in 5m HNO ₃ @ 25°C	1 hr
ML04	brecciated Cibola gneiss within the fault zone (unit 9 of Abbott and Goodwin, in press). The nearest known Tertiary intrusive is less than 10 m away.	35°13.63", 106°15.69"	1988	A: 25.9 ± 2.6	22 secs in 5m HNO ₃ @ 25°C	1 hr
ML05	sheared Quaternary surficial deposit within the fault zone (unit 2 of Abbott and Goodwin, in press)	35°13.62", 106°15.66"	1988	A: 59.3 ± 6 Z: 53.5 ± 3.0	22 secs in 5m HNO ₃ @ 25°C	6 and 9 hrs

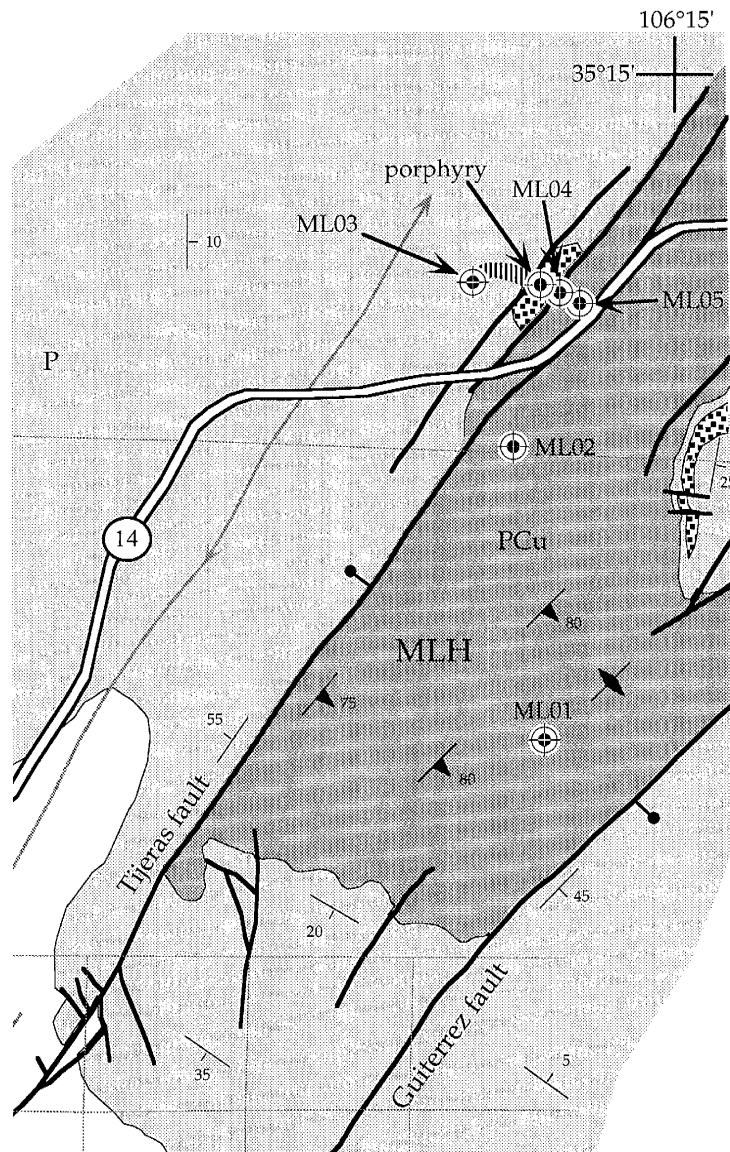


Figure 3-3. Sample localities for fission-track analysis. Map area is enlarged from upper right part of Fig. 3-2.

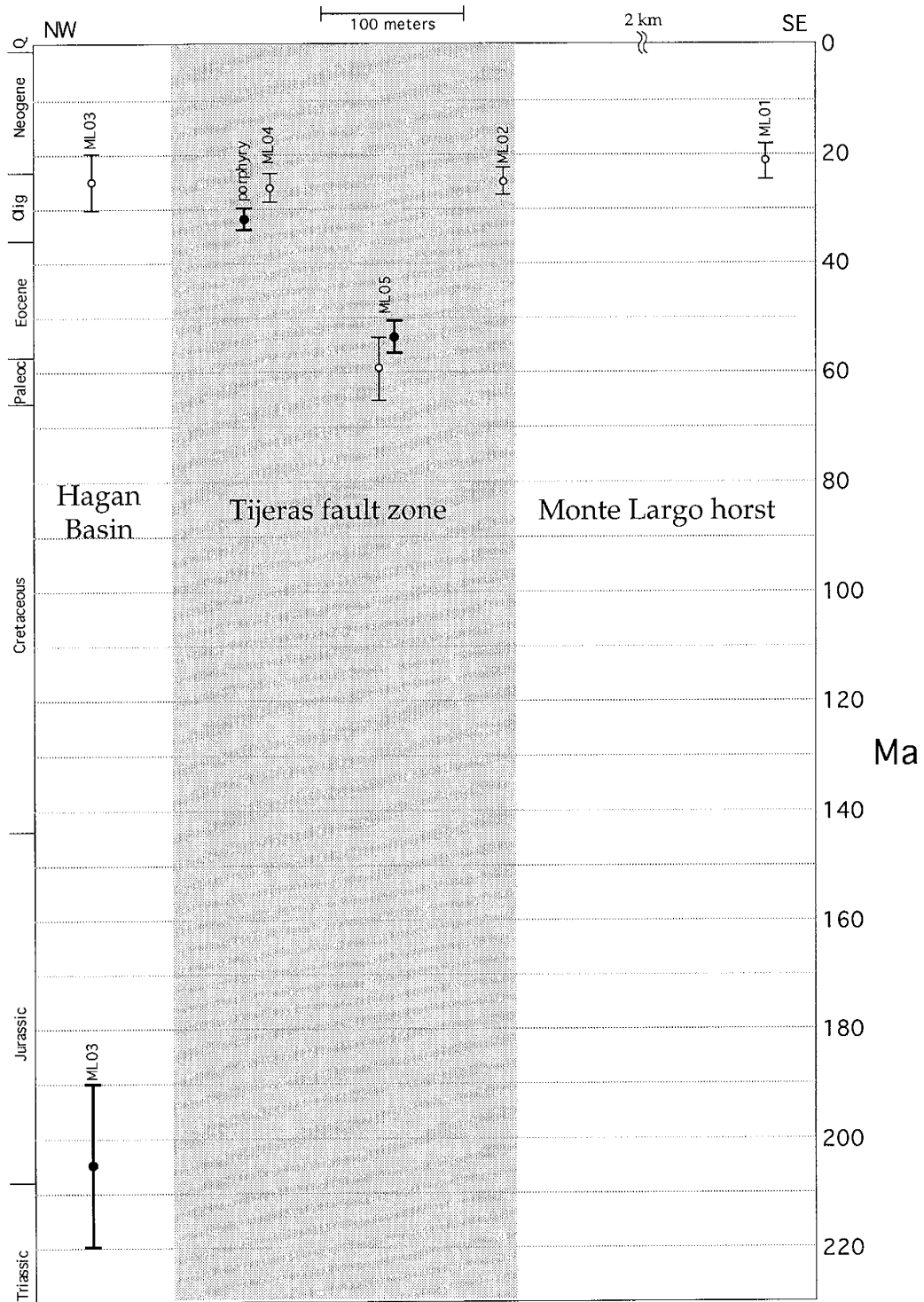


Figure 3-4. Comparison of fission-track dates in and adjacent to the Tijeras fault. Error bars represent 1 standard deviation. Open circles are apatite fission-track dates; solid dots are zircon fission-track dates.

published dates for the Sandia Mountains (Kelley & Duncan, 1984), and suggest regional denudation in the late Oligocene and early Miocene.

Zircon fission-track dates on the samples vary widely. The zircon fission-track date on the porphyritic intrusive rock (ML04) is 31.9 ± 2.0 Ma. The rock has a porphyritic texture defined by 1-5 mm phenocrysts of hornblende and altered plagioclase set in an aphanitic matrix. The porphyritic texture and aphanitic matrix suggest rapid cooling and crystallization, probably related to emplacement at shallow crustal levels. The zircon fission-track date records the time since cooling below the closure temperature of zircon; since this is expected to occur rapidly following shallow intrusion, it is taken as an approximate emplacement and crystallization age. The zircon fission-track date of the porphyritic intrusive rock falls within the range of K-Ar dates on hornblende crystals in the porphyritic intrusive rocks in the nearby Ortiz Mountains, which vary from 26 to 34 Ma (Bachman and Mehnert, 1978; Kay, 1986; Maynard et al., 1990). These dates were similarly interpreted as approximate emplacement ages, and are consistent with our interpretation of the zircon fission-track date as an approximate emplacement age.

The porphyritic intrusive rock records intense brecciation (Abbott and Goodwin, 1995) which cannot be older than the age of the rock (32 ± 2 m.y.). Faults in the porphyritic intrusive rock are overlain by undeformed Quaternary(?) surficial deposits, and therefore are older than the Quaternary(?) (Abbott and Goodwin, 1995). These data suggest fault movement in the Neogene.

The Abo siltstone (ML03) was deposited in Permian time. The zircon fission-track age on the Abo siltstone, however, is Late Triassic to Early Jurassic. Clearly, this does not reflect the age(s) of the source rocks, as it is younger than the depositional age of the siltstone. The zircon age could represent either a closure temperature, recording exhumation following burial, or partial annealing of the sample. Individual grains exhibit a broad range in ages (Appendices D and E), suggesting that the apparent fission-track age of the sample records partial annealing subsequent to deposition.

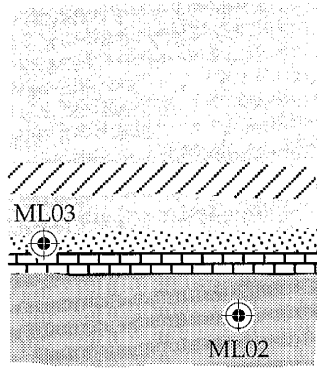
The Quaternary surficial deposit (ML05) is composed of grains that have zircon fission-track ages that range from late Paleozoic to Pliocene. A large fraction of the grains are Paleogene in age, and probably were incorporated from the porphyritic intrusive rock, which is in fault contact with the deposit. Three grains have ages between 3.2 ± 1.0 and 4.3 ± 2.0 Ma, and probably represent a Pliocene volcanic source (e.g. Bachman and Mehnert, 1978). Apatite fission-track dates on individual grains in the sample are also highly variable, ranging from 17.5 ± 7.4 to 124.0 ± 34.0 Ma. Several grains in the surficial deposit have apatite fission-track dates that are Mesozoic in age. These dates are dissimilar to those in bedrock samples from both this area and the Sandia Mountains to the west (Kelley and Duncan, 1984). Several grains in the surficial deposit have apatite fission-track dates that are Mesozoic in age. These dates are dissimilar to those in both the bedrock samples in this area as well as those in samples from the Sandia Mountains to the west (Kelley & Duncan, 1984). Multiple populations of grain ages and a broad age spectrum (Appendix E) indicate that the surficial deposit retains the apatite and zircon fission-track ages of the source rocks, and that it has not been re-heated enough in the fault zone to reset the fission-track ages.

Apatite fission-track ages of rocks adjacent to the porphyritic intrusive rock are similar to those far away from the intrusion. This suggests that emplacement of the porphyritic intrusive rock in the fault zone had a negligible effect on the thermal histories of the rocks in the fault zone and did not reset the apatite fission-track ages. This is consistent with the interpretation that the zircon fission-track age of the porphyritic intrusive rock approximates the emplacement age of the intrusion. The porphyritic intrusive rock therefore was emplaced before the time of regional cooling below the closure temperature of apatite.

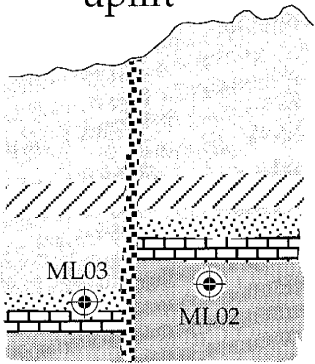
Similar apatite fission-track dates on both sides of the Tijeras fault (Fig. 3-4) preclude substantial vertical displacement in the Late Oligocene and Early Miocene. Therefore, rotation of the Monte Largo horst / Tijeras graben fault block occurred either prior to or after this time. If uplift of the horst pre-dated the time of cooling below the closure temperature of apatite, rocks of the same elevation on either side of the fault would have similar apatite fission-track

Figure 3-5. Schematic illustration of the effect of the timing of uplift of the Monte Largo horst on fission-track dates. If uplift preceded cooling below the fission-track closure temperature (left path), rocks of equal elevation on either side of the fault will have similar fission-track ages. If uplift post-dated cooling below the fission-track closure temperature (right path), rocks of equal stratigraphic position on either side of the fault will have similar fission-track ages. Laramide uplift best fits the observed fission-track ages.

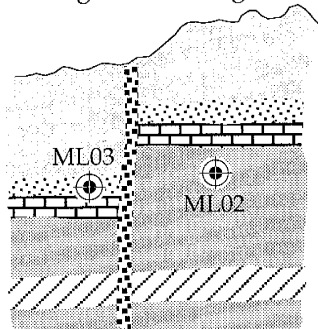
Mesozoic (pre-faulting)



Laramide uplift

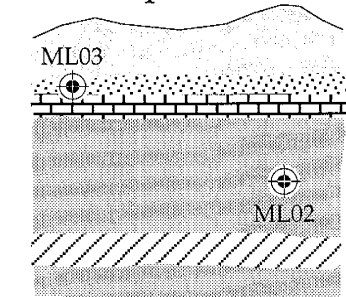


uplift of the MLH pre-dates regional cooling

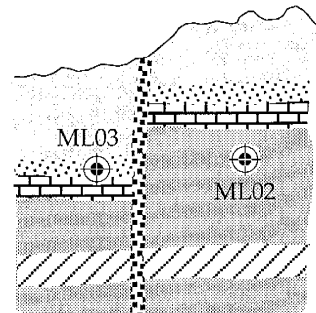


rocks of equal elevation on either side of the fault have similar fission-track ages

Neogene uplift

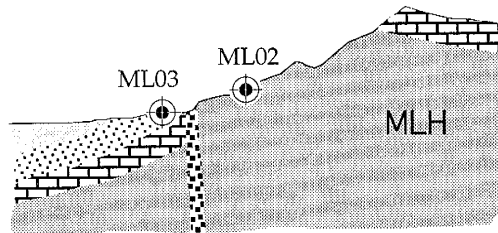


uplift of the MLH occurs subsequent to regional cooling



rocks of equal stratigraphic position on either side of the fault have similar fission-track ages

present day



ages (Fig. 3-5). The effect of current elevation on the apatite fission-track dates is probably small because all of the samples were taken within a narrow range of elevations. The largest difference in elevation is about 146 m, which will have a negligible effect on apatite fission-track ages for normal uplift rates. This model is consistent with the observed uniformity in the apatite fission-track ages across the Tijeras fault.

If uplift of the horst post-dated the time of cooling below the closure temperature of apatite, rocks of equal stratigraphic position on either side of the fault would have similar apatite fission-track ages (Fig. 3-5). The granites on the southeast fault block (ML01, ML02) are about 700 m stratigraphically lower than the Abo siltstone (ML03) on the northwest fault block. The magnitude of the effect of stratigraphic position cannot be accurately determined because the denudation rate for this area during the time of cooling is unknown. However, a rough estimate of the effect may be calculated by assuming a denudation rate. A denudation rate of 81 m/m.y. during the late Oligocene and early Miocene was determined for the Sandia Mountains (Kelley and Duncan, 1984). As this rate was determined from rocks on a flank of the Rio Grande rift, it is taken to be a maximum estimate for the Golden area, which has not experienced such dramatic uplift. Assuming this rate, if rise of the Monte Largo horst post-dated the time of cooling below the closure temperature of apatite, the Abo siltstone (ML03) might record a date that is more than 8 m.y. older than Proterozoic rocks on the northwest fault block that are equal in stratigraphic position to those sampled on the southeast block:

$$(700 \text{ m}) \times (1 \text{ m.y.}/81 \text{ m}) > 8 \text{ m.y.}$$

Removing the effect of stratigraphic position, decreases, rather than increases, the uniformity of apatite fission-track ages. As apatite fission-track dates are fairly uniform across the Tijeras fault, uplift of the horst probably pre-dated the late Oligocene. As Upper Cretaceous strata are faulted in the Tijeras graben, rotation of the Tijeras graben / Monte Largo horst fault block must have post-dated deposition of the Upper Cretaceous strata. Therefore, the likely timing of this deformation is constrained between the Late Cretaceous and the late Oligocene, and the deformation probably occurred during the Laramide orogeny.

Confined track lengths are a sensitive record of thermal history. There is a range of track lengths in any sample because each track forms at a different time and partially anneals to a different extent. A sample with a simple and rapid cooling history will have a narrow, unimodal distribution of track lengths. More complex thermal histories produce more complex distributions (Naeser, 1989; Wagner and Van den Haute, 1992).

Apatite confined track lengths for samples ML02 and ML04 are presented in Figure 3-6 and Appendix F. A statistically significant number of measurements in sample ML02 allowed modelling of the thermal history of that sample. The model illustrates a slow, simple cooling history of the Monte Largo horst in the Neogene (Fig. 3-7), which suggests that the horst did not experience rapid exhumation in the Neogene. This is consistent with our interpretation that the Monte Largo horst was uplifted prior to the Neogene, during the Laramide orogeny.

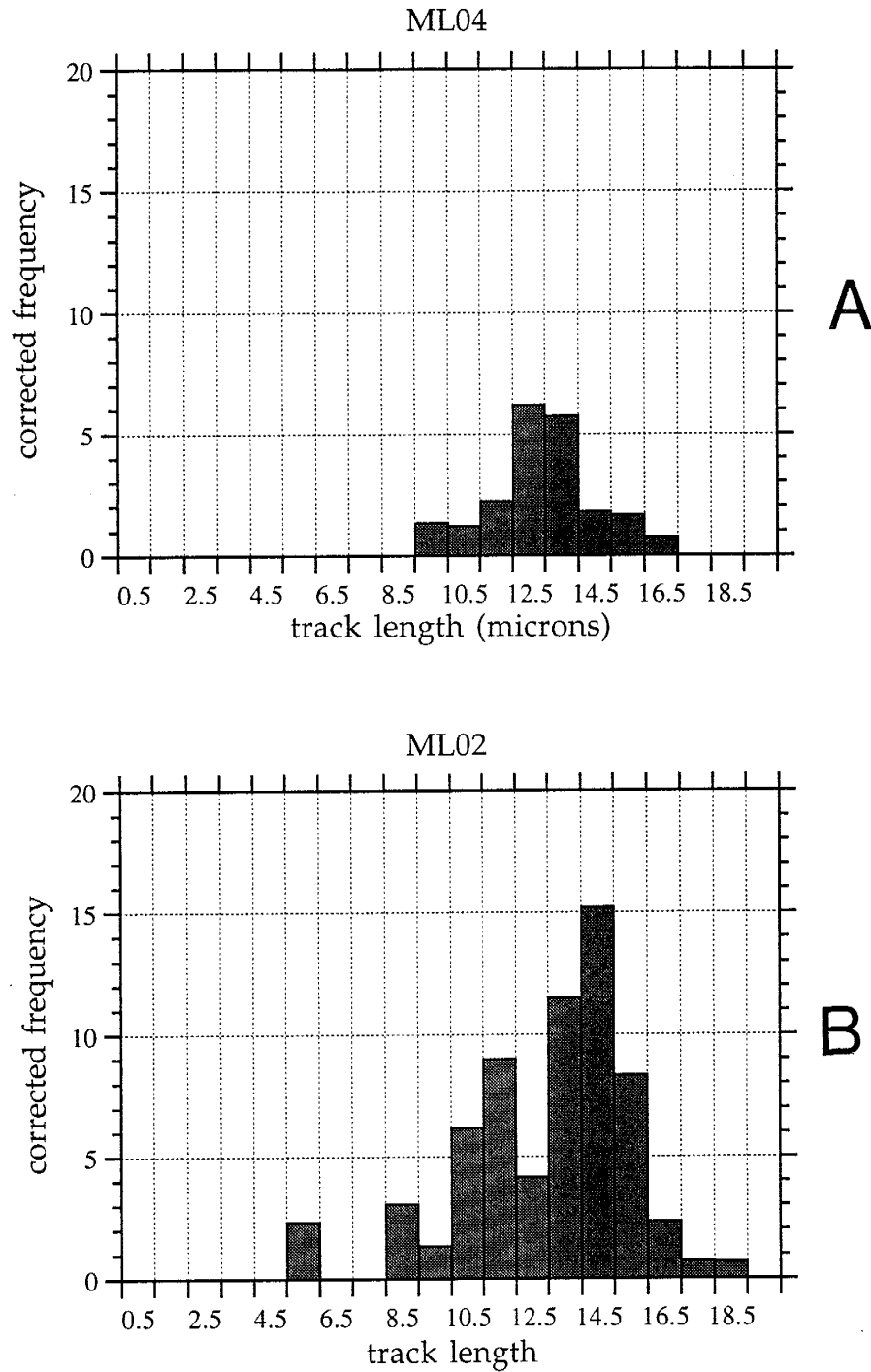


Figure 3-6. Histograms of confined fission-track lengths in apatite. Number of tracks for each cell are corrected to account for track-length bias, which recognizes that longer confined tracks have a higher probability of being etched and revealed than shorter tracks. (a) 21 track length measurements from sample ML04. (b) 65 track length measurements from sample ML02.

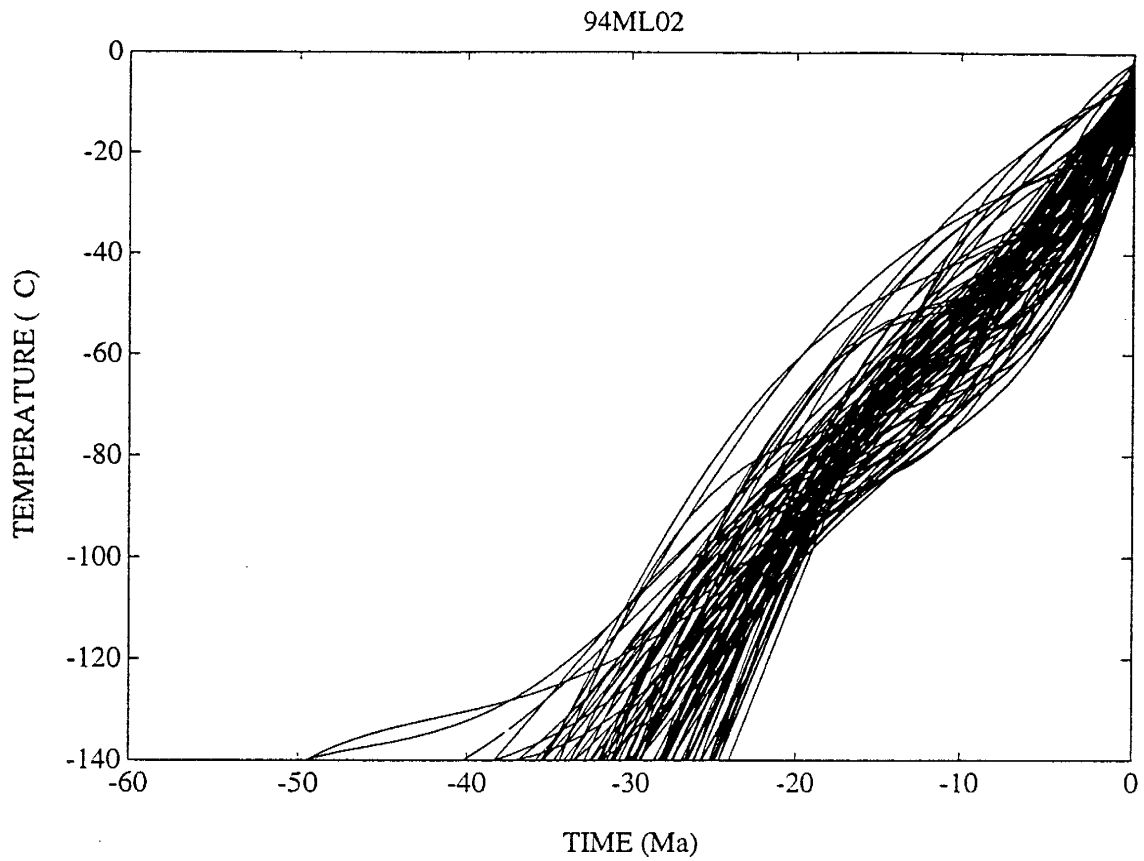


Figure 3-7. Time-temperature inversion model (Corrigan, 1991) for sample ML02. Plot shows 100 thermal history solutions compatible with the observed apatite track-length distribution. Solutions illustrate relatively slow and simple cooling of the Monte Largo horst in the Neogene.

FAULTS AND FAULT SLICKENSIDES

The orientations of faults and slickensides help constrain the sense of motion and timing of deformation on the Tijeras-Cañoncito fault system. Several populations of faults have been identified, most of which are distinctly oblique to the trend of the fault system. We interpret these populations of slickensides in terms of Riedel shear geometries. The orientation of each population, combined with kinematic indicators, suggest a certain sense of movement on the Tijeras-Cañoncito fault system. The timing of deformation is constrained by comparing the sense of movement recorded by rocks of different ages with our current understanding of the tectonic history of north-central New Mexico. For example, east-west to northeast-southwest shortening during the Laramide orogeny would have favored right-lateral transtensional motion on the Tijeras-Cañoncito fault system (Cather, 1992). Given our understanding of the tectonics of the Rio Grande rift, we expect that the Tijeras-Cañoncito fault system would have accommodated left-lateral motion if it were active in the Neogene (Fig. 3-8).

We follow Fleuty (1975) in defining a fault slickenside as a polished and commonly, though not invariably, striated brittle shear surface. Slickenlines, linear structures on a slickenside that form parallel to the direction of movement, can be subdivided into those that form by friction (slickenside striae) and those that form by mineral growth (slickenfibers). Crystallization of slickenfibers is taken to occur on the lee side of an asperity, so a slickenstep (Fleuty, 1975) forms perpendicular to slickenlines and facing the direction of movement of the missing block (Petit, 1987). Secondary fractures may develop on a slickenside, and their orientations can be used to determine the sense of slip (Petit, 1987). The criteria we used to determine the sense of shear on a fault slickenside are described by Petit (1987).

The orientations of 289 faults were measured in units ranging from Proterozoic to Quaternary in age (Figs. 3-9 through 3-14; Appendices C and G). Of these, 189 have slickensides with slickenlines. The pitch of slickenlines was measured on each slickenside surface. Slickenlines that pitch $\leq 45^\circ$ record dominantly strike-slip motion; slickenlines that

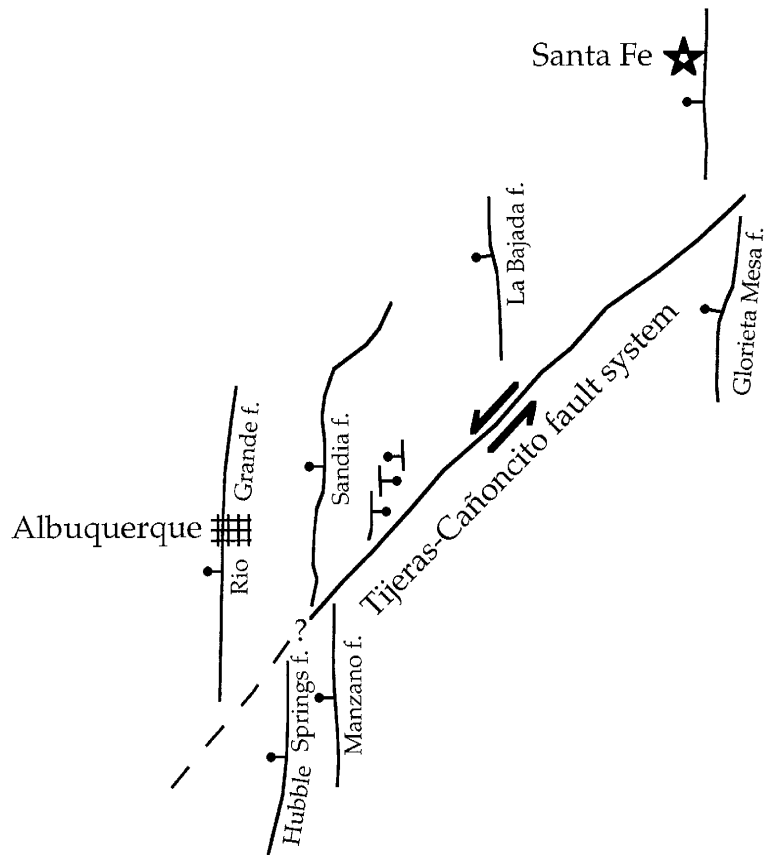
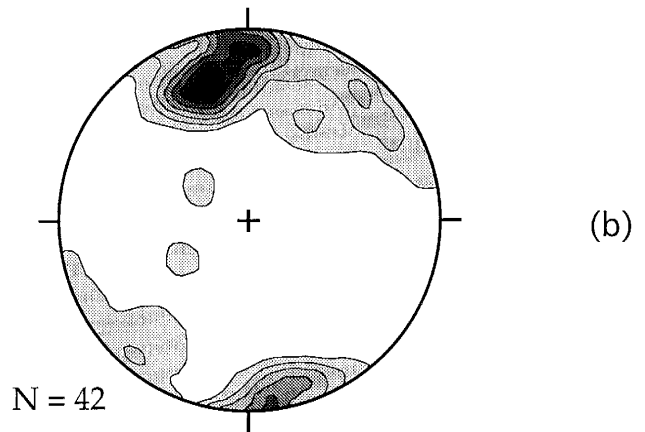
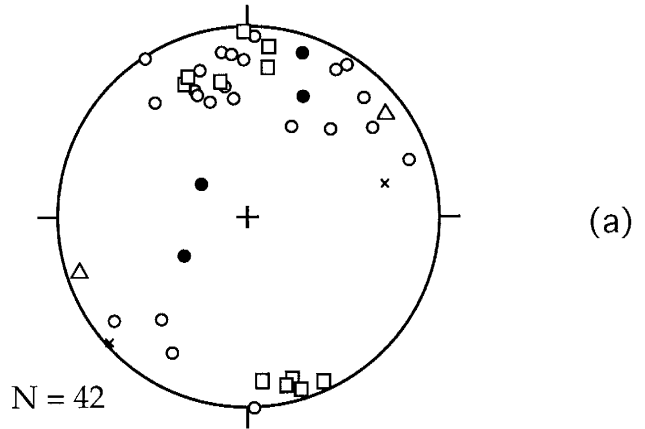


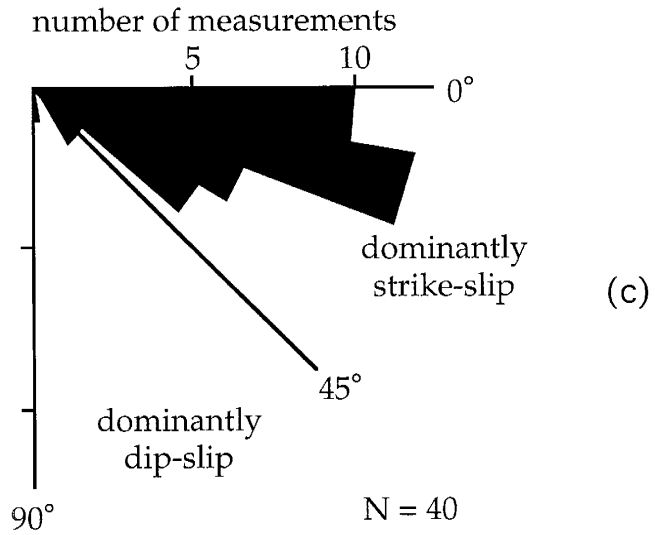
Figure 3-8. Schematic diagram of Neogene rifting. Left-lateral transtensional motion on the northeast-striking Tijeras-Cañoncito fault system, coupled with greater extension on the northwest side of the fault system, may have accommodated east-west extension during the Neogene and Quaternary.

Figure 3-9. Minor fault and slickenline data from the Proterozoic Tijeras greenstone. (a) Equal area, lower hemisphere projection of poles to minor faults. Dominant component of the sense of slip on each slickenside is indicated. (b) Poles to faults contoured in multiples of random distribution (mrd). White is less than 1 mrd, each subsequent contour represents an increase in one mrd. The data are plotted and contoured using the program and method of Starkey (1977). (c) Pitches of slickenlines from slickenside surfaces. Each petal is 10° .

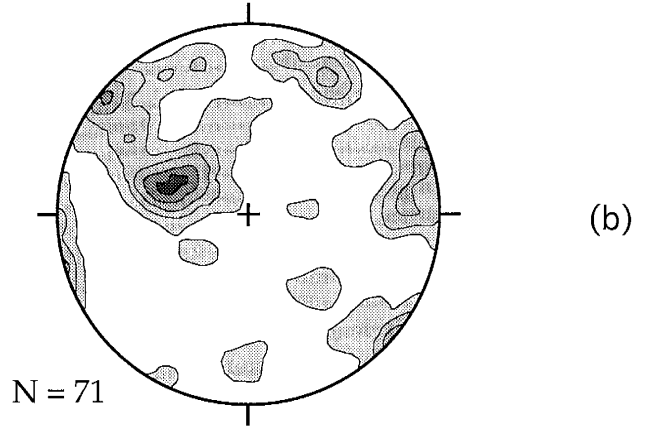
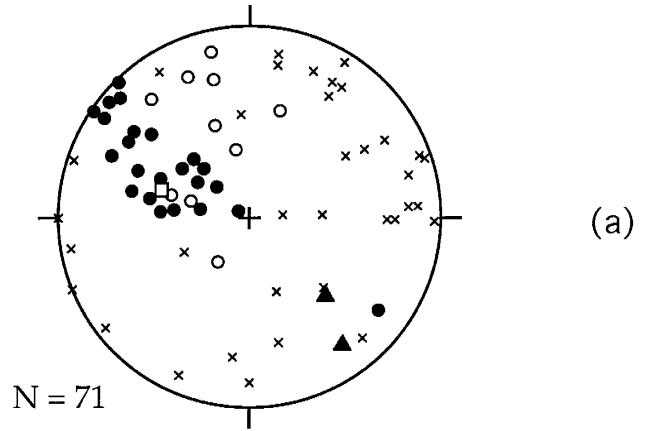
- × fault, no slickenlines
- strike slip fault
pitch $\leq 45^\circ$
- right-lateral
- △ left-lateral
- dip slip fault
pitch $> 45^\circ$
- normal
- ▲ reverse



Proterozoic
Tijeras greenstone



- × fault, no slickenlines
- strike slip fault pitch $\leq 45^\circ$
- dip slip fault pitch $> 45^\circ$
- right-lateral
- △ left-lateral
- normal
- ▲ reverse



Proterozoic
Cibola gneiss

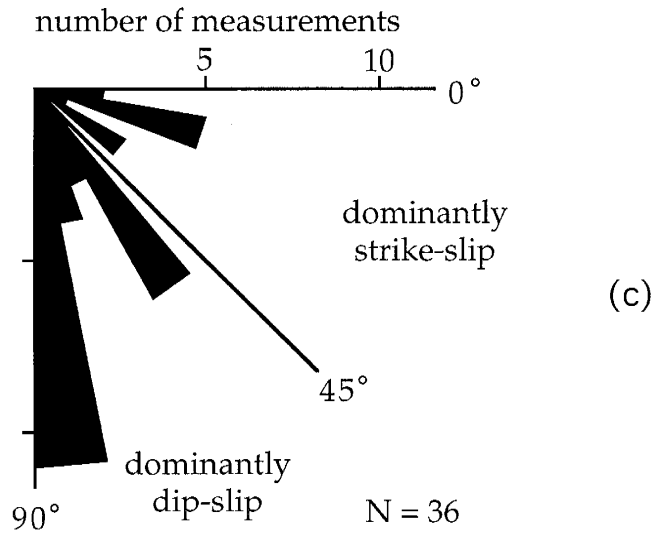
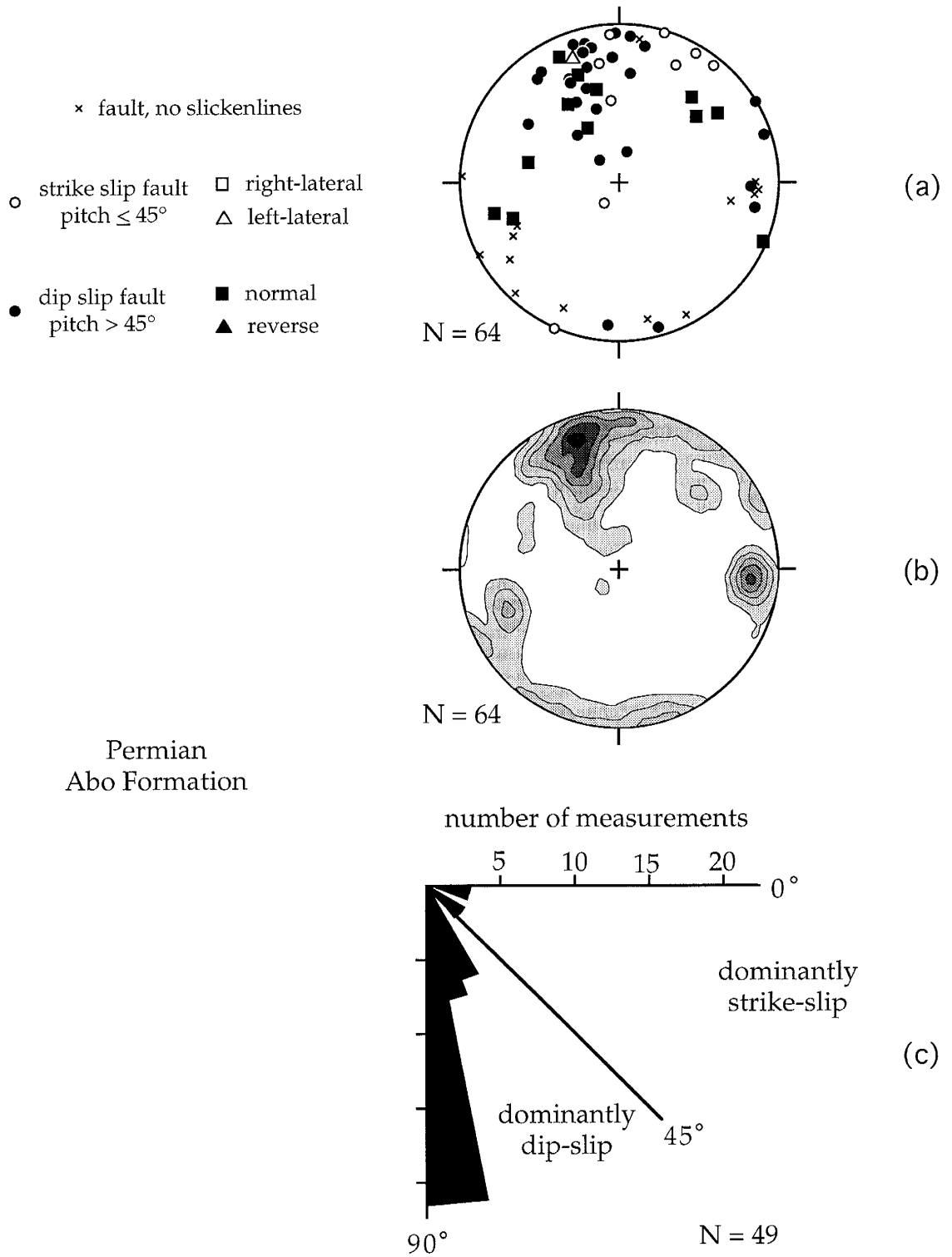
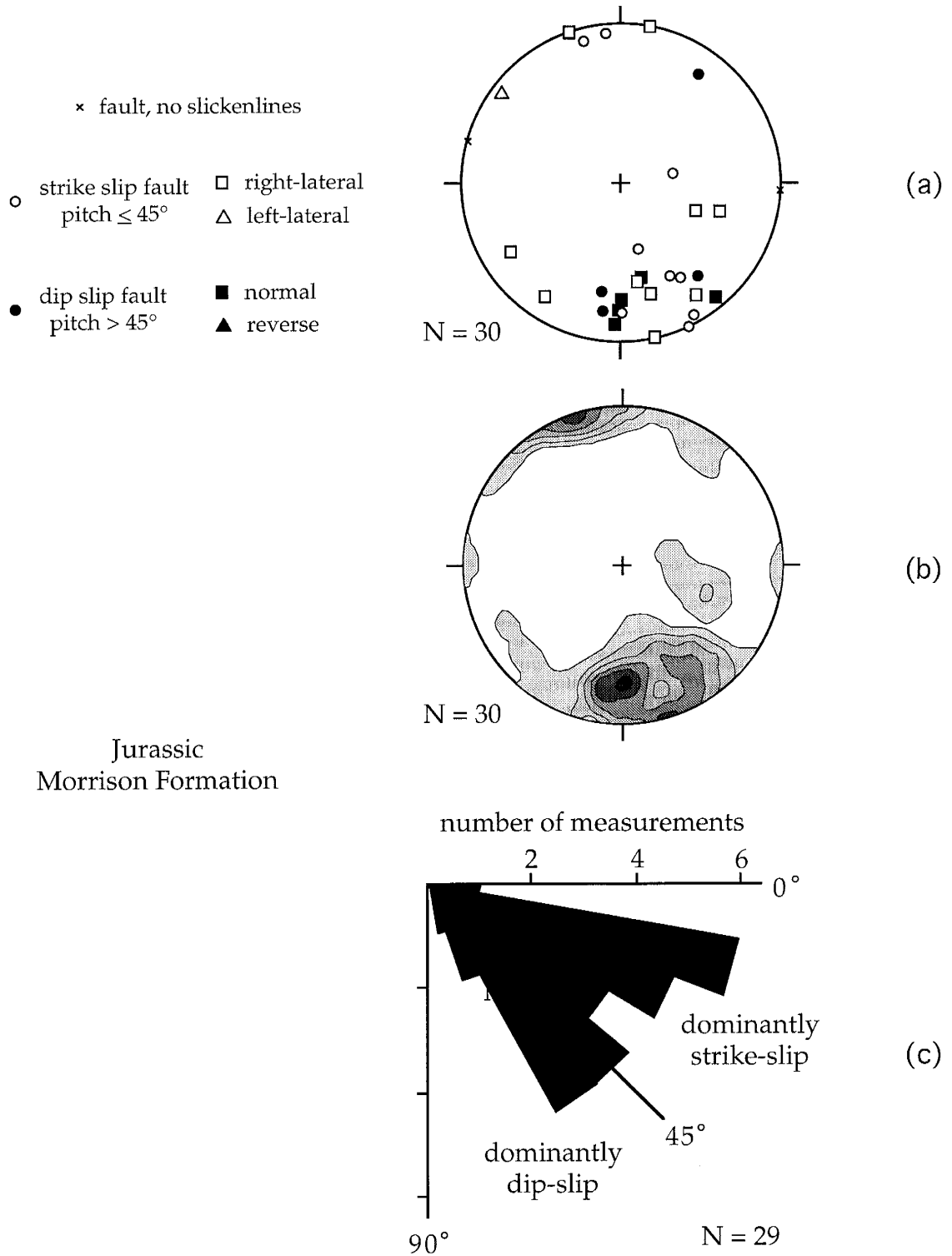


Figure 3-10. Minor fault and slickenline data for the Proterozoic Cibola gneiss. Refer to caption of Fig. 3-9 for explanation.



Permian
Abo Formation

Figure 3-11. Minor fault and slickenline data for the Permian Abo Formation. Refer to caption of Fig. 3-9 for explanation.



Jurassic
Morrison Formation

Figure 3-12. Minor fault and slickenline data for the Jurassic Morrison Formation. Refer to caption of Fig. 3-9 for explanation.

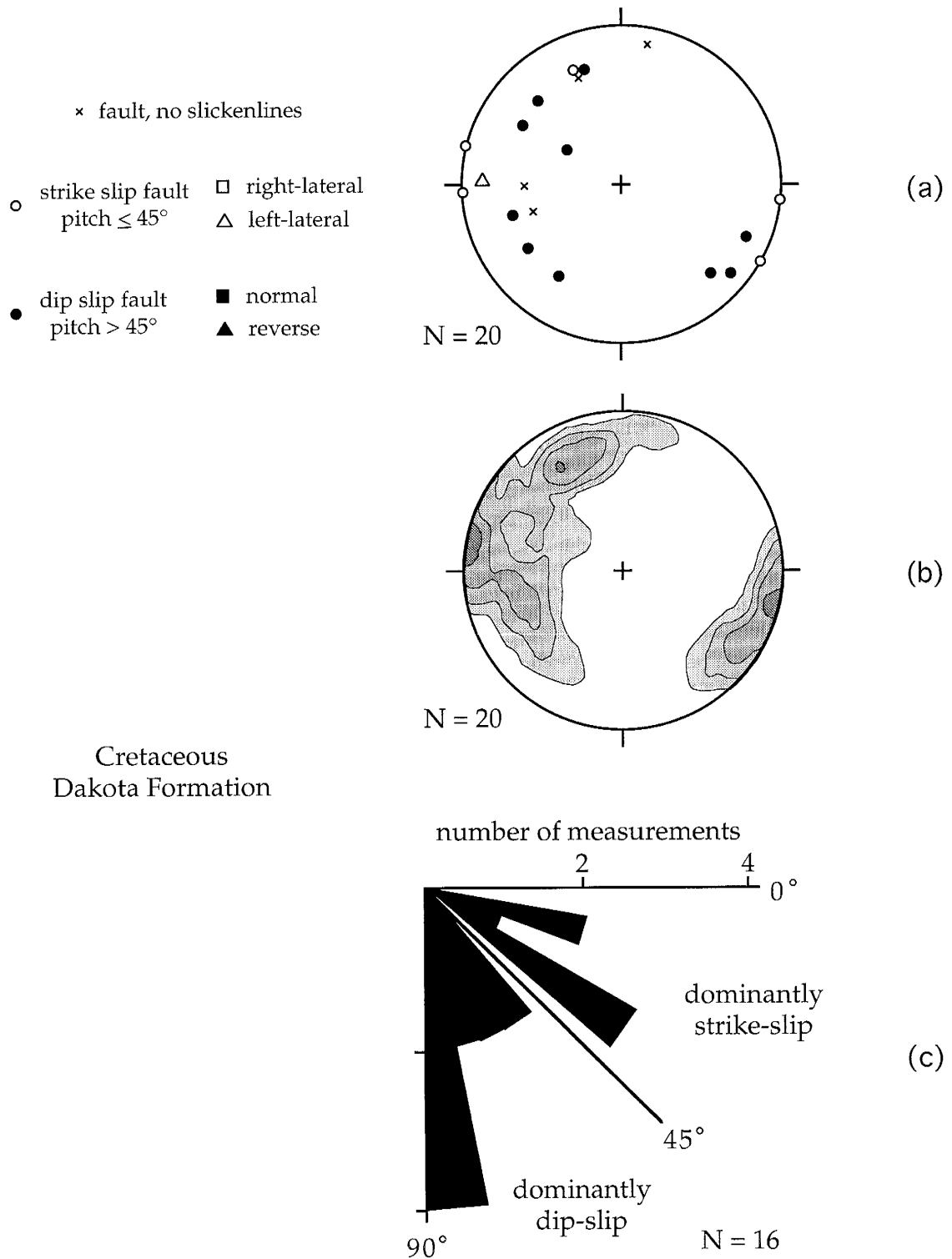


Figure 3-13. Minor fault and slickenline data for the Cretaceous Dakota Formation. Refer to caption of Fig. 3-9 for explanation.

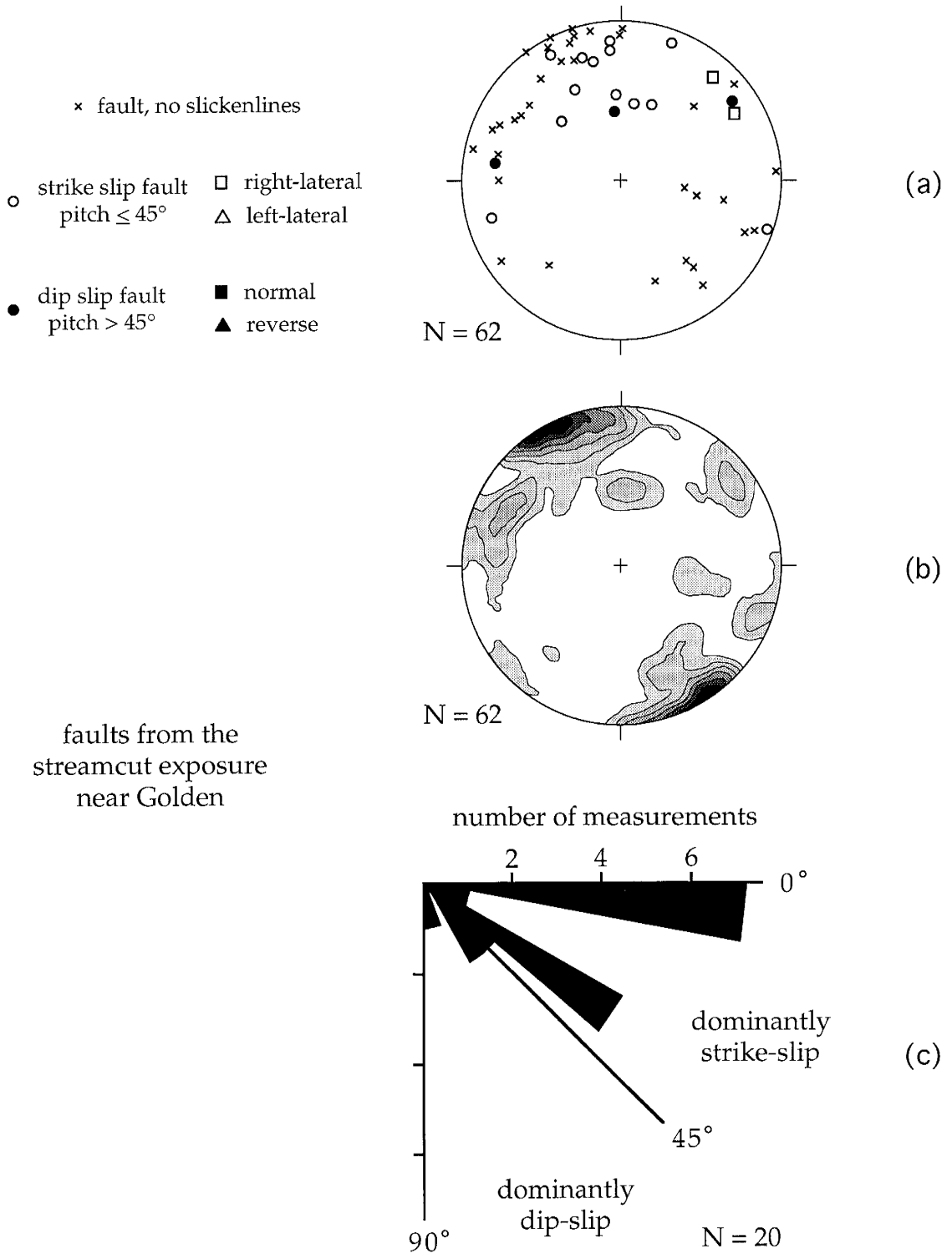


Figure 3-14. Minor fault and slickenline data from the streamcut exposure near Golden. Refer to caption of Fig. 3-9 for explanation.

pitch $>45^\circ$ record dominantly dip-slip motion. The sense of slip was determined from secondary fractures or slickenfibers on 48 of the slickensides. The faults are grouped by geographic location, which also generally corresponds to grouping by geologic age. Locations of fault measurements are shown on Figure 3-2. Note that the measurements were taken from different areas in the fault system. For example, measurements were taken adjacent to the Tijeras fault, within the Tijeras graben, and from an area adjacent to the east-striking fault that bounds the southwestern end of the graben.

East-northeast-striking faults

The most pronounced population of faults strikes east-northeast, dips sub-vertically, and has slickenlines that vary in pitch with position in the fault system. In most exposures adjacent to the Tijeras fault, slickenlines typically pitch $\leq 45^\circ$ (Figs. 3-9, 3-14 and 3-15). Northwest of the Tijeras graben, however, the slickenlines are generally oblique, with the pitch of most between 10° and 60° (Fig. 3-12). Twenty slickensides measured adjacent to the Tijeras fault record right-lateral motion; of these, five have a significant normal component of movement and one records a significant reverse component of slip. One records normal movement with a left-lateral component. This population of faults is properly oriented for slip as synthetic right-lateral Riedel shears during right-lateral transtensional motion on the Tijeras-Cañoncito fault system (Fig. 3-16a). Their orientations are inconsistent with Riedel shears developed during left-lateral strike-slip motion (cf. Fig. 3-16b). Further, they cut all rocks Cretaceous in age and older. In sec. 15, T10N, R5E, detailed mapping has demonstrated apparent right-lateral offsets of Mesozoic strata across map-scale, east-northeast-striking, high-angle faults (Fig. 3-17). The east-northeast-striking population of faults is therefore interpreted to be Laramide in age. One bit of evidence that seems to contradict this interpretation is the fact that this population of faults is also found in the Oligocene porphyritic intrusive rock in the streamcut exposure (Fig. 2-8). As the porphyritic intrusive



Figure 3-15. ENE-striking fault slickenside in the Tijeras greenstone with well developed horizontal slickenside striae indicating strike-slip motion. 15 cm ruler for scale.

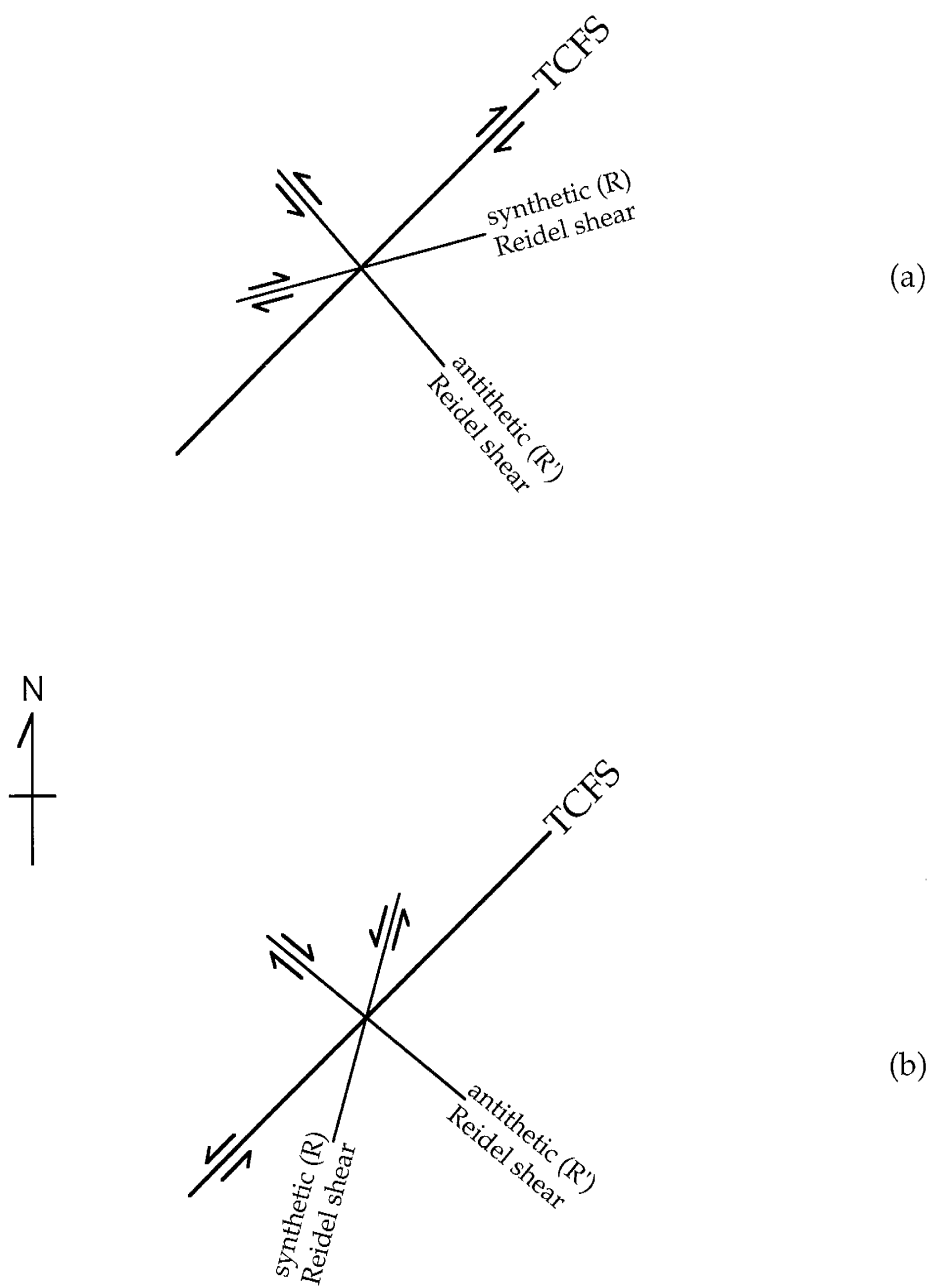


Figure 3-16. Anticipated Riedel shear geometries. (a) right-lateral strike-slip motion on the Tijeras-Cañoncito fault system. (b) left-lateral strike-slip motion on the Tijeras-Cañoncito fault system.

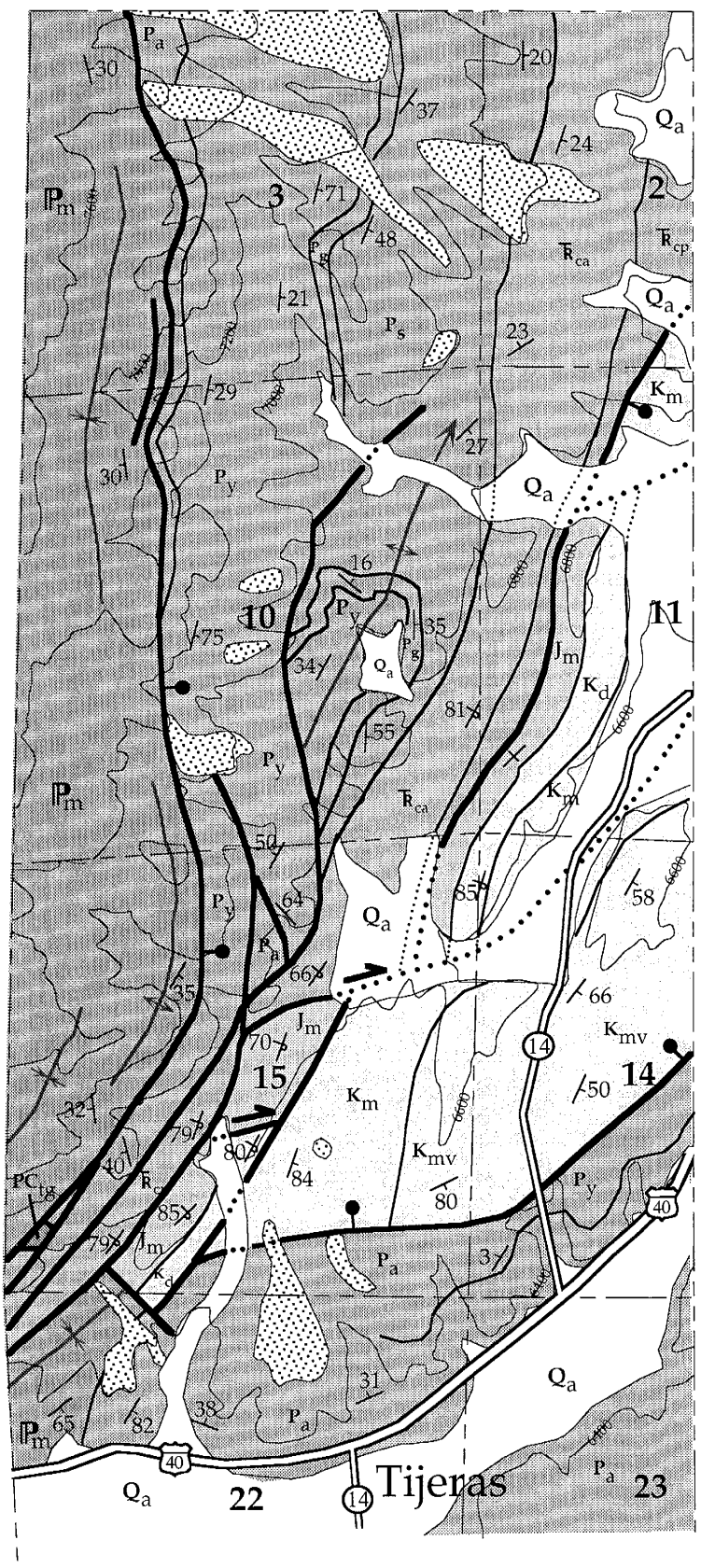
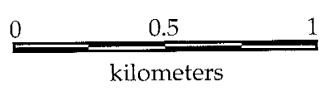
Figure 3-17. Simplified geologic map of the northeastern part of the Tijeras 7.5' quadrangle near the southwestern end of Tijeras graben. Note right-lateral separations of vertically-oriented Mesozoic sedimentary rocks across ENE-striking faults. Map contributed to Karlstrom et al. (1994).

- Qa Quaternary alluvium
- Quaternary or late Tertiary gravel
- Cretaceous sedimentary rocks
 - Kmv** Mesaverde Gp
 - Km** Mancos Fm
- Jurassic sedimentary rocks
 - Jm** Morrison Fm
- Triassic sedimentary rocks, Chinle Gp
 - R_{ca}** Aqua Zarca Fm
 - R_{cp}** Petrified Forest Fm
- Permian sedimentary rocks
 - Ps** San Andres Limestone
 - Pg** Glorieta Sandstone
 - Py** Yeso Formation
 - Pa** Abo Formation
- Pennsylvanian sedimentary rocks
 - P_m** Madera Group
- Proterozoic metamorphic rocks
 - PC_{tg}** Tijeras greenstone

- 45 strike and dip of bedding
- strike of vertical bedding
- 45 strike and dip of overturned bedding

- fault, ball on downthrown side, dotted where concealed
- depositional contact, dotted where concealed
- anticline, arrow points in downplunge direction
- syncline, arrow points in downplunge direction

contour interval = 200 feet



rock is post-Laramide in age, it might appear that this is evidence for post-Laramide right-lateral motion. This, however, is generally inconsistent with the Neogene tectonic history of north-central New Mexico. One possibility is that these faults are extensions of reactivated Laramide faults that propagated into the porphyritic intrusive rock during the Neogene and/or Quaternary. Alternatively, these faults may record Oligocene or early Miocene right-lateral motion on the Tijeras-Cañoncito fault system. This hypothesis is supported by the work by Best (1988), which suggests that a northerly least principle stress orientation persisted until the late Oligocene or early Miocene. A third possibility is that these faults accommodated Neogene right-lateral slip in a local transfer zone in an otherwise dominantly left-lateral regime.

Near the southwestern margin of the Tijeras graben (Fig. 3-11), slickenlines on east-northeast-striking slickensides record dominantly dip-slip motion. Four of the five faults with kinematic indicators record normal displacement; one records dominantly left-lateral motion with a reverse component. These minor faults are in proximity and strike parallel to the major fault that bounds the Tijeras graben, which has more than 1200 m of vertical stratigraphic separation (Fig. 3-17). The spatial association and similarity in orientation of all of these faults suggests that they are genetically related. That is, we suggest the majority of these faults are normal faults. The major fault that bounds the southwestern end of the Tijeras graben probably acted as a releasing bend between the Tijeras and Guitierrez faults during right-lateral strike-slip motion on the fault system. This fault probably accommodated rotation of the Tijeras graben - Monte Largo horst fault block during the Laramide orogeny, causing subsidence of the Tijeras graben and uplift of the Monte Largo horst. The one fault that records left-lateral plus reverse motion was probably reactivated in the Neogene.

Northwest-striking faults

A second population of faults is composed of sub-vertical, northwest-striking faults oriented roughly perpendicular to the Tijeras-Cañoncito fault system. This population is evident throughout the area (Figs. 3-10 through 3-14). Slickenlines on all of these faults record a component of strike-slip motion. We interpret these to be antithetic Riedel shears, though their orientation alone does not suggest a particular sense of shear (Fig. 3-16). Secondary fractures on one slickenside, and slickenfibers on another slickenside in the Tijeras greenstone, both record left-lateral strike-slip motion. The pitch of slickenlines on both of these is less than or equal to 5° . This is consistent with right-lateral strike-slip motion on the Tijeras fault (Fig. 3-16a), and thus probably records Laramide right-lateral strike-slip motion on the Tijeras fault. Conversely, four slickenside surfaces in this population exhibit secondary fractures that record right-lateral strike-slip motion, two of which record a significant component of normal movement. This is consistent with left-lateral strike-slip motion on the Tijeras-Cañoncito fault system. The fault system could have accommodated rifting through left-lateral transtension in the Neogene and Quaternary (Fig. 3-8), and thus these are interpreted to be Neogene and/or Quaternary in age.

At the southwest margin of the Tijeras graben, the pitch of slickenlines in this population varies from 60° to 80° . Slickenfibers and/or secondary fractures on three slickensides in the Abo Formation that contribute to this population record a dominant component of normal motion. It appears that, within the area we have interpreted as a releasing bend between the Tijeras and Guitierrez faults, some northwest-striking minor faults accommodated extension.

North- and north-northeast-striking faults

A third population is composed of north- and north-northeast-striking sub-vertical faults. It is evident in the Cibola gneiss, Abo Formation and Dakota Sandstone (Figs. 3-10, 3-11,

and 3-13), as well as in Proterozoic, Upper Paleozoic, and Oligocene rocks in the streamcut exposure near Golden (Fig. 3-14). This population is found both adjacent to the Tijeras fault and adjacent to and within the Tijeras graben. One slickenside in the Dakota Formation exhibits secondary fractures that record left-lateral strike-slip motion. Four slickensides in the Abo Formation record normal movement. These slickensides are properly oriented for slip as synthetic left-lateral Riedel shears during left-lateral strike-slip motion on the Tijeras-Cañoncito fault system (Fig. 3-16b). They are also properly oriented for slip as normal faults during formation of the Rio Grande rift. These faults are therefore interpreted to be related to rifting in the Neogene and/or Quaternary.

Two slickensides located in the Morrison Formation record right-lateral strike-slip motion. Both are relatively low-angle faults compared to most others in the fault system, dipping between 40° and 53°. The significance of these data is unknown.

Kelley and Northrop (1975) reported high-angle, reverse slickenfibers on a north-striking slickenside in the Madera Formation, near the Flatirons fault, and interpreted them as reflecting Laramide high-angle, reverse faulting. However, these slickenfibers are present on bedding planes on the limb of a drag fold, and are more likely the result of bedding-parallel slip during the normal, east-side-down, development of the drag fold.

Northeast-striking faults

In the Cibola gneiss and the Morrison Formation, a population of faults strikes northeast to north-northeast and dips steeply to moderately to the southeast and east-southeast. This population is not evident in the other formations in other locations. It consists largely of faults having slickenlines that record a dominant component of dip-slip motion, though some slickensides have slickenlines that pitch between 20° and 30°. Kinematic indicators on two of these record dominantly right-lateral strike-slip motion; though one records dominantly left-lateral strike-slip motion. Each of these record a measurable

component of normal movement. Secondary fractures on two dip-slip slickensides record normal displacement. The slickensides recording right-lateral strike-slip motion are consistent with deformation during the Laramide orogeny; the normal faults could have been active during either Laramide-age shortening or Neogene extension.

Two northeast-striking, northwest-dipping faults with slickensides in the Cibola gneiss are notable because they are the only two measured slickensides in the fault system that record a dominant component of reverse motion. The age and significance of these is unknown.

Summary of slickenside data and interpretations

In summary, there are several discernible populations of slickensides within the Tijeras-Cañoncito fault system, few of which are parallel to the system ($\sim 045^\circ$, 90°). Slickensides vary in pitch from 0° (pure strike-slip) to 90° (pure dip-slip), (Fig. 3-18). The relative amounts of strike-slip and dip-slip motion vary with position in the fault system.

Several populations of faults that are oblique to the Tijeras-Cañoncito fault system are interpreted to be Riedel shears. The orientation of the Riedel shears and kinematic indicators on them suggest both right- and left-lateral strike-slip motion on the fault system. Riedel shears that suggest right-lateral strike-slip motion are interpreted to be Laramide in age because east-west to northeast-southwest shortening during the Laramide orogeny would favor right-lateral transtensional motion on the Tijeras-Cañoncito fault system. These Riedel shears are found in rocks of all ages along the Tijeras fault. East-northeast-striking normal faults in the Abo Formation southwest of the graben and an adjacent map-scale fault are also interpreted to be Laramide in age because their orientation is consistent with a releasing bend in the right-lateral strike-slip regime of the Laramide orogeny, accommodating rotation of the Tijeras graben - Monte Largo horst fault block. Therefore, we interpret the variation in slickenside orientations and movement directions to be related to strain partitioning between different areas, rather than a function of the geologic age of faulting.

Riedel shears that suggest left-lateral strike-slip motion on the fault system are interpreted to be Neogene or Quaternary in age because left-lateral motion on the Tijeras-Cañoncito fault system could accommodate rift-related east-west extension (Fig. 3-8).



Figure 3-18. Two fault surfaces in the Abo Formation of similar orientation that record different kinematic histories. The fault on the right has well developed sub-horizontal slickenside striae, indicating strike-slip movement. The fault on the left has well developed down-dip slickenside striae, indicating dip-slip motion. Faults strike ENE. 15 cm ruler for scale.

CONCLUSIONS

There is no conclusive evidence to suggest or refute Proterozoic or Paleozoic movement on the Tijeras-Cañoncito fault system. The oldest documented movement is Laramide in age. The fault system accommodated right-lateral transtensional motion in the Laramide, as indicated by:

- 1) Paleocurrent analysis and stratigraphic thickening of the strata of the Galisteo basin that indicate that the fault system controlled extensional subsidence in the Paleogene (Abbott et al., 1995).
- 2) Apatite fission-track dates (21.4 ± 3.3 to 25.9 ± 2.6 Ma) and deformation of Cretaceous strata in the Tijeras graben that are best explained by rotation of the Monte Largo horst/ Tijeras graben fault block during the interval between Late Cretaceous and late Oligocene time.
- 3) Separations of Mesozoic stratigraphy (Fig. 3-17) and folds oblique to the fault system (Kelley and Northrop, 1975; Lisenbee et al., 1979; Chapin and Cather, 1981), both of which suggest right-lateral motion.
- 4) Minor faults that are interpreted as right-lateral synthetic and antithetic shears based on orientations relative to the fault system and kinematic indicators. In most exposures adjacent to the Tijeras fault, slickenlines are dominantly strike-slip, though typically they have components of both right-lateral and normal motion.
- 5) Evidence that the major fault that bounds the southwestern end of the Tijeras graben acted as a releasing bend between the Tijeras and Guitierrez faults during right-lateral strike-slip motion on the fault system.

These observations also suggest that the geometry of the Tijeras-Cañoncito fault system was largely established during the Laramide orogeny. Right-lateral motion on the Tijeras-Cañoncito fault system during the Laramide orogeny is inconsistent with the interpretation of Slack and Campbell (1976) that the Tijeras-Cañoncito fault system was a left-lateral conjugate wrench system to the right-lateral Rio Puerco fault zone.

The fault system may have been locally reactivated in the Oligocene (Woodward, 1984; Kay, 1986; Maynard et al., 1990; Maynard et al., 1991). However, late Oligocene - early Miocene apatite fission-track ages on both sides of the Tijeras fault near Golden precludes substantial vertical displacement on the fault during this time. Evidence that the Tijeras-Cañoncito fault system was active as a left-lateral transtensional system in the Neogene includes:

- 1) Intense brecciation of a 32 ± 2 Ma porphyritic intrusive rock by the Tijeras fault.
 - Faults in the porphyritic intrusive rock are overlain by undeformed Quaternary(?) surficial deposits, and therefore are older than Quaternary(?) in age (Abbott and Goodwin, 1995).
- 2) Slickensides in Proterozoic, Upper Paleozoic, and Mesozoic rocks that record left-lateral and normal slip on surfaces that strike east-northeast to north-northeast, and synthetic and antithetic Riedel shear geometries that suggest left-lateral transtension on the Tijeras-Cañoncito fault system.
- 3) Abbott and Goodwin (1995) noted normal separation on small-scale, north-striking faults, and suggested that rift-related extension could be accommodated by normal slip on north-striking faults and left-lateral transtensional movement on the northeast-striking Tijeras-Cañoncito fault system.

There is unequivocal evidence that the Tijeras-Cañoncito fault system was active in the Quaternary. Near the village of Golden, Quaternary activity on the Tijeras fault is illustrated by a fault which cuts Quaternary(?) surficial deposits but is overlain by Holocene(?) sediments (Abbott and Goodwin, 1995). In Tijeras Canyon, Quaternary(?) colluvium and Tijeras greenstone are locally juxtaposed by the Tijeras fault (Lisenbee et al., 1979). The apparent displacement direction of this fault (northwest-side-down) is opposite that of the fault near Golden, but the relative timing of faulting in the two locations has not been determined.

COMBINED REFERENCES

- Abbott, J. C., and Goodwin, L. B., 1995, A spectacular exposure of the Tijeras fault, with evidence for Quaternary motion, New Mexico Geological Society, Guidebook 46.
- Abbott, J. C., Cather, S. M., and Goodwin, L. B., 1995, Paleogene synorogenic sedimentation in the Galisteo basin related to the Tijeras-Cañoncito fault system, New Mexico Geological Society, Guidebook 46.
- Allen, J. R. L., 1967, Notes on some fundamentals of paleocurrent analysis, with reference to preservation potential and sources of variance: *Sedimentology*, v. 9, p. 75-88.
- Atkinson, W. W., 1961, Geology of the San Pedro Mountains, Santa Fe County, New Mexico, New Mexico Bureau of Mines and Mineral Resources, Bulletin 77, 49 p.
- Baars, D. L., 1982, Paleozoic history of the Albuquerque trough: implications of basement control on Rio Grande Rift: New Mexico Geological Society, Guidebook 33, p. 153-157.
- Bachman, G. O., 1975, Geologic Map of the Madrid Quadrangle, Santa Fe and Sandoval Counties, New Mexico: U. S. Geological Survey, Geologic Quadrangle Map GQ-1268, scale 1:62,500.
- Bachman, G. O., and Mehnert, H. H., 1978, New K-Ar dates and the late Pliocene to Holocene geomorphic history of the central Rio Grande region, New Mexico: Geological Society of America Bulletin, v. 89, p. 283-292.
- Beck, W. C., and Chapin, C. E., 1991, Structural data from the Joyita Uplift: implications for Ancestral Rocky Mountain deformation within central and southern New Mexico: New Mexico Geological Society, Guidebook 42, p. 183-190.
- Best, M. G., 1988, Early Miocene change in direction of least principle stress, southwestern United States: conflicting inferences from dikes and metamorphic core-detachment fault terranes: *Tectonics*, v. 8, no. 2, p. 249-259.
- Booth, F. O., 1976, Geology of the Galisteo Creek Area, Lamy to Cañoncito, Santa Fe County, New Mexico [M.S. thesis]: Golden, Colorado School of Mines, 122 p.

- Bruns, J. J., 1959, Petrology of the Tijeras Greenstone, Bernalillo County, New Mexico [M.S. thesis]: Albuquerque, University of New Mexico, 119 p.
- Cabezas, P., 1991, The southern Rocky Mountains in west-central New Mexico- Laramide structures and their impact on the Rio Grande rift extension: *New Mexico Geology*, v. 13, no. 2, p. 25-37.
- Cather, S. M., 1989, Post-Laramide tectonic and volcanic transition in west-central New Mexico: *New Mexico Geological Society, Guidebook 40*, p. 91-97.
- Cather, S. M., 1992, Suggested revisions to the Tertiary tectonic history of north-central New Mexico: *New Mexico Geological Society, Guidebook 43*, p. 109-122.
- Cavin, W. J., 1985, Precambrian geology of the Manzanita Mountains, Bernalillo County, New Mexico [M.S. thesis]: Albuquerque, University of New Mexico, 144 p.
- Chapin, C. E., 1988, Axial basins of the northern and central Rio Grande rifts; *in* Sloss, L. L., ed., *Sedimentary Cover - North American Craton: U.S.: The Geology of North America*, vol. D-2: Boulder, Colorado, Geological Society of America, p. 165-170.
- Chapin, C. E., 1989, Volcanism along the Socorro accommodation zone, Rio Grande rift, New Mexico: *New Mexico Bureau of Mines and Mineral Resources, Memoir 46*, p. 46-57.
- Chapin, C. E., and Cather, S. M., 1981, Eocene tectonics and sedimentation in the Colorado Plateau - Rocky Mountain area: *Arizona Geological Society, Digest*, v. 14, p. 173-198.
- Chapin, C. E., Chamberlin, R. M., Osburn, G. R., Sanford, A. R., and White, D. L., 1978, Exploration framework for the Socorro geothermal area, New Mexico: *New Mexico Geological Society, Special Publication 7*, p. 115-129.
- Chapin, M. A. and Nelson, E. P., 1986, Laramide basement-involved deformation in the Fra Cristobal Range, south-central New Mexico: *New Mexico Geological Society, Guidebook 37*, p. 107-114.

- Chester, F. M., Friedman, M., and Logan, J. M., 1985, Foliated cataclasites, *Tectonophysics*, v. 111, p. 139-146.
- Connolly, J. R., 1981, *Geology of the Precambrian rocks of Tijeras Canyon, Bernalillo County, New Mexico* [M.S. thesis]: Albuquerque, University of New Mexico, 147 p.
- Connolly, J. R., 1982, Structure and metamorphism in the Precambrian Cibola gneiss and Tijeras greenstone, Bernalillo County, New Mexico: *New Mexico Geological Society, Guidebook* 33, p. 197-202.
- Corrigan, J., 1991, Inversion of apatite fission-track data for thermal history information, *Journal of Geophysical Research*, v. B-96, no. 6, p. 10,347-10,360.
- Disbrow, A. E. and Stoll, W. C., 1957, *Geology of the Cerrillos area, Santa Fe County, New Mexico*: New Mexico Bureau of Mines and Mineral Resources, Bulletin 48, 73 p.
- Emerick, W. L., 1950, *Geology of the Golden area, Santa Fe County, New Mexico* [M.S. thesis]: Albuquerque, University of New Mexico, 66 p.
- Fleuty, M. J., 1975, Slickensides and slickenlines: *Geological Magazine*, v. 112, no. 3, p. 319-322.
- Gibbons, J. F., 1990, Tectonic disruption of Tijeras Canyon drainage: *New Mexico Geology*, v. 12, no. 4, p. 93.
- Goolsby, R. S., 1965, *Geology of the Lamy-Canoncito Area, Santa Fe County, New Mexico* [M.S. thesis]: Albuquerque, University of New Mexico, 68 p.
- Gorham, T. W., 1979, *Geology of the Galisteo Formation, Hagan Basin, New Mexico* [M.S. thesis]: Albuquerque, University of New Mexico, 136 p.
- Gorham, T. W. and Ingersoll, R. V., 1979, Evolution of the Eocene Galisteo Basin, north-central New Mexico: *New Mexico Geological Society, Guidebook* 30, p. 219-224.
- Hamilton, W. B., 1981, Plate tectonic mechanism of Laramide deformation; *in* Boyd, D. W., and Lillegraven, J. A., eds., *Rocky Mountain foreland basement tectonics*: Laramie, University of Wyoming Contributions to Geology, v. 19, p. 87-92.

- Harrison, E. P., 1949, Geology of the Hagan coal basin [Ph. D. dissertation]: Albuquerque, University of New Mexico, 177 p.
- Harrison, T. M., Armstrong, R. I., Naeser, C. W., and Harakal, J. E., 1979, Geochronology and thermal history of the Coast Plutonic Complex, near prince Rupert, British Columbia, Canadian Journal of Earth Sciences, v. 16, p. 400-410.
- Hayden, F. N., 1869, Third annual report of the United States geological survey of the territories embracing Colorado and New Mexico, including a report by Percifor Frazer, Jr., titled 'On mines and minerals of Colorado': Washington, D. C., Department of the Interior.
- Holmes, W. H., 1877, Report on the San Juan district, Colorado: U. S. Geological Survey Geog. Survey Terr., 9th Annual Report for 1875, p. 245, 248.
- Hurford, A. J., 1985, On the closure temperature for fission tracks in zircon: Nuclear Tracks and Radiation Measurement, v. 10, p. 415.
- Huzarski, J. R., 1971, Petrology and structure of the eastern Monte Largo Hills, New Mexico [M.S. thesis]: Albuquerque, University of New Mexico, 45 p.
- Ingersoll, R. V., Cavazza, W., Baldrige, W. S., and Shafiqullah, M., 1990, Cenozoic sedimentation and paleotectonics of north-central New Mexico: implications for initiation and evolution of the Rio Grande rift: Geological Society of America Bulletin, v. 102, p. 1280-1296.
- Johnson, R. B., 1975, Geologic map of the Galisteo Quadrangle, Santa Fe County, New Mexico: U. S. Geological Survey, Geological Quadrangle Map GQ-1234, scale 1:24,000.
- Karlstrom, K., et al., 1994, Geologic map of the Tijeras 7.5' quadrangle, New Mexico Bureau of Mines and Mineral Resources, Socorro, New Mexico, Open-file Report 396.
- Karlstrom, K. E., and Daniel, C. G., 1993, Restoration of Laramide right-lateral strike slip in northern New Mexico using Proterozoic piercing points: tectonic implications from the Proterozoic to the Cenozoic: Geology, v. 21, p. 1139-1142.

- Kay, B. D., 1986, Vein and breccia gold mineralization and associated igneous rocks at the Ortiz Mine, New Mexico, U.S.A. [M.S. thesis]: Golden, Colorado School of Mines, 179 p.
- Keller, G. R., and Cather, S. M., eds., 1994, Basins of the Rio Grande Rift: Structure, Stratigraphy, and Tectonic Setting: Boulder, Colorado, Geological Society of America, Special Paper 291, 304 p.
- Kelley, S. A., and Duncan, I. J., 1984, Tectonic history of the northern Rio Grande rift derived from apatite fission-track geochronology, New Mexico Geological Society, Guidebook 35, p. 67-73.
- Kelley, V. C., 1982, The right-relayed Rio Grande rift, Taos to Hatch, New Mexico: New Mexico Geological Society, Guidebook 33, p. 147-151.
- Kelley, V. C., and Northrop, S. A., 1975, Geology of Sandia Mountains and vicinity, New Mexico: New Mexico Bureau of Mines and Mineral Resources, Memoir 29, 136 p.
- Kirby, E., Karlstrom, K. E., Andronicos, C. L., and Dallmeyer, R. D., 1995, Tectonic setting of the Sandia pluton: An orogenic 1.4 Ga granite in New Mexico: *Tectonics*, v. 14, no. 1, p. 185-201.
- Krishnaswami, S., Lal, D., Prabhu, N., and Macdougall, D., 1974, Characteristics of fission-tracks in zircon: Applications to geochronology and cosmology: *Earth and Planetary Science Letters*, v. 22, p. 51-59.
- Lambert, P. W., 1961, Petrology of the Precambrian rocks of part of the Monte Largo area, New Mexico [M.S. thesis]: Albuquerque, University of New Mexico, 108 p.
- Lewis, C. J., and Baldrige, W. S., 1994, Crustal extension in the Rio Grande rift, New Mexico: Half-grabens, accommodation zones, and shoulder uplifts in the Ladron Peak - Sierra Lucero area; *in* Keller, G. R., and Cather, S. M., eds., Basins of the Rio Grande Rift: Structure, Stratigraphy, and Tectonic Setting: Boulder, Colorado, Geological Society of America Special Paper 291, p. 135-155.
- Lisenbee, A. L., 1967, Geology of the Cerro Pelon - Arroyo de la Jara area, Santa Fe County, New Mexico [M.S. thesis]: Albuquerque, University of New Mexico, 112 p.

- Lisenbee, A. L., 1976, Shale diapirism and the structural development of the Galisteo syncline, Santa Fe County, New Mexico: New Mexico Geological Society, Special Publication 6, p. 88-94.
- Lisenbee, A. L., Woodward, L. A., and Connolly, J. R., 1979, Tijeras-Cañoncito fault system - a major zone of recurrent movement in north-central New Mexico: New Mexico Geological Society, Guidebook 30, p. 89-99.
- Lozinsky, R. P., 1988, Stratigraphy, sedimentology, and sand petrology of the Santa Fe Group and pre-Santa Fe Tertiary deposits in the Albuquerque Basin, central New Mexico [Ph. D. dissertation]: Socorro, New Mexico Institute of Mining and Technology, 298 p.
- Lozinsky, R. P., 1994, Cenozoic stratigraphy, sandstone petrology, and depositional history of the Albuquerque Basin, central New Mexico: *in* Keller, G. R., and Cather, S. M., eds., Basins of the Rio Grande Rift: Structure, Stratigraphy, and Tectonic Setting: Boulder, Colorado, Geological Society of America Special Paper 291, p. 73-81.
- Lucas, S. G., 1982, Vertebrate paleontology, stratigraphy, and biostratigraphy of Eocene Galisteo Formation, north-central New Mexico: New Mexico Bureau of Mines and Mineral Resources, Circular 186, 34 p.
- Machette, M. N., 1982, Quaternary and Pliocene faults in the La Jencia and southern part of the Albuquerque-Belen Basins, New Mexico: Evidence of fault history from fault scarp morphology and Quaternary geology: New Mexico Geological Society, Guidebook 33, p. 161-169.
- Martinez, R., 1989, Summary of Laramide Orogeny in New Mexico; *in* Lorenz, J. C. and Lucas, S. G., eds., Energy Frontiers in the Rockies: Albuquerque, Albuquerque Geological Society, p. 171-176.
- May, S. J., and Russell, L. R., 1994, Thickness of the syn-rift Santa Fe Group in the Albuquerque Basin and its relation to structural style; *in* Keller, G. R., and Cather, S. M., eds., Basins of the Rio Grande Rift: Structure, Stratigraphy, and Tectonic Setting: Boulder, Colorado, Geological Society of America Special Paper 291, p. 113-123.

- Maynard, S. R., Nelsen, C. J., Martin, K. W., and Schutz, J. L., 1990, Geology and gold mineralization of the Ortiz Mountains, Santa Fe County, New Mexico: *Mining Engineering*, v. 42, p. 1007-1011.
- Maynard, S. R., Woodward, L. A., and Giles, D. L., 1991, Tectonics, intrusive rocks, and mineralization of the San Pedro - Ortiz porphyry belt, north-central New Mexico: *New Mexico Bureau of Mines and Mineral Resources, Bulletin 137*, p. 57-69.
- Miall, A. D., 1978, Lithofacies types and vertical profile models in braided rivers: A summary; *in* Miall, A. D., ed., *Fluvial Sedimentology*: Canadian Society of Petroleum Geologists, *Memoir 5*, p. 597-604.
- Miller, J. P., Montgomery, A., and Sutherland, P. K., 1963, Geology of part of the southern Sangre de Cristo Mountains, New Mexico: *New Mexico Bureau of Mines and Mineral Resources, Memoir 11*, 106 p.
- Molenaar, C. M., 1977, Stratigraphy and depositional history of upper Cretaceous rocks of the San Juan Basin area, New Mexico and Colorado, with a note on economic resources: *New Mexico Geological Society, Guidebook 28*, p. 159-166.
- Molenaar, C. M., 1983, Major depositional cycles and regional correlations of Upper Cretaceous rocks, southern Colorado Plateau and adjacent areas; *in* Reynolds, M. W., and Dolly, E. E., eds., *Mesozoic paleogeography of the west-central United States*: Society of Economic Geologists and Mineralogists, Rocky Mountain section, Rocky Mountain Paleogeography Symposium 2, p. 201-224.
- Myers, D. A. and McKay, E. J., 1976, Geologic Map of the north end of the Manzano Mountains, Tijeras and Sedillo Quadrangles, Bernalillo County, New Mexico: U. S. Geological Survey, *Miscellaneous Geologic Investigations Map I-968*, scale 1:24,000.
- Naeser, C. W., 1979, Fission-track dating and geologic annealing of fission-tracks; *in* Jager, E., and Hunziker, J. C., eds., *Lectures in Isotope Geology*: Springer-Verlag, New York, p. 154-169.

- Naeser, C. W., and Naeser, N. D., 1989, Laboratory procedures and techniques; *in* Crowley, K. D., Naeser, C. W., and Naeser, N. D., eds., *Fission-track Analysis: Theory and Applications: Geological Society of America, Short Course*, chapter 3.
- Naeser, N. D., 1989, Thermal history of sedimentary basins; *in* Crowley, K. D., Naeser, C. W., and Naeser, N. D., eds., *Fission-track Analysis: Theory and Applications: Geological Society of America, Short Course*, chapter 5.
- Petit, J. P., 1987, Criteria for the sense of movement on fault surfaces in brittle rocks: *Journal of Structural Geology*, v. 9, no. 5/6, p.597-608.
- Russell, L. R., and Snelson, S., 1990, Structural style and tectonic evolution of the Albuquerque Basin segment of the Rio Grande rift; *in* Pinet, B., and Bois, C., eds., *The potential of deep seismic profiling for hydrocarbon exploration: Paris, Editions Technip*, p. 175-207.
- Russell, L. R., and Snelson, S., 1994, Structure and tectonics of the Albuquerque Basin segment of the Rio Grande rift: Insights from seismic reflection data; *in* Keller, G. R., and Cather, S. M., eds., *Basins of the Rio Grande Rift: Structure, Stratigraphy, and Tectonic Setting: Boulder, Colorado, Geological Society of America Special Paper 291*, p. 83-112.
- Salyards, S. L., Ni, J. F., and Aldrich, M. J., Jr., 1994, Variation in paleomagnetic rotations and kinematics of the north-central Rio Grande rift, New Mexico; *in* Keller, G. R., and Cather, S. M., eds., *Basins of the Rio Grande Rift: Structure, Stratigraphy, and Tectonic Setting: Boulder, Colorado, Geological Society of America Special Paper 291*, p. 59-71.
- Sanford, A. R., Jaksha, L. H., and Cash, D. J., 1991, Seismicity of the Rio Grande rift in New Mexico; *in* Slemmons, D. B., Engdahl, E. R., Zoback, M. D., and Blackwell, D. D., eds., *Neotectonics of North America, Geological Society of America, Decade Map*, v. 1, p. 229-244.
- Sibson, R. H., 1977, Fault rocks and fault mechanisms: *Journal of the Geological Society of London*, v. 133, p. 191-213.

- Slack, P. B., and Campbell, J. A., 1976, Structural geology of the Rio Puerco fault zone and its relationship to central New Mexico tectonics; *in* Woodward, L. A., and Northrop, S. A., eds., Tectonics and mineral resources of southwestern North America: New Mexico Geological Society, Special Publication 6, p. 46-52.
- Smith, N. D., 1972, Some sedimentary aspects of planar cross-stratification in a sandy braided river: *Journal of Sedimentary Petrology*, v. 42, no. 3, p. 624-634.
- Starkey, J., 1977, The contouring of orientation data represented in spherical projection: *Canadian Journal of Earth Sciences*, v. 14, p. 268-277.
- Stearns, C. E., 1943, The Galisteo Formation of north-central New Mexico: *Journal of Geology*, v. 51, p. 301-319.
- Stearns, C. E., 1953, Tertiary geology of the Galisteo-Tonque area, north-central New Mexico: *Geological Society of America Bulletin*, v. 64, p. 459-508.
- Vernon, R. H., 1986, Oriented growth of sillimanite in andalusite, Placitas - Juan Tabo area, New Mexico, U.S.A.: *Canadian Journal of Earth Sciences*, v. 24, p. 580-590.
- Wagner, G., and Van den Haute, P., 1992, *Fission-Track Dating*: Ferdinand Enke Verlag, Germany, 285 p.
- Woodward, L. A., 1984, Basement control of Tertiary intrusions and associated mineral deposits along Tijeras-Canoncito fault system, New Mexico: *Geology*, v. 12, p. 531-533.

APPENDIX A

Sedimentological data from the Galisteo basin in the Cerrillos-Lamy area. Site numbers are keyed to maps in Plate 1. Bedding orientation is given as the strike direction, dip value, and dip direction. Informal lithostratigraphic unit is indicated. Percentages of conglomerate, sandstone, and mudstone in an outcrop are given under cg-ss-ms. Miall facies (1978) and maximum and mean clast sizes (in cm) at most sites are also provided. Types of paleocurrent indicators (PI) include solitary (α) and grouped (o) planar crossbeds, solitary (θ) and grouped (π) channel crossbeds, imbricated pebbles and cobbles (I), and ripple cross-laminations (r). Orientation of paleocurrent indicator is given as the strike and dip of foreset on planar crossbeds and ripple cross-laminations, and of the face of imbricated clasts. The pitch (rake) of the channel axis measured in the plane of bedding is given for channel crossbeds; direction of flow is given as "out" (of the ground), or "in" (into the ground). The quality of each measurement is given as good or poor, depending on the degree to which three-dimensional control on the structure could be established in the field. Restored paleocurrent azimuths were computed by restoring bedding to horizontal by one rotation about the line of strike. Clast composition indicates the percentages of quartzite (qtz), limestone (ls), sandstone (ss), mudstone (ms), granitic (gran), and metamorphic (meta) clasts.

site	unit	bedding	cg-ss-ms	Miall	max clast	mean clast	PI	paleocurrent	qual.	restored	clast composition
1	lower	061, 71 nw		Sp			α	056, 50 nw	good	140	
2	lower	083, 79 nw		Sp			o	043, 79 nw	good	130	
3	lower	063, 82 se		Sp			α	038, 60 nw	good	122	
4	lower	059, 85 nw		Sp			α	065, 60 nw	good	161	
5	lower	065, 71 nw		St			π	85 sw (out)	good	341	
6	lower	061, 78 nw		Sp			o	040, 57 nw	good	112	
7	lower	051, 90		St			π	75 ne (out)	good	308	
8	lower	055, 85 nw		St			π	85 sw (out)	good	330	
9	?	067, 73 nw		Sp			α	084, 70 n	good	236	
10	?	063, 78 nw		Sp			α	051, 66 se	good	351	
11	?	057, 60 nw		Sp			o	027, 68 nw	good	48	
12	?	045, 80 nw		Sp			α	034, 90	poor	2	
13	?	036, 71 nw		Sp			α	027, 60 w	poor	90	
14	?	021, 64 nw		Gm, Gt	4	1.5	o	000, 78 w	poor	349	95 qtz, 5 ss
15	?	006, 80 w		Gp	2	1	α	337, 73 w	poor	22	
16	upper	050, 30 se		Sp	1	0.5	α	320, 20 ne	poor	356	
17	upper	050, 30 se		Gt	4	1.5	π	90 (out)	poor	320	
18	upper	027, 37 se		Sp	1	0.5	α	000, 29 e	good	344	
19	upper	045, 36 se		Sp	4	2	α	026, 27 e	good	355	75 qtz, 25 ls
20	upper	045, 36 se		Sp	3	2	α	030, 43 se	good	67	75 qtz, 25 ls
21	upper	000, 42 e		Sp	1	0.5	α	000, 65 e	good	90	50 ls, 50 qtz
22	upper	063, 65 se		Gp, Gt	8	5					90 qtz, 10 ls
23	upper	063, 29 se		Gp	8	3	α	063, 36 se	good	341	85 ss, 5 ms, 5 ls, 5 qtz
24	upper	063, 29 se		Gp	20	3	I	70 s (out)	good	352	85 ss, 5 ms, 5 ls, 5 qtz
25	upper	062, 75 se		Sr	3	0.5	r	038, 55 se	good	2	
26	upper			Gt	8	3					90 qtz, 5 ss, 5 ls
27	upper	081, 81 s		Sp			α	051, 68 se	good	211	

28	upper	060, 62 se	Gt	20	1								95 qtz, 5 meta, 5 gran, 5 ls
29	upper	060, 62 se	Sp	2	0.5	α	076, 56 se		good		94		95 qtz, 5 meta, 5 gran, 5 ls
30	upper	062, 44 e	Sr			r	085, 70 se		poor		208		
31	upper	058, 42 e	Sp			α	061, 61 se		poor		159		
32	upper	041, 51 e	Sp			α	030, 51 se		good		25		
33	upper	050, 38 se	Gt			⊖	086, 9 s		poor		313		
34	upper	049, 31 se	Sp			o	062, 43 se		poor		179		
35	upper	049, 31 se	Sp										
36	upper	032, 27 se	Sp			α	029, 38 se		good		112		
37	upper	032, 27 se	Sp			o	028, 25 se		good		160		
38	upper	032, 27 se	Sp			o	050, 34 se		good		183		
39	upper	032, 27 se	Sp			o	356, 42 e		good		44		
40	upper	032, 27 se	Sp			o	343, 48 e		good		36		
41	upper	023, 36 e	Sp			α	029, 50 e		good		135		
42	upper	022, 39 e	Sp			o	013, 52 e		good		81		
43	upper	025, 31 e	Sp			o	065, 33 e		good		43		
44	upper	046, 45 e	St	6	0.6	π	90 (in)		good		136		50 ss, 25 qtz, 25 ls
45	upper	052, 39 e	Sp			α	043, 29 e		good		345		
46	upper	052, 39 e	Sp			o	080, 52 s		good		217		
47	upper	052, 39 e	Sp			o	283, 43 s		poor		258		
48	upper	052, 39 e	Sp			o	061, 58 se		good		171		
49	upper	048, 57 e	Sp			o	059, 43 e		good		293		
50	upper	048, 41 e	Sp			o	040, 58 e		good		116		
51	upper	028, 29 se	Sp			o	035, 46 e		good		137		
52	upper	079, 35 se	Gp	6	2	α	277, 11 s		good		340		80 ls, 10 ss, 5 qtz, 5 meta
53	upper	066, 35 se	Gp	45	1.5	I	35 ne (in)		poor		102		90 ls, 10 ss
54	upper	069, 39 se	Sp	3	1.5	α	033, 53 e		good		82		
55	upper	051, 31 se	Sp	20	6	α	000, 53 e		poor		61		35 ss, 35 ls, 30 qtz
56	upper	031, 30 se	Sp			α	059, 45 se		good		184		40 ss, 40 qtz, 20 ls

57	upper	031, 30 se		Sp	30	4	α	014, 37 se	poor	54	41 ss, 40 qtz, 20 ls
58	upper	042, 29 se		Sp	10	3	α	066, 34 se	good	213	42 ss, 40 qtz, 20 ls
59	upper	017, 32 e		Sp			α	064, 45 se	poor	194	
60	upper	033, 33 e		Sp	8	3	α	072, 48 s	good	198	35 ss, 35 qtz, 30 ls
61	upper	054, 85 se		Sp	10	1	α	033, 59 se	good	358	50 ls, 25 ss, 25 qtz
62	upper	045, 63 se		St	10	2	Θ	45 ne (in)	good	90	
63	upper	046, 30 se	0-60-40	Sp	8	2	α	023, 31 e	good	38	35 ss, 35 ls, 30 qtz
64	upper	053, 32 se	0-100-0	Sp			π	035, 35 se	good	55	
65	upper	072, 20 se	0-100-0	Sp	2	0.5	α	284, 48 s	good	210	
66	upper	065, 28 se	0-100-0	Sp	4	1	α	282, 22 s	good	283	40 ls, 40 ss, 20 qtz
67	upper	035, 17 e	0-100-0	Sp	5	2	α	010, 34 e	poor	80	35 ls, 35 ss, 30 qtz
68	upper	046, 15 se	0-100-0	Sp	8	2	α	068, 31 se	good	175	35 ls, 35 ss, 30 qtz
69	upper	044, 88 se	0-100-0	Sp			α	034, 69 nw	poor	111	
70	upper	355, 25 e	0-100-0	Sp			o	327, 53 e	good	41	
71	upper	298, 35 e	0-100-0	Sp			o	341, 25 e	good	161	
72	upper	027, 29 se	0-100-0	Sp			o	354, 34 e	good	28	
73	upper	340, 19 e	0-100-0	Sp			o	348, 38 e	good	85	
74	upper	022, 21 e	0-100-0	Sp			o	044, 36 se	good	158	
75	upper	000, 16 e	0-100-0	Sp			o	001, 42 e	poor	91	
76	upper	027, 53 e	0-100-0	Sp			α	023, 70 se	good	106	
77	upper	302, 32 ne	0-100-0	Sp			o	350, 23 e	good	165	
78	upper	328, 36 ne	0-100-0	Sp			o	314, 30 ne	good	295	
79	upper	013, 24 e	0-100-0	Sp			o	001, 37 e	good	70	
80	upper	328, 21 e	0-100-0	Sp			α	342, 35 e	poor	89	
81	upper	330, 30 ne	0-100-0	St			π	45 ne (in)	good	15	
82	upper	013, 17 e	0-100-0	Sp			o	022, 31 se	poor	122	
83	upper	020, 13 e	0-100-0	Sp			o	024, 24 se	good	119	
84	upper	043, 70 nw	0-30-70	Sp			o	045, 71 nw	poor	270	

113	lower	286, 10 n	1-70-29	Sp	2	mU	α	318, 28 ne	good	60	
114	lower	344, 10 e	0-70-30	Sp	mU	mU	α	320, 19 n	poor	21	
115	lower	330, 15 ne	0-70-30	Sp	cL	mU	α	020, 33 e	good	135	
116	lower	330, 15 ne	0-70-30	Sp	cL	mU	α	354, 31 e	good	100	
117	lower	320, 10 e	1-70-29	Sp	2	mU	α	330, 30 e	good	63	50 qtz, 50 ms
118	lower	345, 5 e	0-70-30	Sp	cL	mU	α	310, 20 ne	good	28	
119	lower	300, 7 ne	0-70-30	Sp	0.5	cU	α	286, 35 n	good	12	100 qtz
120	lower	300, 3 ne	0-70-30	St		mU					
121	lower	331, 10 ne	0-70-30	Sp	mL	mL	α	298, 19 ne	good	359	
122	lower	310, 13 ne	0-70-30	Sp	cL	cL	α	029, 29 se	good	142	
123	lower	009, 11 e	0-70-30	Sp	mU	mU	α	335, 22 ne	poor	38	
124	lower	022, 15 se	0-70-30	Sp	cU	cU	α	310, 32 n	good	15	
125	lower	328, 10 ne	0-70-30	Sp	cL	cL	α	028, 32 se	good	134	
126	lower	305, 18 ne	0-70-30	Sp	mU	mL	α	305, 26 ne	good	25	
127	lower	352, 15 e	0-70-30	Sp	mU	mU	α	300, 15 ne	poor	326	
128	lower	286, 15 n	0-70-30	Sp	mU	mU	α	013, 19 se	good	141	
129	lower	298, 35 e	0-70-30	Sp	mU	mU	α	012, 32 e	good	154	
130	lower	330, 23 e	0-70-30	Sp	cU	cU	α	310, 39 ne	good	18	
131	lower				1.5	cL					75 qtz, 25 ss
132	lower	335, 10 ne	0-60-40	Sp	1	mL	o	064, 22 se	poor	178	85 qtz, 15 ss
133	lower	003, 11 e	0-60-40	Sp	mU	mU	α	023, 32 se	poor	121	
134	lower	305, 10 e	0-60-40	Sp	cU	mU	α	013, 23 se	poor	128	
135	lower	305, 10 e	0-60-40	Sp	cU	mU	α	295, 25 ne	poor	17	
136	lower	350, 12 e	0-60-40	Sp	cL	cL	α	340, 31 ne	good	62	
137	lower	313, 23 ne	0-70-30	Sp	mU	mU	α	307, 24 ne	poor	337	
138	lower	329, 6 e	0-70-30	Sp	0.5	mU	α	030, 20 se	poor	138	80 qtz, 10 ms, 10 ss
139	lower	329, 6 e	0-70-30	Sp	0.5	mU	o	034, 21 se	good	142	80 qtz, 10 ms, 10 ss
140	lower	329, 6 e	0-70-30	Sp	0.5	mU	o	320, 42 ne	good	48	80 qtz, 10 ms, 10 ss

141	lower	329, 6 e	0-70-30	Sp	mU	mU	α	332, 50 ne	good	62	
142	lower	340, 15 ne	0-70-30	Sp	cL	mU	α	324, 30 ne	good	38	
143	lower	010, 17 e	0-70-30	Sp	2	mU	α	344, 45 ne	good	63	80 qtz, 10 ms, 10 ss
144	lower	050, 11 se		Sp	1.5	mU	α	326, 12 ne	poor	10	
145	lower	050, 11 se		Sp	1.5	mU	α	028, 30 se	good	107	
146	lower	340, 10 ne	0-70-30	Sp	0.5	mL	α	326, 54 ne	poor	54	90 qtz, 5 ss, 5 ms
147	lower	337, 10 ne	0-70-30	Sp	1	mU	α	330, 25 ne	poor	57	95 qtz, 3 ss, 2 ms
148	lower	337, 10 ne	0-70-30	Sp	mU	mU	α	336, 24 ne	poor	61	
149	lower	342, 12 ne	0-60-40	Sp	cL	mU	α	304, 33 ne	good	18	
150	lower	324, 16 ne	0-60-40	Sp	0.5	mU	α	312, 34 ne	good	32	90 qtz, 5 ms, 5 ss
151	lower	315, 10 ne	0-60-40	Sp	1.5	mU	o	326, 28 ne	good	61	90 qtz, 5 ms, 5 ss
152	upper	335, 10 ne	0-60-40	Sp	mL	mL	o	350, 33 e	good	84	
153	upper	011, 10 e	0-60-40	Sp	1	mU	α	077, 28 se	poor	187	85 qtz, 15 ss+ms
154	upper	004, 15 e	1-60-39	Sp	4	cU	α	297, 25 n	poor	352	
155	upper	005, 5 e	1-60-39	Sp	2	cU	α	055, 24 se	poor	155	85 qtz, 10 ls, 5 ss
156	upper	329, 5 sw	0-60-40	Sp	mL	mL	α	340, 15 w	poor	257	85 qtz, 10 ls, 5 ss
157	upper	346, 10 ne	0-60-40	Sp	mL	mL	o	300, 30 ne	good	12	
158	upper	321, 10 ne	5-50-45	Sp	30	cL	α	030, 43 se	good	131	65 ss, 35 ls
159	lower	048, 20 nw	0-60-40	Sp	mU	mU					
160	lower	065, 20 nw	0-60-40	Sp	mU	mU	α	304, 36 ne	poor	64	
161	lower	047, 20 nw	0-60-40	Sp	mU	mU	α	312, 17 ne	good	93	
162	lower	085, 40 n	0-60-40	Sp	mU	mU					
163	lower		3-60-37		3	mU					50 qtz, 50 ss
164	lower	039, 15 nw	0-60-40	Sp	mU	mU	α	053, 27 nw	poor	338	
165	lower	030, 15 nw	0-60-40	Sp	mU	mU	α	089, 23 n	poor	37	
166	lower	052, 15 nw	0-60-40	Sp	mU	mU	o	277, 24 n	good	331	
167	lower	357, 15 e	10-60-30	Sp	3	cL	α	309, 50 s	poor	208	90 qtz, 10 ss
168	lower	028, 42 se	3-60-37	Sp	3	cL	α	028, 32 se	poor	304	

169	lower	000, 70 e	5-60-35	Sp	2	cL	α	031, 63 se	poor	200	90 qtz, 10 ss
170	lower	000, 50 e	5-60-35	Sp	3	mU	o	023, 50 se	good	188	90 qtz, 10 ss
171	lower	047, 10 se	5-70-25	Sp	3	mU	o	049, 31 se	poor	141	90 qtz, 10 ss
172	lower	054, 15 se	5-70-25	Sp	2	mU	o	005, 32 e	poor	69	90 qtz, 10 ss
173	lower	015, 10 e	10-70-20	Sp	2	mU	o	352, 31 e	poor	72	90 qtz, 10 ss
174	lower	015, 10 e	10-70-20	Sp	2	mU	o	342, 18 e	poor	42	90 qtz, 10 ss
175	lower	354, 15 e	10-70-20	Sp	4	mU	α	063, 29 se	poor	183	90 qtz, 10 ss
176	lower	354, 15 e	10-70-20	Sp	2	mU	α	337, 17 ne	poor	4	90 qtz, 10 ss
177	lower	322, 2 e	10-70-20	Sp	mU	mU	α	351, 17 e	poor	85	
178	lower	051, 12 se	5-70-25	Sp	mU	mU	α	031, 35 se	poor	111	
179	lower	039, 43 nw	0-60-40	Sp	mU	mU	α	010, 45 w	poor	217	
180	lower	059, 42 nw	0-70-30	Sp	mU	mU					
181	lower	040, 23 nw	0-75-25	Sp	1	mU	α	316, 10 ne	poor	106	75 qtz, 25 ss
182	lower	326, 33 ne	5-70-25	Sp	0.5	mU	o	016, 12 e	poor	217	75 qtz, 25 ss
183	lower	308, 15 ne	0-70-30	Sp	mU	mL	o	048, 5 se	poor	202	
184	lower	308, 15 ne	0-70-30	Sp	mU	mL	o	080, 24 n	poor	327	
185	lower	324, 18 ne	0-70-30	Sp	mU	mU	α	050, 20 se	good	183	
186	lower	320, 10 ne	0-70-30	Sp	mU	mU	α	076, 30 se	poor	179	
187	lower	357, 18 e	0-70-30	Sp	mU	mU	α	011, 44 e	poor	109	
188	lower	010, 33 w	0-70-30	Sp	mU	mU	α	039, 42 nw	poor	354	
189	lower	006, 35 w	0-70-30	Sp	mU	mL	α	000, 20 w	good	102	
190	lower	058, 13 nw	0-70-30	Sp	mU	mL	α	006, 23 e	good	113	
191	lower	043, 15 nw	0-70-30	Sp	mU	mL	o	302, 30 ne	good	58	
192	lower	043, 15 nw	0-70-30	Sp	mU	mL	o	064, 35 nw	good	345	
193	lower	005, 12 e	0-70-30	Sp	mU	mL	o	086, 10 s	good	235	
194	lower	034, 16 nw	0-70-30	Sp	mL	mL	o	005, 8 e	good	114	
195	lower	034, 16 nw	0-70-30	Sp	mL	mL	o	025, 36 nw	good	290	
196	lower	073, 13 n	1-70-29	Sp	1	mL	α	350, 13 e	good	121	

197	lower	347, 10 e	1-70-29	Sp	1.5	mL	α	054, 25 se	good	168	100 ms
198	lower	280, 10 n	1-70-29	Sp	1	mL	α	311, 23 n	good	57	
199	lower	277, 8 n	0-70-30	Sp	mL	mL	α	312, 26 n	poor	53	
200	lower	318, 10 ne	0-70-30	Sp	mL	mL	α	307, 20 s	poor	221	
201	lower	292, 6 n	0-70-30	Sp	mL	mL	o	318, 15 n	good	55	
202	lower	292, 6 n	0-70-30	Sp	mL	mL	o	071, 27 w	good	332	
203	lower	056, 10 nw	0-70-30	Sp	mL	mL	α	009, 11 e	good	121	
204	lower	056, 10 nw	0-70-30	Sp	mL	mL	α	349, 14 e	poor	105	
205	lower	056, 10 nw	0-70-30	Sp	mL	mL					
206	lower	060, 8 nw	0-70-30	Sp	mL	mL	α	030, 14 se	good	133	
207	lower	307, 11 n	0-70-30	Sp	mL	mL	α	285, 31 ne	good	3	
208	lower	308, 9 ne	0-70-30	Sp	mL	mL	α	305, 32 ne	good	34	
209	lower	303, 10 ne	0-80-20	Sp	mL	mL	o	342, 32 ne	poor	84	
210	lower	280, 4 n	0-80-20	Sp	mL	mL					
211	lower	021, 27 nw	3-70-27	Sp	1.5	fU	α	274, 18 n	good	72	90 qtz, 10 ss
212	lower	021, 27 nw	3-70-27	Sp	1.5	fU	α	090, 24 n	good	57	90 qtz, 10 ss
213	lower	067, 14 se	0-60-40	Sp	mL	fU	α	280, 17 n	good	356	
214	upper	314, 19 ne	0-50-50	Sp	1.5	cU	o	012, 24 e	poor	151	100 ms
215	upper	314, 19 ne	0-50-50	Sp	1.5	cU	o	354, 24 e	poor	136	100 ms
216	upper	314, 19 ne	0-50-50	Sp	1.5	cU	o	240, 20 ne	poor	148	100 ms
217	upper	314, 19 ne	0-50-50	Sp	cU	cL	o	000, 17 e	poor	166	
218	upper	026, 25 se	0-60-40	Sp	cL	mL	α	322, 38 ne	poor	17	
219	upper	000, 5 e	0-60-40	Sp	mU	fU	o	344, 21 e	poor	67	
220	upper	000, 5 e	0-60-40	Sp	mU	fU	o	310, 17 ne	poor	21	
221	upper	310, 13 ne	0-60-40	Sp	mL	mL	α	293, 26 ne	good	7	
222	upper	017, 14 e	0-70-30	Sr	mL	mL	r	000, 0	poor	288	
223	upper	336, 11 n	0-70-30	Sr	mL	mL	r	277, 17 s	poor	210	
224	upper	348, 7 e	0-70-30	Sp	mU	mL	α	009, 22 e	good	107	
225	upper	279, 10 n	0-70-30	Sp	cU	mU	α	351, 32 e	good	97	

226	upper	322, 8 e	5-70-25	Sp	2	mU	o	000, 20 e	good	109	100 qtz
227	upper	281, 7 n	5-70-25	Sp	15	cL	o	340, 10 e	poor	114	100 ms
228	upper	281, 7 n	0-70-30	Sp	cU	cL	o	354, 17 e	poor	107	
229	upper	281, 7 n	0-70-31	Sp	mL	mL	α	346, 12 e	poor	112	
230	upper	082, 7 n	0-70-32	Sp	1	mU	α	062, 21 se	poor	144	85 qtz, 15 ss
231	upper	307, 9 ne	0-70-33	Sp	1.5	mU	o	013, 17 se	poor	136	85 qtz, 15 ss
232	upper	307, 9 ne	0-70-34	Sp	2	mU	o	002, 21 e	poor	115	85 qtz, 15 ss
233	upper	297, 9 ne	0-70-35	Sp	2	mU	o	293, 32 n	poor	20	85 qtz, 15 ss
234	upper	086, 37 n	0-10-90	Sp	1	mL	α	008, 12 e	poor	17	100 qtz
235	upper	089, 9 n	0-5-95	Sp	mL	mL					
236	upper	057, 9 nw	0-50-50	Sp	mU	mL	o	077, 24 n	poor	357	
237	upper	067, 21 nw	0-50-50	Sp	mL	fU	o	300, 23 ne	poor	86	
238	upper	054, 55 nw	0-60-40	St	fU	fU					
239	upper	054, 50 nw	0-60-40	Sp	fU	fU	α	083, 57 n	poor	47	
240	upper	075, 8 n	0-60-40	Sp	mL	mL	o	036, 24 se	poor	136	
241	upper	075, 8 n	0-60-40	Sp	mL	mL	o	339, 27 ne	poor	84	
242	upper	075, 8 n	0-60-40	Sp	mL	mL	o	326, 23 ne	good	73	
243	upper	075, 8 n	0-60-40	Sp	mL	mL	o	288, 28 n	poor	28	
244	upper	275, 11 n	0-60-40	Sp	mL	mL	α	008, 11 e	poor	143	
245	upper	275, 11 n	0-60-40	Sp	mL	mL	α	014, 16 e	poor	135	
246	upper	315, 8 ne	0-50-50	Sp	mL	mL	α	307, 37 n	poor	37	
247	lower	065, 2 nw	0-30-70	Sp	mL	mL	α	077, 31 nw	good	347	
248	lower	283, 20 n	0-30-70	Sp	mL	mL	α	320, 33 ne	good	82	
249	lower	064, 3 nw	0-30-70	Sp	mL	mL	α	323, 26 ne	poor	58	
250	lower	050, 6 nw	0-40-60	Sp	mL	mL	α	052, 17 nw	poor	324	
251	lower	270, 4 n	0-60-40	Sp	mL	mL	o	343, 30 s	poor	247	
252	lower	270, 4 n	0-60-40	Sp	mL	mL	o	299, 16 ne	poor	36	
253	lower	270, 2n	2-65-33	Sp	5	mL	α	071, 19 se	poor	162	90 qtz, 10 ss

254	lower	270, 2n	0-65-35	Sp	mL	mL	α	012, 23 w	poor	279
255	lower	292, 8 n	0-65-35	Sp	mL	mL	α	333, 11 s	good	226
256	lower	292, 8 n	0-65-35	Sp	mL	mL	α	343, 14 s	good	238
257	lower	292, 2 n	0-65-35	Sp	mL	mL	α	019, 17 sw	good	116
258	lower	295, 4 n	0-65-35	Sp	mL	mL	α	290, 21 s	good	202
259	lower	295, 2 n	0-65-35	Sp	mL	mL	α	069, 19 sw	good	163
260	lower	295, 3 n	0-65-35	Sp	mL	mL	α	322, 31 ne	good	55
261	lower	295, 4 n	0-65-35	Sp	mL	mL	o	325, 20 ne	good	58
262	lower	075, 5 ne	0-60-40	Sp	mL	mL	α	312, 29 s	good	216
263	lower	075, 5 ne	5-60-35	Sp	4	mL	α	319, 18 s	good	218 100 qtz
264	lower	075, 6 n	0-60-40	Sp	mL	mL	α	344, 20 w	poor	240
265	lower	038, 18 nw	0-70-30	Sp	mL	mL	α	083, 38 n	good	17
266	lower	038, 8 nw	0-70-30	Sp	mL	mL	o	330, 12 ne	good	84
267	lower	080, 10 n	0-70-30	Sp	mL	mL	o	280, 34 n	good	16
268	lower	015, 16 w	0-75-25	Sp	mL	mL	α	328, 1 sw	good	107
269	lower	070, 24 nw	0-75-25	Sp	mL	mL	α	090, 42 n	good	20
270	lower	070, 31 n	0-75-25	Sp	mL	mL	α	276, 43 n	poor	42
271	lower	074, 25 nw	0-75-25	Sp	mL	mL	α	295, 43 ne	good	55
272	lower	070, 16 n	0-75-25	Sp	mL	mU	α	283, 24 n	good	48
273	lower	016, 5 s	0-30-69	Sp	1.5	mL	α	317, 25 ne	good	37 100 qtz
274	lower	016, 5 s	0-30-70	Sp	mL	mL	α	020, 27 e	poor	111
275	lower	000, 8 e	0-30-70	Sp	mL	mL	α	047, 35 se	good	148
276	lower	000, 8 e	0-30-70	Sp	mL	mL	α	044, 30 se	good	146
277	lower	000, 8 e	0-30-70	Sp	mL	mL	α	326, 29 ne	good	42
278	lower	000, 8 e	0-30-70	Sp	mL	mL	α	322, 43 ne	good	45
279	lower	000, 8 e	0-30-70	Sp	mL	mL	α	330, 50 ne	good	45
280	lower	000, 8 e	0-30-70	Sp	mL	mL	α	082, 23 s	good	192
281	lower	000, 8 e	0-30-70	Sp	mL	mL	α	332, 46 ne	good	57

282	lower	040, 5 se	0-30-70	Sp	mL	mL	o	038, 10 se	poor	125	
283	lower	040, 5 se	0-30-70	Sp	mL	mL	o	044, 15 se	good	139	
284	lower	040, 5 se	0-30-70	Sp	mL	mL	o	012, 17 e	poor	90	
285	lower	350, 6 e	0-30-70	Sp	mL	mL	o	350, 27 e	poor	79	
286	lower	350, 6 e	0-30-70	Sp	mL	mL	o	330, 25 ne	poor	52	
287	lower	350, 6 e	0-30-70	Sp	mL	mL	α	315, 15 se	poor	237	
288	?	346, 13 e	0-55-45	Sp	mL	mL	α	346, 35 e	good	74	
289	?	040, 13 se	0-55-45	Sp	mL	mL	α	090, 24 s	poor	212	
290	?	045, 12 se	0-55-45	Sp	mL	mL	α	300, 6 ne	poor	339	
291	?	000, 8 e	0-60-40	Sp	mU	mL	o	000, 24 e	poor	90	
292	?	000, 8 e	0-60-40	Sp	mU	mL	α	044, 27 se	poor	150	
293	?	000, 4 e	0-60-40	Sp	mU	mL	α	341, 38 ne	poor	69	
294	?	340, 6 e	0-60-40	Sp	mU	mL	α	351, 26 e	poor	83	
295	?	326, 10 ne	0-60-40	Sp	mU	mL	α	065, 18 se	good	182	
296	?	326, 10 ne	0-60-40	Sp St	2	mL	α	282, 9 s	good	220	100 qtz
297	upper	070, 20 n	3-40-57	St	2	mU	⊖	090, 20 n	poor	77	90 qtz, 10 ss
298	upper	013, 25 w	0-50-50	Sp	mL	mL	α	043, 25 nw	good	22	
299	upper	071, 21 nw	0-55-45	Sp	0.5	mL	α	294, 26 ne	poor	76	
300	upper	313, 13 ne	0-55-45	Sp	cU	cL	α	299, 30 ne	poor	18	
301	upper	313, 13 ne	0-55-45	Sp	1	cL	α	285, 30 n	poor	356	95 qtz, 3 ms, 2 ls
302	upper	286, 24 n	0-55-45	Sp	0.5	mL	α	346, 24 e	poor	135	
303	upper	286, 24 n	0-55-45	Sp	0.5	mL	α	280, 5 n	poor	199	
304	upper		5-55-40	Gm	12	cL					60 qtz, 40 ls
305	upper	013, 22 s	0-60-40	Sp	1	cL	α	049, 18 nw	good	300	95 qtz, 5 ms
306	upper	013, 22 s	0-60-40	Sp	1	cL	α	270, 3 s	poor	275	95 qtz, 5 ms
307	upper	055, 24 nw	0-60-40	Sp	cU	cL	α	345, 15 sw	poor	184	
308	upper	040, 23 nw	0-60-40	Sp	cL	cL	α	002, 55 w	poor	257	
309	upper	040, 23 nw	0-60-40	Sp	cL	cL	α	011, 35 w	good	250	

310	upper	039, 25 nw	0-60-40	Sp	cL	cL	α	033, 35 nw	good	295	
311	lower	016, 13 w	15-70-15	Sp	5	mU	o	032, 32 w	poor	310	
312	lower	016, 13 w	15-70-15	Sp	8	mU	o	358, 40 w	poor	261	
313	lower	016, 13 w	15-70-15	Sp	5	mU	α	035, 40 w	good	311	70 qtz, 20 ss, 10 ms
314	lower	046, 11 nw	0-85-15	Sp	mL	mL	α	078, 25 nw	good	8	70 qtz, 20 ss, 10 ms
315	lower	025, 22 nw	10-70-20	Sp	4	mU	o	080, 22 n	good	50	70 qtz, 20 ss, 10 ms
316	lower	025, 22 nw	10-70-20	Sp	3	mU	o	030, 15 se	poor	118	70 qtz, 20 ss, 10 ms
317	lower	145, 18 nw	5-55-40	Sp Gm	2	1	α	135, 32 ne	poor	32	
318	lower	005, 21 w	5-55-40	Sp Gm	2	1	α	040, 30 nw	good	348	
319	lower	066, 15 n	5-55-40	Sp Gm	2	1	α	127, 37 ne	good	57	
320	lower	066, 15 n	5-55-40	Sp Gm	2	1	α	107, 27 n	good	46	
321	lower	035, 15 nw	5-55-40	Sp Gm	2	1	α	090, 38 n	good	20	
322	lower	035, 15 nw	5-55-40	Sp Gm	2	1	α	155, 34 nw	poor	80	
323	lower	030, 10 nw	5-55-40	Sp Gm	2	1	α	028, 55 nw	good	297	
324	lower	030, 13 nw	5-55-40	Sp Gt	6	1	α	127, 20 nw	poor	65	
325	lower	030, 13 nw	5-55-40	Sp Gt	6	1	α	004, 32 w	good	259	
326	lower	030, 13 nw	5-55-40	Sp Gt	2	1	α	015, 35 w	good	278	
327	lower	030, 13 nw	5-55-40	Sp Gt	2	1	α	005, 43 w	good	256	
328	lower	050, 20 nw	5-55-40	Sp Gt	2	1	α	110, 30 n	good	58	
329	upper	100, 45 n		Sp			α	070, 52 n	poor	288	
330	upper	125, 37 n		Sp			α	122, 65 n	poor	28	
331	upper	135, 55 n		Sp			α	113, 53 n	poor	302	
332	upper	120, 52 n		Sp			α	133, 57 n	poor	98	
333	upper	125, 57 n		Sp			α	117, 65 n	poor	353	
334	upper	092, 45 n		Sp			α	105, 35 n	poor	150	
335	upper	131, 77 n		Sp			α	000, 75 e	poor	141	
336	upper	089, 13 n		Sp			α	130, 33 n	poor	57	
337	upper	101, 56 n		Sp			α	119, 51 n	poor	128	

APPENDIX B

Detailed log of the streamcut exposure near Golden (Fig. 2-1). Section measured and described from southeast (upstream) to northwest (downstream).

<u>Unit</u>	<u>Description</u>	<u>Width (m)</u>
1	Quaternary(?) pebbly gravel surficial deposit. Largely clast supported, with typical clasts ranging from 1-4 cm in diameter. The unit has a moderately well developed horizontal stratification defined by flat-lying tabular pebbles. In a zone 10-15 cm wide immediately adjacent to unit 2, the horizontal stratification has been completely overprinted by a strong vertical fabric defined by vertically oriented elongate pebbles. The fabric is interpreted to be created by re-orientation of pebbles along a fault contact with unit 2 (Figs. 2-2a and 2-6).	> 1
2	Quaternary(?) carbonate-rich mottled clay. This unit is predominantly clay, but also contains several outsized cobbles up to 30 cm in maximum diameter. The unit has a strong, northeast-trending, sub-vertical fabric defined by anastomosing white fault gouge zones and vertically oriented elongate cobbles. The contact with unit 3 is a vertical zone 5-10 cm wide of anastomosing gouge-filled faults orientated 062°, 90° (Figs. 2-2a and 2-6).	0.5
3	Oligocene(?) porphyritic intrusive rock. Most of the unit is strongly brecciated, though lens-shaped pods of somewhat less fractured rock are locally present. This unit contains several zones 5-30 cm wide of anastomosing gouge-filled faults. The contact with unit 4 is a zone of anastomosing faults 5 cm wide (Figs. 2-2a and 2-6).	2.5
4	Dark brown breccia zone. Identification of the parent rock(s) was not possible due to very strong brecciation, though the presence of some quartz grains suggests that it may have been derived in part from the Cibola gneiss. There is a very strong cataclastic fabric oriented 050°, 90°. The contact with unit 5 is a gradational zone of anastomosing faults 5 cm wide, oriented 072°, 62° NW (Fig. 2-2a).	1.2
5	Proterozoic Cibola gneiss. This unit is composed of roughly equal amounts of relatively intact blocks of gneiss and a matrix of strongly brecciated gneiss (Fig. 2-2a). The blocks are typically 1-2 m in diameter, and preserve the original gneissic foliation. The strongly	

brecciated gneiss has a well developed cataclastic fabric, which generally strikes east-northeast and dips 40° - 70° NNW. The fabric locally wraps around the intact blocks. Iron staining is common. Gouge filled fault zones 1-40 cm wide are common throughout the unit. The gneiss is overlain by a Holocene(?) imbricated gravel surficial deposit, which appears to be faulted in two places (Fig. 2-7). In one place, a large, elongate cobble in the surficial deposit lies in the plane of a fault in the Cibola gneiss. This cobble may have rotated by faulting. In a second place, about 1.5 m downstream, a fault appears to juxtapose Cibola gneiss against the imbricated gravel surficial deposit. Excavation, however, demonstrates that the fault is truncated by a channel deposit, and therefore is older than the surficial deposit.

17.7

6 Proterozoic Cibola gneiss. The unit is largely intact Cibola gneiss, though locally it is punctuated by brecciated rock. A steeply southeast-dipping gneissic foliation is clearly visible in most of the unit, though 1- 20 cm wide zones of fault gouge and breccia are locally evident. A fault oriented 130° , 60° NE separates this unit from unit 7. 11.0

7 Proterozoic Cibola gneiss. Most of the unit is strongly brecciated and altered. A 1-m-wide block of relatively intact Cibola gneiss retains a gneissic foliation, though the block itself is highly fractured and shatters easily under the blow of a hammer (Fig. 2-5). Numerous 1-4 cm wide fault gouge zones are present; many of these zones are contorted and may be traced for only a few centimeters. An older fault oriented 129° , 86° N is cut by a younger fault oriented 078° , 85° S with an apparent left-lateral offset of a few centimeters. The contact with unit 8 is a contorted fault gouge zone 1-5 cm wide. 3.8

8 Upper Paleozoic(?) black shales, Proterozoic Cibola gneiss, and limestone of the Pennsylvanian Madera Group (Fig. 2-2b). This unit is a zone in which faulting has mixed rocks of different lithologies and ages. Most of this unit is black, brown, and tan shales interbedded with numerous 1-2-cm-thick beds of limestone and a 10-cm-wide tan sandstone bed. This is probably part of the Pennsylvanian Sandia Formation or Madera Group. Bedding is complexly folded, and is unrecognizable in the shales. The limestone beds are generally discontinuous over 10-30 cm, but a few may be traced across the 1 m height of the outcrop. Individual limestone beds are clearly folded, but often these folds appear to involve only one limestone bed, with adjacent beds having a different fold pattern. There are two larger folds that involve several beds. Both of these are tight and steeply plunging with fold hinges oriented 100° , 62° and 171° , 66° . The Upper Paleozoic(?) black shales locally contain pods of very strongly brecciated Proterozoic Cibola gneiss. Near the center of the unit,

Proterozoic Cibola gneiss and limestones of the Pennsylvanian Madera Group are mixed into the black shales. The Cibola gneiss is very strongly brecciated and contains numerous zones of fault gouge. The gneiss resembles grus in hand sample. There is a well developed, sub-vertical, cataclastic fabric in the gneiss, but no evidence of the original gneissic foliation. The Cibola gneiss contains several pods of black shale that also contain a sub-vertical fabric. Some shale pods are at least 80 cm long and 30 cm wide. A knocker of gray limestone of the Madera Group is set in a matrix of very strongly brecciated Cibola gneiss (Figs. 2-2b and 2-4). The block is oriented sub-vertically, parallel to the cataclastic fabric in the gneiss. Another block of gray fossiliferous limestone of the Madera Group trends northeast and stands sub-vertically about 2.5 m high. It is set in black shales. The block is teardrop-shaped in cross-section; the top is about 1.3 m thick, and it pinches out at the streambed. It also appears to pinch out along strike. A sharp fault contact separates this unit from unit 9. 17.6

9 Proterozoic Cibola gneiss. The gneiss is very strongly brecciated, and the original gneissic foliation has been destroyed. The gneiss has the appearance of grus, and is easily dug out of the streamcut with a pick. Numerous sub-vertical faults strike 072° . A vertical fault striking 066° marks the contact with unit 10. 4.8

10 Zone of extreme shearing. Identification of the parent rock is not possible in the field. Several fault gouge zones are present. There are a few quartz-rich clasts 2-5 cm in diameter, which suggests that at least part of the unit may be derived from the Cibola gneiss. A fault oriented 052° , 82° W separates this unit from unit 11. 1.2

11 Proterozoic Cibola gneiss. This unit is similar to unit 9. A few brecciated quartz-rich clasts 1-3 cm in diameter are present in this very strongly brecciated unit. The contact with unit 12 is a fault oriented 053° , 90° . 0.8

12 Oligocene(?) porphyritic intrusive rock. The porphyritic intrusive rock is light tan and intensely brecciated. The unit is highly brecciated, and is easily excavated with a pick. No intact, unfractured blocks are present. The contact with unit 13 is abrupt. 2.2

13 Fault gouge. This unit consists of dark gray to black clay containing several clasts of porphyritic intrusive rock 4-8 cm in diameter, and was probably derived from the porphyritic intrusive rock. The clay unit is oriented 060° , 85° NW, and varies from 10-20 cm in thickness. The contact with unit 14 is abrupt. 0.2

- 14 Proterozoic Cibola gneiss. This unit is very similar to unit 9. The rock is strongly brecciated; no evidence of the original gneissic foliation exists, and there are no intact blocks of gneiss. A few intensely brecciated quartz-rich clasts are present, as well as numerous 1-2 cm thick fault gouge zones. The contact with unit 15 is abrupt. 1.7
- 15 Fault gouge. This unit is similar to unit 13. The contact with unit 16 is abrupt. 0.2
- 16 Oligocene(?) porphyritic intrusive rock. Most of this unit is intensely brecciated in the same manner as unit 12, though more intact blocks are locally present (Fig. 2-3). These blocks are fractured and shatter easily under the blow of a hammer. In hand sample, light-colored rectangular grains 1-5 cm in diameter are visible, and are interpreted to be plagioclase crystals that have since altered to clays. Also visible in hand sample are black, lath-shaped crystals generally 5 mm long, which are probably hornblende. There are numerous high-angle fault gouge zones 1-2 cm in width. A fault oriented 062° , 71° SE separates this unit from unit 17. 6.2
- 17 Rock flour. Identification of the parent material is impossible in the field. The unit is tan in color, and does not exhibit a cataclastic fabric. A fault oriented 049° , 90° separates unit 17 from unit 18. 0.5
- 18 Oligocene(?) porphyritic intrusive rock. This unit is similar in character to unit 16. Most of the unit is intensely brecciated, though several intact blocks are present. In this unit an older fault oriented 000° , 66° E is cut by a younger fault oriented 071° , 82° SE. A fault oriented 072° , 84° SE separates this unit from unit 19. 2.5
- 19 Permian(?) sandstones. Sandstones are yellowish-brown and tan and are cemented with carbonate. This unit may be derived from the San Ysidro Member of the Permian Yeso Formation. The unit was brecciated into clasts 2-4 cm in diameter and subsequently cemented. 4.4
- bedrock not exposed 12.9
- 20 Permian(?) sandstone. Coarse, red sandstone is locally brecciated. Sand grains are 1-5 mm in diameter. This unit is probably from the Permian Abo Formation. 0.4
- bedrock not exposed 0.8

- 21 Limestone of the Pennsylvanian Madera Group. Gray, fossiliferous limestone with numerous chert nodules. Bedding is oriented 046°, 65°SE. A single fault slickenside oriented 019°, 87°W has fault striae with a pitch of 38°N, recording oblique-slip motion. 4.3
- bedrock not exposed 3.7
- 22 Limestone of the Pennsylvanian Madera Group. Thick, gray, fossiliferous limestone beds. 3.9
- bedrock not exposed 6.4
- 23 Limestone of the Pennsylvanian Madera Group. Thick, gray, fossiliferous limestone beds oriented 160°, 57° NE. 5.1
- bedrock not exposed 2.7
- 24 Fault gouge. The gouge is yellowish-brown and gray and exhibits a steeply dipping cataclastic foliation. Smaller gouge zones cross-cut the cataclastic foliation. This unit is in fault contact with unit 25. 1.2
- 25 Permian Abo Formation, approximately 75% maroon mudstone and 25% sandstone. Bedding in all mudstones is destroyed and replaced by a cataclastic foliation oriented 025°, 90°. Sandstone beds are generally only slightly fractured. Two bed orientations are: 000°, 90° and 026°, 65°W. The latter has a slickenside surface oriented 008°, 70°E with fault striae having a pitch of 82°N, recording dip-slip motion on a high-angle fault. 6.9
- bedrock not exposed 5.7
- 26 Permian Abo Formation. Red sandstones and mudstones are cut by several gouge zones 1-10 cm thick. Two of these zones are oriented 145°, 80°NE and 080°, 90°. 3.8
- bedrock not exposed 1.2
- 27 Permian Abo Formation, approximately 80% red sandstone and 20% red mudstone. Bedding dips approximately 40°NE, which is considerably less steep than elsewhere upstream in the main part of the fault zone. The sandstone is locally intensely brecciated

with a well developed cataclastic foliation. The foliation wraps around a series of fault-bounded blocks about 0.5 m across. The faults that bound the blocks are high-angle, dipping $\geq 72^\circ$. The resulting geometry of blocks resembles a series of horsts and grabens. A few meters downstream, reduction spots have been offset by a number of small, high-angle faults with apparent offsets of 1-5 cm. This creates a similar geometry of horsts and grabens on a smaller scale. Many fault gouge zones are present, though the fault gouge is less clayey and more silty than upstream. All bedding in mudstones has been destroyed. 11.1

bedrock not exposed 5.7

28 Permian Abo Formation. This unit is composed of beds of red sandstone oriented 165° , 37°E . It is essentially intact, but includes abundant slickenside surfaces. 3.3

29 Permian Abo Formation. Bedding in red mudstone is locally preserved. 2.9

Total width = 162 m

APPENDIX C

Minor fault and fault slickenside data for rocks in the streamcut exposure near Golden. Faults vary in scale from hand-sample-size slickenside surfaces to outcrop-scale faults. Pitch refers to the angle of pitch (rake) of slickenlines on a slickenside surface. Orientations of the metamorphic foliation in the Cibola gneiss at the measurement sites are presented, as are bedding orientations in the Upper Paleozoic strata. Sense-of-slip on a slickenside surface is interpreted using the criteria outlined by Petit (1987). Oblique slickenlines record two components of motion (strike-slip and dip-slip). The dominant component is listed first; the subordinate component is listed second. Sense-of-slip criteria on slickensides are subdivided into those that form by friction (secondary fractures) and those that form by mineral growth (slickenfibers).

unit(s)	lithologic unit(s)	fault	pitch	foliation / bedding	sense of slip	sense of slip criteria
2 and 3	unit 2 & Olp	062, 90				
3	Olp	065, 80 nw				
3	Olp	012, 40 w				
4	unit 4	050, 90				
5	Cibola gneiss	072, 62 nw		071, 76 nw		
5	Cibola gneiss	070, 57 nw		073, 73 nw		
5	Cibola gneiss	012, 68 e		073, 73 nw		
5	Cibola gneiss	006, 33 w		064, 80 nw		
5	Cibola gneiss	140, 83 sw				
5	Cibola gneiss	031, 65 se				
5	Cibola gneiss	050, 50 nw				
5	Cibola gneiss	066, 70 ne				
5	Cibola gneiss	039, 64 se				
5	Cibola gneiss	090, 83 s				
6	Cibola gneiss	011, 56 w				
6	Cibola gneiss	050, 55 nw				
6	Cibola gneiss	022, 76 e				
6	Cibola gneiss	025, 73 se				
6	Cibola gneiss	135, 55 sw		030, 90		
6	Cibola gneiss	030, 65 se				
6 and 7	Cibola gneiss	130, 60 ne		035, 75 se		
7	Cibola gneiss	084, 82 n				
7	Cibola gneiss	021, 78 w				
7	Cibola gneiss	129, 86 n				
7	Cibola gneiss	078, 85 s				
8	black shales	051, 70 se		090, 90		
9	Cibola gneiss	072, 90				
9 and 10	gneiss and unit 10	066, 90				
10 and 11	gneiss and unit 10	052, 82 w				
11 and 12	gneiss and Olp	053, 90				
12	Olp	024, 74 w				
16 and 17	Olp and unit 17	062, 71 se				
17 and 18	Olp and unit 17	049, 90				
18	Olp	071, 82 se				
18	Olp	000, 62 e				
18 and 19	Olp and Yeso(?)	072, 84 se				
19	Yeso(?)	090, 81 s				

21	Madera	019, 87 w	38 n	046, 65 se		
25	Abo	008, 70 e	82 e	026, 65 w		
26	Abo	145, 80 ne				
26	Abo	080, 90				
27	Abo	052, 73 nw		118, 40 n		
27	Abo	012, 85 e		118, 40 n		
27	Abo	061, 85 se		118, 40 n		
27	Abo	177, 86 w		122, 39 n		
28	Abo	075, 65 w	4 w	165, 37 e		
28	Abo	164, 73 e	0	165, 37 e		
28	Abo	085, 70 s	25 w	165, 37 e		
28	Abo	086, 76 s	0	165, 37 e		
28	Abo	150, 71 sw	5 e	165, 37 e	right-lateral & reverse	secondary fractures
28	Abo	057, 90	10 s	165, 37 e		
28	Abo	112, 42 s	37 se	165, 37 e		
28	Abo	100, 40 s	41 w	165, 37 e		
28	Abo	060, 80 s	35 sw	165, 37 e		
28	Abo	087, 44 s	45 e	165, 37 e		
28	Abo	132, 75 sw	37 nw	165, 37 e	right-lateral & normal	secondary fractures
28	Abo	145, 74 sw	73 nw	165, 37 e		
28	Abo	110, 80 s	0	165, 37 e		
28	Abo	085, 35 s	52 ne	165, 37 e		
28	Abo	052, 80 nw	54 ne	165, 37 e		
28	Abo	063, 53 s	0	165, 37 e		
28	Abo	044, 44 s	35 sw	165, 37 e		
28	Abo	070, 69 s	0	165, 37 e		

APPENDIX D

Fission-track age data

FISSION TRACK AGE DATA										
PROJECT NAME:	TJERAS FAULT		DATE:	3/29/95		FT AGE:	31.9 Ma			
SAMPLE NUMBER:	PORPHYRY		LATITUDE:	* N		UPPER CI:	36.2 Ma			
LAB NUMBER:	NMT		LONGITUDE:	*W		LOWER CI:	28.2 Ma			
REACTOR RUN NUMBER:	RR-10-19-94Z		ELEVATION (M):			STD ERR:	1.99 Ma			
NEUTRON FLUX:	1.600E+15		MICROSCOPE:	LEITZ		C. COEFF:	0.961			
# SPON TRACKS (FLUX)	600		MAGNIFICATION:	1000X		CHIP:	12.642		19	
# IND. TRACKS (FLUX)	4000		ROCK TYPE:	PORPHYRY		AVG. AGE:	31.0 Ma			
NUMBER OF GRAINS:	20		MINERAL:	ZIRCON		STD. ERR:	1.1			
GRAIN #	# GRIDS	AREA USED (SQ. CM)	Ns	RHO(S) (/CM ²)	Ni	RHO(I) (/CM ²)	RATIO (Ns/Ni)	URANIUM (PPM)	AGE (MA)	STD.DEV. (MA)
1. Y,SH	15	9.6E-06	30	3.125E+06	58	1.208E+07	0.52	725.0	24.7	5.7
2. Y,E	9	5.8E-06	17	2.951E+06	33	1.146E+07	0.52	687.5	24.6	7.4
3. Y,SH	10	6.4E-06	22	3.437E+06	33	1.031E+07	0.67	618.8	31.8	8.9
4. Y,E	25	1.6E-05	32	2.000E+06	43	5.375E+06	0.74	322.5	35.5	8.4
5. Y,SH	25	1.6E-05	65	4.063E+06	125	1.563E+07	0.52	937.5	24.8	4.0
6. Y,E	9	5.8E-06	22	3.819E+06	44	1.528E+07	0.50	916.7	23.9	6.3
7. Y,SH	25	1.6E-05	119	7.438E+06	147	1.838E+07	0.81	1102.5	38.6	5.1
8. Y,E	20	1.3E-05	84	6.562E+06	113	1.766E+07	0.74	1059.4	35.5	5.3
9. Y,E	25	1.6E-05	72	4.500E+06	100	1.250E+07	0.72	750.0	34.4	5.5
10. Y,E	15	9.6E-06	21	2.188E+06	37	7.708E+06	0.57	462.5	27.1	7.5
11. Y,E	20	1.3E-05	52	4.062E+06	74	1.156E+07	0.70	693.7	33.5	6.2
12. Y,E	20	1.3E-05	41	3.203E+06	67	1.047E+07	0.61	628.1	29.2	5.9
13. Y,E	16	1.0E-05	46	4.492E+06	70	1.367E+07	0.66	820.3	31.4	6.1
14. Y,E	25	1.6E-05	54	3.375E+06	63	7.875E+06	0.86	472.5	40.9	7.8
15. Y,E	25	1.6E-05	54	3.375E+06	75	9.375E+06	0.72	562.5	34.4	6.3
16. Y,SH	15	9.6E-06	23	2.396E+06	40	8.333E+06	0.58	500.0	27.5	7.3
17. Y,SH	15	9.6E-06	22	2.292E+06	37	7.708E+06	0.59	462.5	28.4	7.7
18. Y,E	9	5.8E-06	15	2.604E+06	23	7.986E+06	0.65	479.2	31.1	10.4
19. Y,E	8	5.1E-06	15	2.930E+06	24	9.375E+06	0.63	562.5	29.8	9.9
20. Y,E	8	5.1E-06	14	2.734E+06	20	7.813E+06	0.70	468.8	33.4	11.7
		2.2E-04	820	3.779E+06	1226	1.130E+07	0.67	678.1		

FISSION TRACK AGE DATA										
PROJECT NAME:	TJERAS FAULT		DATE:	3/29/95		FT AGE:	53.5 Ma			
SAMPLE NUMBER:	94ML05		LATITUDE:	* N		UPPER CI:	59.9 Ma			
LAB NUMBER:	NMT		LONGITUDE:	*W		LOWER CI:	47.9 Ma			
REACTOR RUN NUMBER:	RR-10-19-94Z		ELEVATION (M):			STD ERR:	2.98 Ma			
NEUTRON FLUX:	1.610E+15		MICROSCOPE:	LEITZ		C. COEFF:	0.120			
# SPON TRACKS (FLUX)	600		MAGNIFICATION:	1000X		CHIP:	554.624		24	
# IND. TRACKS (FLUX)	4000		ROCK TYPE:	SAND SANTA FE FM.		AVG. AGE:	67.5 Ma			
NUMBER OF GRAINS:	25		MINERAL:	ZIRCON		STD. ERR:	16.3			
GRAIN #	# GRIDS	AREA USED (SQ. CM)	Ns	RHO(S) (/CM ²)	Ni	RHO(I) (/CM ²)	RATIO (Ns/Ni)	URANIUM (PPM)	AGE (MA)	STD.DEV. (MA)
1. B,SH	15	9.6E-06	100	1.042E+07	22	4.583E+06	4.55	273.3	215.3	51.6
2. O,SH	25	1.6E-05	85	5.313E+06	136	1.700E+07	0.63	1013.7	30.0	4.4
3. B,E	10	6.4E-06	82	1.281E+07	41	1.281E+07	2.00	764.0	95.6	18.8
4. YB,SR	10	6.4E-06	54	8.438E+06	26	8.125E+06	2.08	484.5	99.3	24.1
5. Y,E	30	1.9E-05	66	3.438E+06	128	1.333E+07	0.52	795.0	24.8	3.9
6. B,SH	15	9.6E-06	49	5.104E+06	47	9.792E+06	1.04	583.9	50.0	10.4
7. B,SH	15	9.6E-06	39	4.063E+06	43	8.958E+06	0.91	534.2	43.5	9.8
8. B,SH	25	1.6E-05	96	6.000E+06	86	1.075E+07	1.12	641.0	53.5	8.3
9. B,SR	25	1.6E-05	221	1.381E+07	48	6.000E+06	4.60	357.8	218.0	36.0
10. B,SR	9	5.8E-06	74	1.285E+07	10	3.472E+06	7.40	207.0	346.9	117.9
11. YB,SH	9	5.8E-06	62	1.076E+07	26	9.028E+06	2.38	538.3	113.8	27.1
12. YB,SR	25	1.6E-05	81	5.063E+06	81	1.013E+07	1.00	603.7	48.0	7.8
13. YB,SH	15	9.6E-06	59	6.146E+06	65	1.354E+07	0.91	807.5	43.6	8.1
14. Y,SH	30	1.9E-05	206	1.073E+07	104	1.083E+07	1.98	646.0	94.7	12.1
15. B,SH	15	9.6E-06	46	4.792E+06	95	1.979E+07	0.48	1180.1	23.3	4.3
16. YB,SH	100	6.4E-05	11	1.719E+05	167	5.219E+06	0.07	311.2	3.2	1.0
17. Y,E	8	5.1E-06	23	4.492E+06	26	1.016E+07	0.88	605.6	42.5	12.3
18. B,SH	12	7.7E-06	60	7.812E+06	24	6.250E+06	2.50	372.7	119.3	29.3
19. B,E	25	1.6E-05	5	3.125E+05	56	7.000E+06	0.09	417.4	4.3	2.0
20. B,SH	25	1.6E-05	3	1.875E+05	36	4.500E+06	0.08	268.3	4.0	2.4
21. B,SH	25	1.6E-05	100	6.250E+06	85	1.063E+07	1.18	633.5	56.4	8.7
22. Y,SH	25	1.6E-05	53	3.313E+06	32	4.000E+06	1.66	238.5	79.3	18.1
23. YB,SH	15	9.6E-06	39	4.063E+06	39	8.125E+06	1.00	484.5	48.0	11.1
24. YB,SH	9	5.8E-06	25	4.340E+06	34	1.181E+07	0.74	703.9	35.3	9.4
25. YB,E	20	1.3E-05	40	3.125E+06	47	7.344E+06	0.85	437.9	40.9	9.0
		3.4E-04	1679	4.885E+06	1504	8.752E+06	1.12	521.9		

FISSION TRACK AGE DATA									
PROJECT NAME:	MONTE LARGO		DATE:	1/20/95		FT AGE:	59.3 Ma		
SAMPLE NUMBER:	94ML5		LATITUDE:	35°13.62' N		UPPER Ct:	72.6 Ma		
LAB NUMBER:	SMU		LONGITUDE:	106°15.66'W		LOWER Ct:	48.5 Ma		
REACTOR RUN NUMBER:	RR-11-29-94A		ELEVATION (M):	1988		STD ERR:	5.95 Ma		
NEUTRON FLUX:	9.000E+15		MICROSCOPE:	OLYMPUS		C. COEFF:	0.736		
# SPON TRACKS (FLUX)	600		MAGNIFICATION:	1250 X		CHIP:	39.052		19
# IND. TRACKS (FLUX)	4000		ROCK TYPE:	SANTA FE SANDSTONE		AVG. AGE:	53.0 Ma		
NUMBER OF GRAINS:	20		MINERAL:	APATITE		STD. ERR:	8.2		
GRAIN #	AREA USED (SQ. CM)	Ns	RHO(S) (/CM ²)	NI	RHO(I) (/CM ²)	RATIO (Ns/NI)	URANIUM (PPM)	AGE (MA)	STD.DEV. (MA)
1. SH	1.6E-05	15	9.375E+05	51	6.375E+06	0.29	68.0	78.7	23.4
2. SR	2.0E-05	4	2.000E+05	12	1.200E+06	0.33	12.8	89.1	51.6
3. SH	2.0E-05	0	0.000E+00	13	1.300E+06	0.00	13.9	0.0	60.0
4. SR	2.0E-05	12	6.000E+05	47	4.700E+06	0.26	50.1	68.4	22.3
5. SH	4.0E-05	6	1.500E+05	46	2.300E+06	0.13	24.5	35.0	15.3
6. SH	4.0E-05	5	1.250E+05	20	1.000E+06	0.25	10.7	67.0	33.6
7. R	2.0E-05	3	1.500E+05	29	2.900E+06	0.10	30.9	27.8	16.9
8. SR	2.0E-05	20	1.000E+06	43	4.300E+06	0.47	45.9	124.0	34.0
9. R	2.0E-05	11	5.500E+05	45	4.500E+06	0.24	48.0	65.5	22.2
10. R	4.0E-05	33	8.250E+05	98	4.900E+06	0.34	52.3	90.0	18.5
11. SH	2.0E-05	0	0.000E+00	6	6.000E+05	0.00	6.4	0.0	150.0
12. R	2.0E-05	7	3.500E+05	30	3.000E+06	0.23	32.0	62.5	26.4
13. SH	2.0E-05	2	1.000E+05	11	1.100E+06	0.18	11.7	48.8	37.5
14. SH	2.0E-05	5	2.500E+05	15	1.500E+06	0.33	16.0	89.1	46.2
15. SR	2.0E-05	9	4.500E+05	23	2.300E+06	0.39	24.5	104.5	41.3
16. R	2.0E-05	0	0.000E+00	5	5.000E+05	0.00	5.3	0.0	173.0
17. SR	2.0E-05	6	3.000E+05	92	9.200E+06	0.07	98.1	17.5	7.4
18. SH	2.0E-05	1	5.000E+04	8	8.000E+05	0.13	8.5	33.6	35.6
19. SH	2.0E-05	1	5.000E+04	9	9.000E+05	0.11	9.6	29.8	31.5
20. SH	2.0E-05	5	2.500E+05	52	5.200E+06	0.10	55.5	25.8	12.2
	4.6E-04	145	3.180E+05	655	2.873E+06	0.22	30.6		

FISSION TRACK AGE DATA

PROJECT NAME:	MONTE LARGO	DATE:	1/20/95	FT AGE:	25.9 Ma
SAMPLE NUMBER:	94ML4	LATITUDE:	35°13.63' N	UPPER CI:	31.7 Ma
LAB NUMBER:	SMU	LONGITUDE:	106°15.69'W	LOWER CI:	21.1 Ma
REACTOR RUN NUMBER:	RR-11-29-94A	ELEVATION (M):	1988	STD ERR:	2.62 Ma
NEUTRON FLUX:	9.000E+15	MICROSCOPE:	OLYMPUS	C. COEFF:	0.909
# SPON TRACKS (FLUX)	600	MAGNIFICATION:	1250 X	CHI²:	11.074 19
# IND. TRACKS (FLUX)	4000	ROCK TYPE:	CIBOLA GNEISS	AVG. AGE:	24.8 Ma
NUMBER OF GRAINS:	20	MINERAL:	APATITE	STD. ERR:	2.3

GRAIN #	AREA USED (SQ. CM)	Ns	RHO(S) (/CM²)	NI	RHO(I) (/CM²)	RATIO (Ns/NI)	URANIUM (PPM)	AGE (MA)	STD.DEV. (MA)
1	8.0E-05	6	7.500E+04	65	1.625E+06	0.09	17.3	24.8	10.6
2	4.0E-05	4	1.000E+05	34	1.700E+06	0.12	18.1	31.6	16.8
3	4.0E-05	10	2.500E+05	125	6.250E+06	0.08	66.7	21.5	7.1
4	4.0E-05	18	4.500E+05	161	8.050E+06	0.11	85.9	30.0	7.6
5	4.0E-05	5	1.250E+05	95	4.750E+06	0.05	50.7	14.2	6.5
6	4.0E-05	15	3.750E+05	115	5.750E+06	0.13	61.3	35.0	9.7
7	2.0E-05	14	7.000E+05	126	1.260E+07	0.11	134.4	29.8	8.5
8	4.0E-05	11	2.750E+05	97	4.850E+06	0.11	51.7	30.5	9.8
9	4.0E-05	8	2.000E+05	54	2.700E+06	0.15	28.8	39.8	15.2
10	2.0E-05	3	1.500E+05	42	4.200E+06	0.07	44.8	19.2	11.5
11	2.0E-05	4	2.000E+05	29	2.900E+06	0.14	30.9	37.0	19.8
12	2.0E-05	2	1.000E+05	36	3.600E+06	0.06	38.4	14.9	10.9
13	4.0E-05	6	1.500E+05	50	2.500E+06	0.12	26.7	32.2	14.0
14	4.0E-05	3	7.500E+04	21	1.050E+06	0.14	11.2	38.3	23.7
15	2.0E-05	3	1.500E+05	56	5.600E+06	0.05	59.7	14.4	8.6
16	4.0E-05	10	2.500E+05	135	6.750E+06	0.07	72.0	19.9	6.6
17	2.0E-05	3	1.500E+05	25	2.500E+06	0.12	26.7	32.2	19.7
18	2.0E-05	1	5.000E+04	20	2.000E+06	0.05	21.3	13.4	13.8
19	2.0E-05	3	1.500E+05	46	4.600E+06	0.07	49.1	17.5	10.5
20	4.0E-05	0	0.000E+00	8	4.000E+05	0.00	4.3	0.0	100.0
	6.8E-04	129	1.897E+05	1340	3.941E+06	0.10	42.0		

FISSION TRACK AGE DATA										
PROJECT NAME:	MONTE LARGO		DATE:	1/20/95		FT AGE:	25.1 Ma			
SAMPLE NUMBER:	94ML3		LATITUDE:	35°13.69' N		UPPER CI:	38.2 Ma			
LAB NUMBER:	SMU		LONGITUDE:	106°15.77'W		LOWER CI:	16.5 Ma			
REACTOR RUN NUMBER:	RR-11-29-94A		ELEVATION (M):	1988		STD ERR:	5.24 Ma			
NEUTRON FLUX:	9.000E+15		MICROSCOPE:	OLYMPUS		C. COEFF:	0.824			
# SPON TRACKS (FLUX)	600		MAGNIFICATION:	1250 X		CHP:	10.134	19		
# IND. TRACKS (FLUX)	4000		ROCK TYPE:	ABO SILTSTONE		AVG. AGE:	26.8 Ma			
NUMBER OF GRAINS:	20		MINERAL:	APATITE		STD. ERR:	5.5			
GRAIN #	AREA USED (SQ. CM)	Ns	RHO(S) (/CM ²)	Ni	RHO(I) (/CM ²)	RATIO (Ns/Ni)	URANIUM (PPM)	AGE (MA)	STD.DEV. (MA)	
1	2.0E-05	0	0.000E+00	3	3.000E+05	0.00	3.2	0.0	352.0	
2	2.0E-05	2	1.000E+05	15	1.500E+06	0.13	16.0	35.8	27.0	
3	7.2E-06	5	6.944E+05	53	1.472E+07	0.09	157.0	25.4	11.9	
4	2.0E-05	1	5.000E+04	10	1.000E+06	0.10	10.7	26.9	28.2	
5	1.6E-05	1	6.250E+04	5	6.250E+05	0.20	6.7	53.6	58.8	
6	2.0E-05	1	5.000E+04	16	1.600E+06	0.06	17.1	16.8	17.3	
7	7.2E-06	1	1.389E+05	3	8.333E+05	0.33	8.9	89.1	103.0	
8	1.2E-05	0	0.000E+00	15	2.500E+06	0.00	26.7	0.0	50.0	
9	7.2E-06	3	4.167E+05	16	4.444E+06	0.19	47.4	50.3	31.7	
10	1.2E-05	1	8.333E+04	12	2.000E+06	0.08	21.3	22.4	23.3	
11	1.2E-05	0	0.000E+00	4	6.667E+05	0.00	7.1	0.0	233.0	
12	7.2E-06	0	0.000E+00	2	5.556E+05	0.00	5.9	0.0	677.0	
13	7.2E-06	1	1.389E+05	6	1.667E+06	0.17	17.8	44.7	48.3	
14	2.0E-05	1	5.000E+04	10	1.000E+06	0.10	10.7	26.9	28.2	
15	7.2E-06	0	0.000E+00	15	4.167E+06	0.00	44.4	0.0	50.0	
16	1.2E-05	1	8.333E+04	12	2.000E+06	0.08	21.3	22.4	23.3	
17	1.2E-05	0	0.000E+00	1	1.667E+05	0.00	1.8	0.0	2655.0	
18	1.2E-05	3	2.500E+05	14	2.333E+06	0.21	24.9	57.4	36.6	
19	2.0E-05	1	5.000E+04	6	6.000E+05	0.17	6.4	44.7	48.3	
20	2.0E-05	4	2.000E+05	60	6.000E+06	0.07	64.0	17.9	9.3	
2.7E-04		26	9.587E+04	278	2.050E+06	0.09	21.9			

FISSION TRACK AGE DATA

PROJECT NAME:	MONTE LARGO	DATE:	1/20/95	FT AGE:	24.9 Ma
SAMPLE NUMBER:	94ML2	LATITUDE:	35°13.21' N	UPPER CI:	30.2 Ma
LAB NUMBER:	SMU	LONGITUDE:	106°16.11' W	LOWER CI:	20.5 Ma
REACTOR RUN NUMBER:	RR-11-29-94A	ELEVATION (M):	2027	STD ERR:	2.41 Ma
NEUTRON FLUX:	9.000E+15	MICROSCOPE:	OLYMPUS	C. COEFF:	0.861
# SPON TRACKS (FLUX)	600	MAGNIFICATION:	1250 X	CHI:	9.199 19
# IND. TRACKS (FLUX)	4000	ROCK TYPE:	GRANITE	AVG. AGE:	26.2 Ma
NUMBER OF GRAINS:	20	MINERAL:	APATITE	STD. ERR:	1.5

GRAIN #	AREA USED (SQ. CM)	Ns	RHO(S) (/CMP)	NI	RHO(I) (/CMP)	RATIO (Ns/NI)	URANIUM (PPM)	AGE (MA)	STD.DEV. (MA)
1	4.0E-05	12	3.000E+05	115	5.750E+06	0.10	61.3	28.0	8.6
2	2.0E-05	8	4.000E+05	95	9.500E+06	0.08	101.3	22.6	8.4
3	2.0E-05	5	2.500E+05	63	6.300E+06	0.08	67.2	21.3	10.0
4	2.0E-05	5	2.500E+05	50	5.000E+06	0.10	53.3	26.9	12.7
5	4.0E-05	4	1.000E+05	54	2.700E+06	0.07	28.8	19.9	10.4
6	4.0E-05	13	3.250E+05	90	4.500E+06	0.14	48.0	38.8	11.6
7	4.0E-05	8	2.000E+05	136	6.800E+06	0.06	72.5	15.8	5.8
8	2.0E-05	8	4.000E+05	64	6.400E+06	0.13	68.3	33.6	12.7
9	2.0E-05	10	5.000E+05	91	9.100E+06	0.11	97.1	29.5	9.9
10	2.0E-05	6	3.000E+05	69	6.900E+06	0.09	73.6	23.4	10.0
11	2.0E-05	4	2.000E+05	35	3.500E+06	0.11	37.3	30.7	16.3
12	4.0E-05	17	4.250E+05	236	1.180E+07	0.07	125.9	19.4	4.9
13	4.0E-05	3	7.500E+04	22	1.100E+06	0.14	11.7	36.6	22.6
14	4.0E-05	5	1.250E+05	52	2.600E+06	0.10	27.7	25.8	12.2
15	2.0E-05	3	1.500E+05	31	3.100E+06	0.10	33.1	26.0	15.8
16	2.0E-05	3	1.500E+05	63	6.300E+06	0.05	67.2	12.8	7.6
17	4.0E-05	12	3.000E+05	100	5.000E+06	0.12	53.3	32.2	9.9
18	2.0E-05	5	2.500E+05	48	4.800E+06	0.10	51.2	28.0	13.2
19	2.0E-05	5	2.500E+05	46	4.600E+06	0.11	49.1	29.2	13.8
20	4.0E-05	9	2.250E+05	106	5.300E+06	0.08	56.5	22.8	8.0
	5.8E-04	145	2.500E+05	1566	5.400E+06	0.09	57.6		

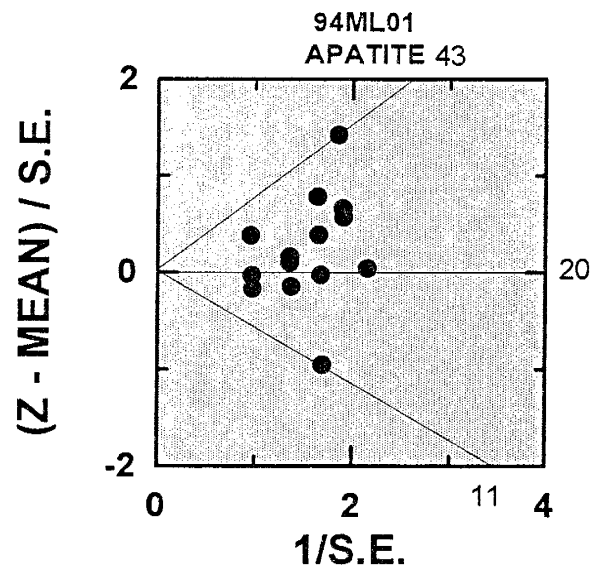
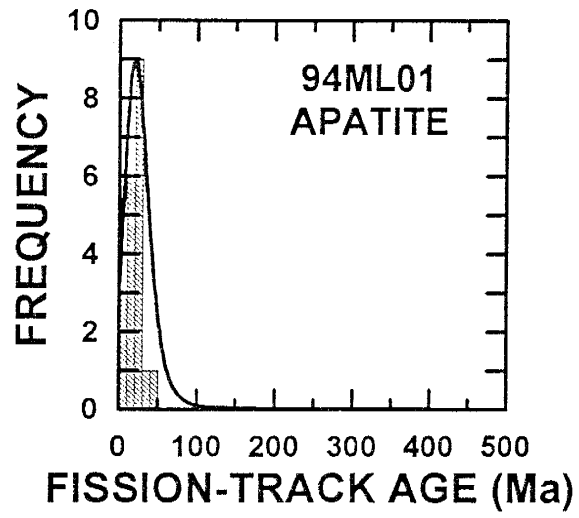
FISSION TRACK AGE DATA

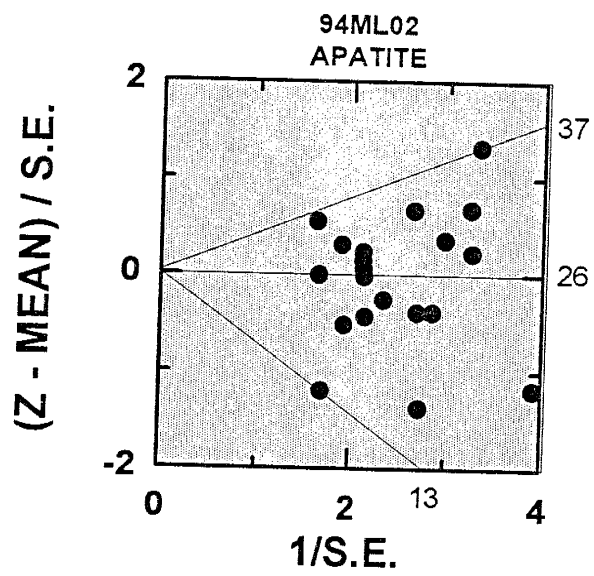
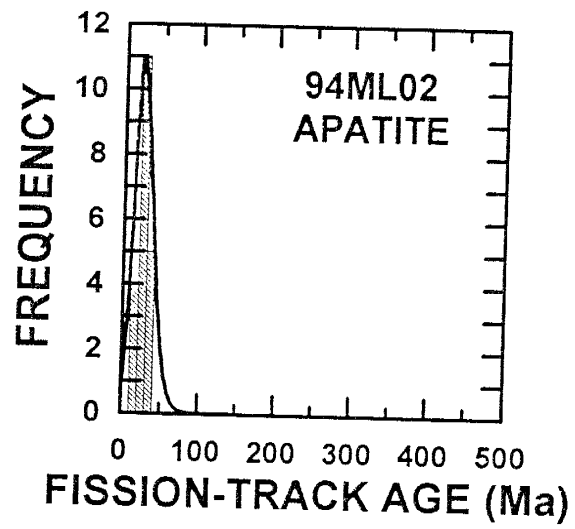
PROJECT NAME:	MONTE LARGO	DATE:	1/20/95	FT AGE:	21.4 Ma
SAMPLE NUMBER:	94ML1	LATITUDE:	35°11.41' N	UPPER CI:	29.2 Ma
LAB NUMBER:	SMU	LONGITUDE:	106°15.51' W	LOWER CI:	15.6 Ma
REACTOR RUN NUMBER:	RR-11-29-94A	ELEVATION (M):	2134	STD ERR:	3.32 Ma
NEUTRON FLUX:	9.000E+15	MICROSCOPE:	OLYMPUS	C. COEFF:	0.813
# SPON TRACKS (FLUX)	600	MAGNIFICATION:	1250 X	CHIP:	6.801 19
# IND. TRACKS (FLUX)	4000	ROCK TYPE:	GRANITE	AVG. AGE:	20.0 Ma
NUMBER OF GRAINS:	20	MINERAL:	APATITE	STD. ERR:	2.5

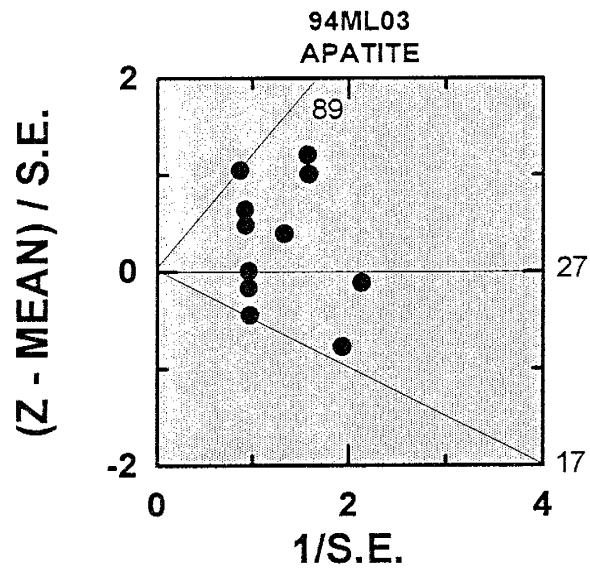
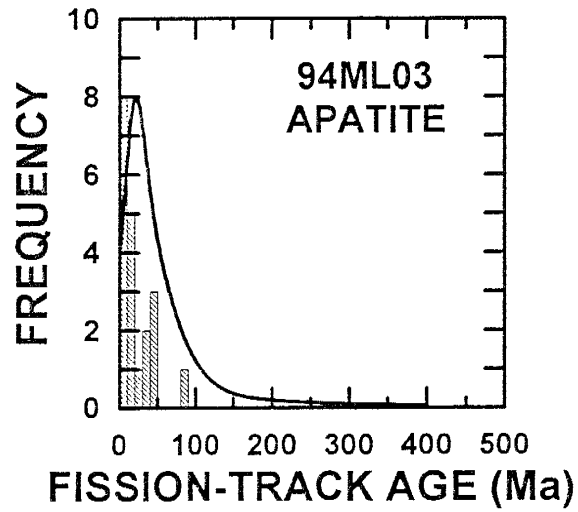
GRAIN #	AREA USED (SQ. CM)	Ns	RHO(S) (/CM ²)	Ni	RHO(I) (/CM ²)	RATIO (Ns/Ni)	URANIUM (PPM)	AGE (MA)	STD.DEV. (MA)
1	8.0E-05	4	5.000E+04	38	9.500E+05	0.11	10.1	28.3	14.9
2	4.0E-05	1	2.500E+04	16	8.000E+05	0.06	8.5	16.8	17.3
3	4.0E-05	2	5.000E+04	24	1.200E+06	0.08	12.8	22.4	16.5
4	2.0E-05	0	0.000E+00	1	1.000E+05	0.00	1.1	0.0	2655.0
5	4.0E-05	1	2.500E+04	14	7.000E+05	0.07	7.5	19.2	19.9
6	4.0E-05	5	1.250E+05	66	3.300E+06	0.08	35.2	20.4	9.5
7	4.0E-05	3	7.500E+04	41	2.050E+06	0.07	21.9	19.7	11.8
8	4.0E-05	1	2.500E+04	16	8.000E+05	0.06	8.5	16.8	17.3
9	4.0E-05	3	7.500E+04	25	1.250E+06	0.12	13.3	32.2	19.7
10	4.0E-05	5	1.250E+05	66	3.300E+06	0.08	35.2	20.4	9.5
11	4.0E-05	0	0.000E+00	19	9.500E+05	0.00	10.1	0.0	37.0
12	4.0E-05	3	7.500E+04	32	1.600E+06	0.09	17.1	25.2	15.3
13	2.0E-05	4	2.000E+05	38	3.800E+06	0.11	40.5	28.3	14.9
14	4.0E-05	3	7.500E+04	71	3.550E+06	0.04	37.9	11.4	6.7
15	2.0E-05	4	2.000E+05	25	2.500E+06	0.16	26.7	42.9	23.2
16	2.0E-05	2	1.000E+05	25	2.500E+06	0.08	26.7	21.5	15.8
17	4.0E-05	0	0.000E+00	8	4.000E+05	0.00	4.3	0.0	100.0
18	2.0E-05	1	5.000E+04	9	9.000E+05	0.11	9.6	29.8	31.5
19	4.0E-05	2	5.000E+04	30	1.500E+06	0.07	16.0	17.9	13.1
20	4.0E-05	4	1.000E+05	40	2.000E+06	0.10	21.3	26.9	14.1
	7.4E-04	48	6.486E+04	604	1.632E+06	0.08	17.4		

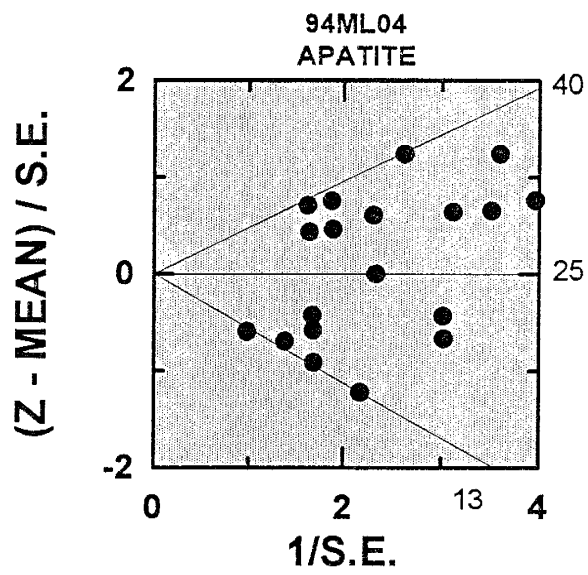
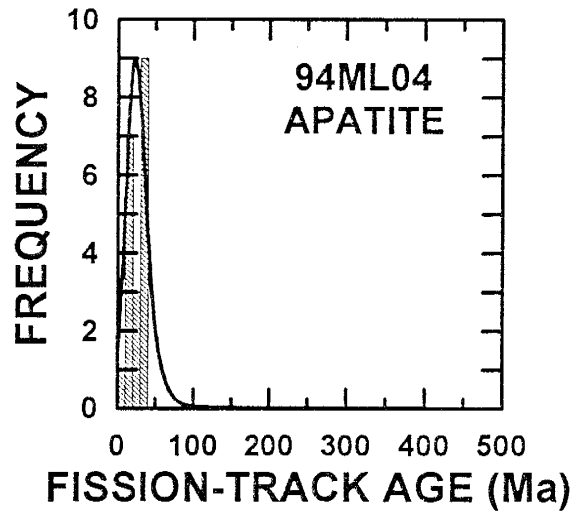
APPENDIX E

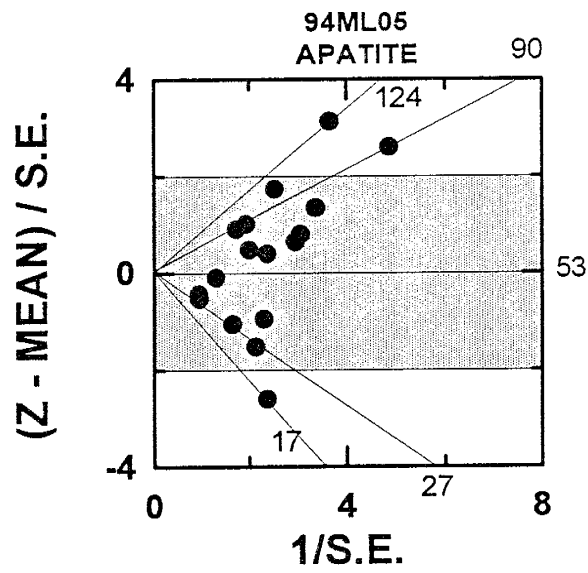
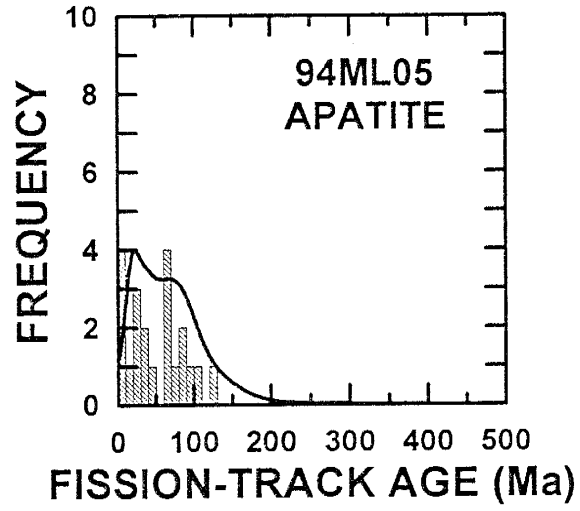
Graphical representation of fission-track age data. Upper figure: fission track age probability density function superimposed on histogram of individual grain ages. The density function indicates the probability that a certain number of grains in a sample will have ages within a given age interval. Lower figure: radial plot diagrams (Galbraith, 1988), which allow comparison of measurements with different standard errors. The variation of single grain ages are plotted as $y = (z_i - z) \text{ s.e.}_i$, where z_i is the individual grain age, z is the mean age, and s.e._i is the standard error of the single grain age, versus $x = 1/\text{s.e.}_i$, a measure of the precision of each grain age. Fission-track age is given by the slope of a straight line from the origin through the data points. The age scale is shown radially around the edge of the plot. Since young grains have precise ages, these grains are easily identified because they plot to the right-hand side of the diagram. If all of the grains belong to a single age population, the points should lie within ± 2 on the y-axis (shaded), which corresponds to lying within ± 2 s.e. Scatter outside of $y = \pm 2$ indicates that multiple age populations are present.

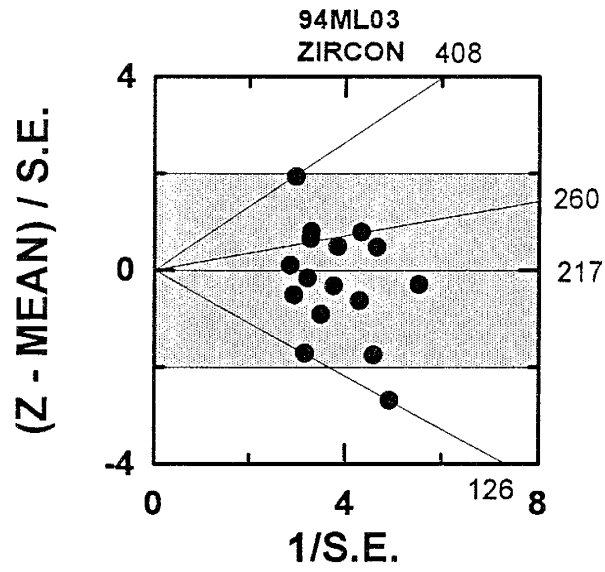
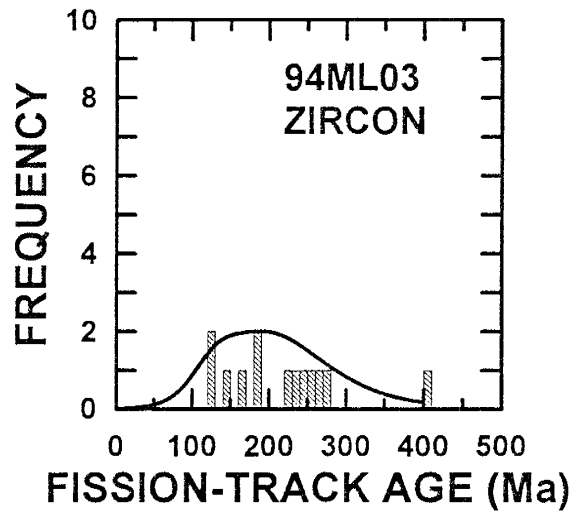


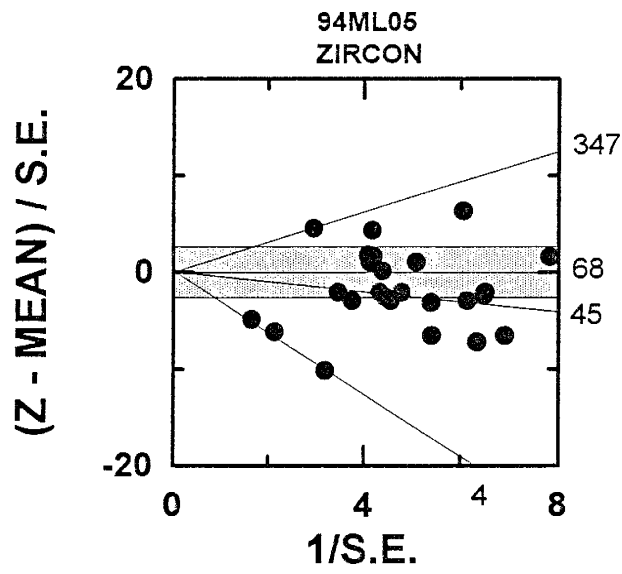
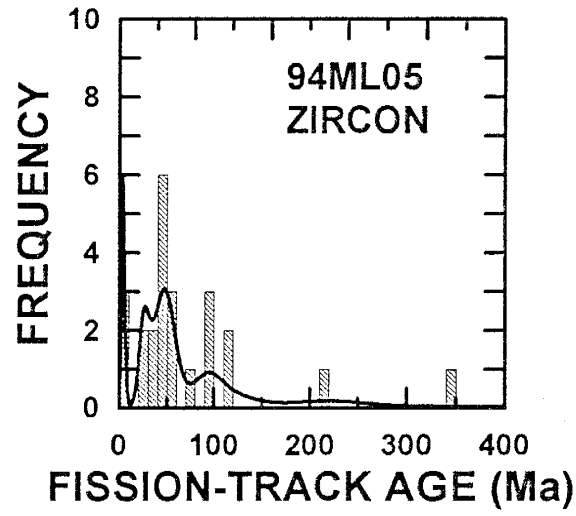


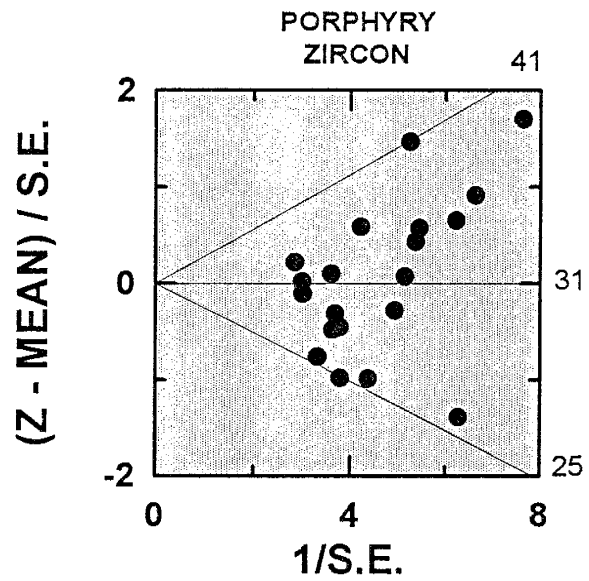
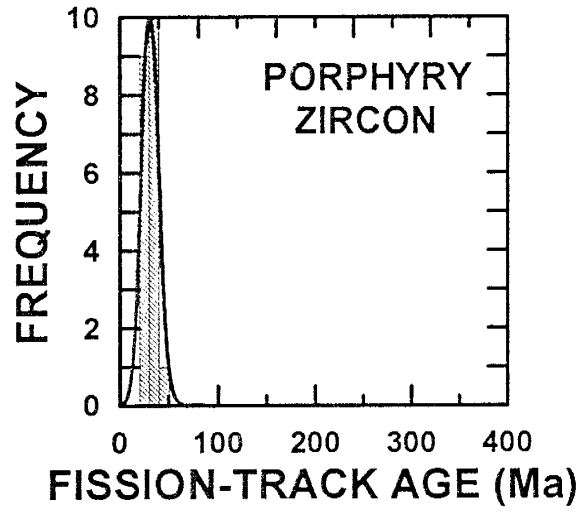












APPENDIX F

(a) Apatite confined fission-track lengths (in microns) for sample ML02. Total count: 65. Minimum track length: 5.8. Maximum track length: 18.5. Mean length: 13.47. Standard deviation: 2.23. Standard error: 0.54.

11.8	15.2	10.9	15.6	10.6
5.8	13.9	14.0	13.6	15.2
18.5	16.8	14.1	14.4	11.7
13.6	13.7	12.1	15.4	14.3
12.6	15.1	14.3	17.1	10.3
15.8	14.7	11.6	9.4	14.3
14.4	12.6	14.3	13.5	15.7
15.6	13.8	10.7	16.5	11.5
13.1	13.7	14.5	8.9	11.9
13.5	14.8	15.0	14.9	11.8
8.1	14.9	13.9	14.2	15.1
10.7	16.5	13.0	11.5	12.6
14.8	13.1	14.1	14.4	11.6

(b) Apatite confined fission-track lengths (in microns) for sample ML04. Total count: 21. Minimum track length: 9.1. Maximum track length: 16.3. Mean length: 13.16. Standard deviation: 1.69. Standard error: 0.72.

15.5	15.2	14.9
12.6	11.7	11.1
12.7	9.1	10.8
13.8	13.4	12.4
13.9	16.3	12.3
12.7	13.4	12.4
13.9	13.9	14.4

APPENDIX G

Minor fault and fault slickenside data. Data for rocks in the streamcut exposure near Golden are presented separately in Appendix C. Data was collected in five lithologic units: Proterozoic Tijeras greenstone, Proterozoic Cibola gneiss, Permian Abo Formation, Cretaceous Mesaverde Group, and the Cretaceous Dakota Formation. See Fig. 3-2 for location of exposures. Faults vary in scale from hand-sample slickenside surfaces to outcrop-size faults. Pitch refers to the angle of pitch (rake) of slickenlines on a slickenside surface. Orientation (strike, dip, dip direction) of the metamorphic foliation in the Tijeras greenstone and Cibola gneiss, and the orientation of bedding in the Abo Formation, Mesaverde Group, and Dakota Formation, is presented for each measurement site. Sense-of-slip is interpreted from slickenside surfaces using the criteria outlined by Petit (1987), or indicated by bedding separations. Oblique slickenlines record two components of motion (strike-slip and dip-slip). The dominant component of each measurement is listed first; the subordinate component is listed second. Sense-of-slip criteria on slickensides is subdivided into those criteria which form by friction (secondary fractures) and those that form by mineral growth (slickenfibers). Offset beds reflect apparent vertical displacement direction.

lithologic unit	fault orientation	pitch	foliation or bedding	sense of slip	sense of slip criteria
greenstone	108, 80 s	50 w	036, 65 nw		
greenstone	144, 69 sw	10 nw	036, 65 nw		
greenstone	083, 53 s	30 w	036, 65 nw		
greenstone	138, 90		036, 65 nw		
greenstone	123, 85 sw	10 se	036, 65 nw		
greenstone	166, 63 w		042, 68 nw		
greenstone	142, 79 sw	5 se	042, 68 nw	left-lateral & normal	secondary fractures
greenstone	163, 84 e	0	042, 68 nw	left-lateral	slickenfibers
greenstone	143, 79 ne	12 se	042, 68 nw		
greenstone	149, 33 ne	46 nw	042, 68 nw		
greenstone	075, 76 n	8 ne	042, 68 nw	right-lateral & normal	slickenfibers
greenstone	120, 71 ne	10 se	042, 68 nw		
greenstone	074, 82 nw	36 sw	042, 68 nw	right-lateral & reverse	slickenfibers
greenstone	066, 83 nw	3 sw	042, 68 nw	right-lateral & reverse	slickenfibers
greenstone	089, 88 s	17 w	042, 68 nw	right-lateral & normal	slickenfibers
greenstone	131, 60 ne	27 se	042, 68 nw		
greenstone	088, 72 s	23 e	042, 68 nw		
greenstone	134, 76 sw	32 se	042, 68 nw		
greenstone	272, 85 s	0	042, 68 nw		
greenstone	057, 90	15 sw	031, 73 nw		
greenstone	051, 67 se	29 sw	031, 73 nw		
greenstone	160, 78 w	10 nw	031, 73 nw		
greenstone	081, 77 s	2 w	031, 73 nw		
greenstone	276, 80 s	16 w	031, 73 nw	right-lateral & normal	secondary fractures
greenstone	067, 71 se	10 ne	031, 73 nw	right-lateral & reverse	slickenfibers
greenstone	078, 78 nw	0	031, 73 nw	right-lateral	slickenfibers
greenstone	121, 79 sw	20 se	031, 73 nw		
greenstone	089, 90	15 w	031, 73 nw		
greenstone	084, 75 s	0	031, 73 nw		
greenstone	097, 69 s	9 w	031, 73 nw	right-lateral & normal	slickenfibers
greenstone	086, 74 n	0	031, 73 nw	right-lateral	slickenfibers
greenstone	067, 61 se	30 sw	031, 73 nw		

greenstone	067, 59 se	25 ne	031, 73 nw		
greenstone	078, 63 se	14 sw	031, 73 nw	right-lateral & normal	slickenfibers
greenstone	079, 60 se	36 sw	031, 73 nw		
greenstone	072, 54 se	57 ne	031, 73 nw		
greenstone	072, 70 se	10 sw	031, 73 nw		
greenstone	114, 59 sw	46 nw	031, 73 nw		
greenstone	064, 68 se	21 ne	031, 73 nw	right-lateral & reverse	slickenfibers
greenstone	115, 44 w	39 se	031, 73 nw		
greenstone	035, 25 se	90	031, 73 nw		
greenstone	133, 53 sw	25 se	031, 73 nw		
Cibola gneiss	049, 47 nw				
Cibola gneiss	170, 85 e				
Cibola gneiss	012, 45 e	57 s			
Cibola gneiss	024, 54 se	55 sw			
Cibola gneiss	018, 36 e	20 sw			
Cibola gneiss	127, 23 ne	15 nw			
Cibola gneiss	149, 59 sw				
Cibola gneiss	014, 54 e	58 s			
Cibola gneiss	025, 69 se	59 s			
Cibola gneiss	008, 33 e	71 s			
Cibola gneiss	035, 71 nw	57 sw			
Cibola gneiss	046, 90	85 sw			
Cibola gneiss	012, 22 e	64 sw			
Cibola gneiss	113, 73 sw				
Cibola gneiss	070, 34 nw				
Cibola gneiss	123, 65 sw				
Cibola gneiss	085, 45 e				
Cibola gneiss	150, 70 sw				
Cibola gneiss	018, 27 e	17 sw			
Cibola gneiss	037, 6 se	88 ne			
Cibola gneiss	037, 67 se	90		normal	offset beds
Cibola gneiss	100, 71 s				
Cibola gneiss	048, 30 se	75 ne			

Cibola gneiss	045, 20 se	80 ne				
Cibola gneiss	045, 46 nw	80 sw			reverse & right-lateral	secondary fractures
Cibola gneiss	047, 36 se	63 ne				
Cibola gneiss	121, 72 sw					
Cibola gneiss	053, 69 nw	80 sw			reverse & right-lateral	secondary fractures
Cibola gneiss	043, 83 se	90				
Cibola gneiss	066, 71 se	7 sw				
Cibola gneiss	142, 85 ne					
Cibola gneiss	035, 83 se	75 sw				
Cibola gneiss	100, 76 s					
Cibola gneiss	040, 86 se	80 sw				
Cibola gneiss	047, 76 nw					
Cibola gneiss	033, 65 se	53 sw				
Cibola gneiss	035, 90	54 sw				
Cibola gneiss	121, 85 sw					
Cibola gneiss	105, 50 s	17 e		033, 77 nw		
Cibola gneiss	075, 65 s	7 ne		033, 77 nw		
Cibola gneiss	161, 85 w			033, 77 nw		
Cibola gneiss	176, 72 w			033, 77 nw		
Cibola gneiss	069, 44 se	32 ne		033, 77 nw		
Cibola gneiss	041, 58 se	81 ne		033, 77 nw		
Cibola gneiss	005, 39 e	83 n		033, 77 nw		
Cibola gneiss	025, 43 se	61 sw		033, 77 nw		
Cibola gneiss	077, 57 nw			033, 77 nw		
Cibola gneiss	152, 32 ne			033, 77 nw		
Cibola gneiss	037, 37 se	72 sw		033, 77 nw		
Cibola gneiss	000, 62 w					
Cibola gneiss	058, 79 se					
Cibola gneiss	078, 31 se	34 e				
Cibola gneiss	159, 90					
Cibola gneiss	036, 28 se	90				
Cibola gneiss	090, 76 n					
Cibola gneiss	000, 65 w					

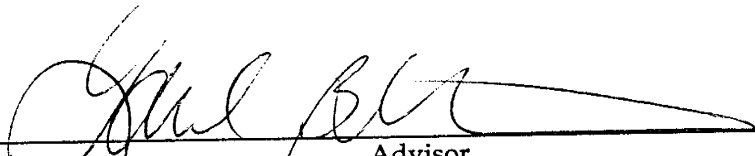
Cibola gneiss	051, 71 se	12 ne			
Cibola gneiss	077, 79 se	16 ne			
Cibola gneiss	165, 75 s				
Cibola gneiss	018, 87 e				
Cibola gneiss	114, 80 n				
Cibola gneiss	147, 50 sw				
Cibola gneiss	125, 73 sw				
Cibola gneiss	001, 86 w				
Cibola gneiss	174, 14 w				
Cibola gneiss	160, 84 w				
Cibola gneiss	097, 63 n				
Cibola gneiss	176, 77 w				
Cibola gneiss	020, 41 e	30 sw			right-lateral & normal
Cibola gneiss	177, 31 w				
Cibola gneiss	000, 90				
Abo	061, 49 se	85 w	077, 23 n		
Abo	310, 13 ne	42 se	287, 23 n		
Abo	281, 17 s	78 e	062, 17 nw		
Abo	300, 85 sw	15 se	062, 17 nw		
Abo	064, 62 se	84 w	062, 17 nw		
Abo	078, 78 s	80 e	062, 17 nw		
Abo	048, 16 se	49 se	062, 17 nw		
Abo	074, 66 s	90	062, 17 nw		
Abo	033, 59 se	60 sw	062, 17 nw		
Abo	088, 86 s	85 w	062, 17 nw		
Abo	076, 81 s	85 w	062, 17 nw		
Abo	295, 90	0	062, 17 nw		
Abo	286, 90	0	062, 17 nw		
Abo	274, 84 s	85 w	062, 17 nw		
Abo	070, 54 se	80 e	062, 17 nw		
Abo	071, 83 se	85 e	062, 17 nw		
Abo	275, 60 s	65 e	062, 17 nw		
Abo	275, 78 n	90	062, 17 nw		

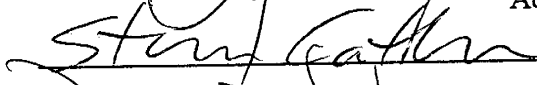
Abo	010, 61 w			062, 17 nw	normal	offset beds
Abo	003, 75 w			090, 10 n	normal	offset beds
Abo	005, 75 w			090, 10 n	normal	offset beds
Abo	096, 70 s	90		090, 10 n		
Abo	280, 78 s	90		090, 10 n		
Abo	325, 74 ne			090, 10 n		
Abo	313, 86 ne			090, 10 n	normal	offset beds
Abo	128, 85 sw	15 se		085, 10 n		
Abo	048, 34 se	90		085, 10 n		
Abo	072, 41 s	75 e		085, 10 n		
Abo	010, 75 w	75 e		085, 10 n		
Abo	052, 74 s	90		085, 10 n		
Abo	000, 73 w			085, 10 n	normal	offset beds
Abo	074, 76 se	90		085, 10 n		
Abo	070, 81 se	32 sw		059, 13 n	left-lateral & reverse	slickenfibers
Abo	278, 80 s			031, 13 nw	normal	offset beds
Abo	152, 90			031, 13 nw		
Abo	078, 78 n			031, 13 nw		
Abo	075, 83 n	85 se		027, 11 nw		
Abo	080, 67 s	15 w		027, 11 nw		
Abo	161, 62 e			027, 11 nw		
Abo	341, 85 w	80 se		027, 11 nw		
Abo	052, 74 se	65 ne		027, 11 nw		
Abo	064, 80 se	72 ne		027, 11 nw	normal & left-lateral	secondary fractures
Abo	064, 63 se	50 ne		027, 11 nw		
Abo	035, 76 se	80 ne		027, 11 nw		
Abo	086, 85 s	0		027, 11 nw		
Abo	329, 90	60 se		027, 11 nw		
Abo	163, 61 e	60 se		027, 11 nw	normal & right-lateral	secondary fractures
Abo	014, 51 e	80 se		027, 11 nw	normal & right-lateral	secondary fractures
Abo	115, 72 s	30 e		027, 11 nw		
Abo	153, 65 e			027, 11 nw		
Abo	167, 71 e	65 se		027, 11 nw	normal & right-lateral	secondary fractures


Abo	056, 52 se	80 e	027, 11 nw	normal & left-lateral	secondary fractures
Abo	068, 65 se	78 ne	027, 11 nw	normal & left-lateral	secondary fractures
Abo	083, 44 s	36 e	027, 11 nw		
Abo	075, 53 se	70 e	090, 15 n	normal & left-lateral	secondary fractures
Abo	114, 76 ne		027, 11 nw		
Abo	001, 71 w	64 s	050, 12 se		
Abo	143, 65 sw	80 se	050, 12 se	normal & left-lateral	secondary fractures
Abo	137, 54 sw	80 se	050, 12 se	normal & left-lateral	slickenfibers
Abo	063, 84 nw		050, 12 se		
Abo	129, 61 sw	70 se	050, 12 se	normal & left-lateral	secondary fractures
Abo	022, 86 w	47 sw	106, 20 n	normal & left-lateral	secondary fractures
Abo	059, 35 se	72 sw	106, 20 n	normal & right-lateral	slickenfibers
Abo	006, 90		106, 20 n		
Morrison	037, 85 se	20 ne	027, 75 e	left-lateral & normal	secondary fractures
Morrison	062, 55 nw	18 ne	027, 75 e		
Morrison	090, 70 n	25 e	027, 75 e		
Morrison	125, 73 sw	55 se	027, 75 e		
Morrison	100, 90	58 e	027, 75 e	right-lateral	secondary fractures
Morrison	078, 90	27 e	027, 75 e	right-lateral	secondary fractures
Morrison	091, 68 n	55 w	027, 75 e	normal & left-lateral	secondary fractures
Morrison	084, 84 s	0	027, 75 e		
Morrison	100, 58 n	78 e	027, 75 e		
Morrison	002, 90		027, 75 e		
Morrison	118, 90		027, 75 e		
Morrison	125, 74 ne	15 se	027, 75 e	right-lateral & normal	secondary fractures
Morrison	075, 82 s	10 ne	027, 75 e		
Morrison	058, 59 nw	40 ne	027, 75 e		
Morrison	075, 60 nw	32 ne	027, 75 e	right-lateral & normal	secondary fractures
Morrison	093, 76 n	63 e	027, 75 e	normal & right-lateral	secondary fractures
Morrison	061, 83 nw	30 sw	027, 75 e		
Morrison	079, 48 n	25 e	027, 75 e	right-lateral & normal	secondary fractures
Morrison	079, 48 n	65 e	027, 75 e	normal & right-lateral	secondary fractures
Morrison	050, 80 nw	46 ne	027, 75 e	normal & right-lateral	secondary fractures


Morrison	070, 90		20 ne			027, 75 e	right-lateral	secondary fractures
Morrison	050, 64 nw		47 ne			027, 75 e		
Morrison	091, 62 n		52 e			027, 75 e	normal & right-lateral	secondary fractures
Morrison	149, 71 ne		36 se			027, 75 e	right-lateral & normal	secondary fractures
Morrison	056, 71 nw		30 ne			027, 75 e	right-lateral & normal	secondary fractures
Morrison	098, 69 n		50 e			027, 75 e		
Morrison	169, 26 w		45 s			027, 75 e		
Morrison	020, 40 w		10 n			027, 75 e	right-lateral & normal	secondary fractures
Morrison	075, 35 n		45 ne			027, 75 e		
Morrison	016, 53 w		16 n			027, 75 e	right-lateral & normal	secondary fractures
Morrison	065, 90		15 ne			027, 75 e		
Dakota	031, 62 se		79 ne			123, 25 s		
Dakota	069, 66 s					123, 25 s		
Dakota	164, 49 e					123, 25 s		
Dakota	164, 61 e		80 s			123, 25 s		
Dakota	045, 67 nw		68 ne			123, 25 s		
Dakota	023, 73 nw		80 n			123, 25 s		
Dakota	067, 68 se		38 ne			123, 25 s		
Dakota	072, 66 e		55 ne			123, 25 s		
Dakota	045, 64 se		60 ne			123, 25 s		
Dakota	000, 52 e					123, 25 s		
Dakota	100, 80 s					123, 25 s		
Dakota	039, 76 nw		70 ne			123, 25 s		
Dakota	029, 90		38 ne			123, 25 s		
Dakota	005, 90		18 n			139, 49 sw		
Dakota	032, 34 e		52 ne			139, 49 sw		
Dakota	179, 90		35 n			139, 49 sw		
Dakota	014, 90		25 n			139, 49 sw		
Dakota	125, 59 n		80 w			139, 49 sw		
Dakota	146, 61 ne		85 nw			139, 49 sw		
Dakota	002, 78 e		18 s			155, 51 w	left-lateral & reverse	secondary fractures

This thesis is accepted on behalf of the faculty
of the Institute by the following committee:



Advisor


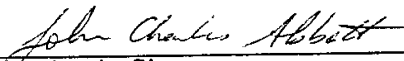




MAY 12, 1995

Date

I release this document to the New Mexico Institute of Mining and Technology.



Student's Signature

May 1995

Date